THE ROLE OF THE GUT MICROBIOME IN BONE AND JOINT

A Dissertation

Presented to the Faculty of the Graduate School

of Cornell University

In Partial Fulfillment of the Requirements for the Degree of

Doctor of Philosophy

By

Jason Daniel Guss

December 2018

THE ROLE OF THE GUT MICROBIOME IN BONE AND JOINT

Jason Daniel Guss, Ph.D.

Cornell University 2018

` Osteoporosis and osteoarthritis affect millions of people worldwide every year. Osteoporosis related fractures totaled 8.9 million worldwide annually and osteoarthritis affects over 30 million people in the US alone. Recently, the gut microbiome has been identified as a factor that can influence chronic conditions associated with bone and joint disease such as obesity, diabetes, metabolic syndrome, inflammatory bowel diseases, and malnutrition. Though the gut microbiome is studied extensively in relation to metabolic diseases and disorders, the role of the gut microbiome in the development and progression of bone and joint disease is largely unexplored.

Recent evidence suggests that the gut microbiome can influence bone mass, however no studies have determined if the mechanical performance of the bone is influenced by the gut microbiome. Therefore, first, we characterize how alterations to the gut microbiome can influence whole bone mechanical performance at skeletal maturity. We evaluate alterations in the gut microbiome caused by genotypic alteration and chronic treatment with antibiotics. Our results demonstrate that disruption of the gut microbiome with antibiotics is associated with reductions in cortical bone mass and whole bone strength, as well as drastic shifts in the composition of the gut microbiome. Furthermore, the changes in whole bone strength are greater than can be explained by the associated changes in bone mass and geometry, suggesting

impaired bone tissue material properties in mice with an altered gut microbiome due to genotypic alteration and chronic antibiotic treatment.

Next, we evaluate the changes in bone tissue composition caused by alterations in the gut microbiome. Additionally, we investigate how the functional profile of the gut microbiome can influence bone tissue material properties through several potential pathways: 1) regulation of nutrient and vitamin absorption/synthesis; 2) regulation of the immune system; 3) translocation of bacterial products. Our results demonstrate that disruption of the gut microbiome with antibiotics causes changes in bone mineral crystallinity, and that the effect is different per mouse genotype. Furthermore, we show that the functional capacity of the gut microbiome is dramatically altered in mice treated with antibiotics. A pathway involving vitamin K, a factor important for bone health, and associated with fracture risk, is suspected as changes in microbial gene pathways for vitamin K synthesis are disrupted leading to reduced vitamin K levels in organs.

Last, we evaluate how alterations in the gut microbiome may influence the development and severity of load-induced osteoarthritis. Here we investigate obesity and metabolic syndrome, two conditions associated with an altered gut microbiome and an increased risk of developing osteoarthritis (OA). We use a mouse model of metabolic syndrome dependent on the gut microbiome, a mouse model of severe obesity/diabetes, and an in vivo non-invasive loading model to induce osteoarthritis-like pathology. Our results demonstrate that metabolic syndrome in the current mouse model does not increase load-induced cartilage damage, while severe obesity leads to increases in cartilage damage, though only after a prolonged loading period. The increased cartilage damage in severely obese mice is associated with increased adiposity, systemic inflammation, and bacterial lipopolysaccharide. We also demonstrate that disruption of

the gut microbiome in the metabolic syndrome mice is associated with decreased load-induced cartilage damage, as well as changes in subchondral bone properties.

Together, the current work suggests the gut microbiome influences both the structure and composition of bone, and can influence the development of osteoarthritis. The current work helps to establish a promising foundation for future lines of investigation evaluating how the gut microbiome influences bone and joint and suggests that there may be a future use for manipulating the gut microbiome in therapies to treat and prevent bone and joint disease.

Biographical Sketch

Jason was salutatorian of Longwood High School 2008 class, and was salutatorian of the 2013 Mechanical Engineering class at State University of New York at Binghamton. In his free time, Jason performs comedy, reads about neuroscience, psychology, and the subconscious mind, and loves to both watch and play sports including basketball, football, and tennis. Jason's future pursuits include high growth technology startup companies and enhancing science communication and engagement.

Acknowledgements

I humbly thank my parents Robert Guss and Shari Guss for their unrelenting support throughout my entire PhD and every other obstacle I've faced throughout my life. Their love and support have sustained my confidence and drive. I would also like to thank my brother Michael Guss for inspiring me to be the best I can be and to always work hard. Additionally, I would like to thank all the other friends that have supported me, made me laugh, and brought joy and support to my life everyday. Last, I would very much like to thank my advisor, Dr. Christopher Hernandez for helping me to learn during such a critical phase of my life, be analytical, and to set a high standard for my work that I feel will positively influence every endeavor I take on for the rest of my life.

Table of Contents

List of Figures

List of Tables

Chapter 1. Introduction

Chapter 1.1 Introduction to the Gut Microbiome

The gut microbiome are the trillions of microorganisms and their products that inhabit the gastrointestinal tract. The gut microbiome is comprised of over a 1000 different species that coexist in a stable, but dynamic equilibrium. The gut microbiome offers unique benefits to the host as the gut microbiome is involved in digestion and metabolism, nutritional absorption, and the development and functioning of the immune system. Alterations to the gut microbiome are linked to various chronic conditions that include: obesity, diabetes, metabolic syndrome, inflammatory bowel diseases, malnutrition, cardiovascular disease, cancer, neurological disorders, and most recently, orthopedic bone and joint disorders.

The following paragraph is from the paper I co-authored titled "Links Between the Microbiome and Bone". The paragraph is reused with permission from Wiley.

(Start of excerpt from Hernandez et al 2016)

The human microbiome is established soon after birth, usually by colonization by microbial flora present in the birth canal [(1)]. The microbiota is shaped subsequently by diet and environmental exposure, and reaches a steady state at about three years of age [(1)]. The great majority of the human microbiome is located within the gastrointestinal system. The human gut microbiota consists of over 1000 distinct microbial species, many of them not yet well characterized. Roughly two-thirds of the microbial species composition is unique to each individual [(2)]. The human gut microbiota is dominated by organisms from the *Bacteroidetes* and *Firmictues* phyla [(3)]. Once established in an individual, the contents of the

microbial community in the gut enter a dynamic equilibrium as the hundreds of different species compete and interact with one another and the host immune system in complex networks of interdependence. The relative abundance of species within the gut flora fluctuates from day to day based on changes in diet [3,4], but in general retains its basal constitutive state despite these transient disruptions. For example, after a stimulus such as a course of antibiotics or short gastrointestinal infection, the contents of the gut microbiota mostly return to their initial state, although the resulting gut microbial community may be less stable than it was prior to treatment [5] and small changes in content may occur (e.g. species with similar function may replace each other [4]). Hence, while the gut microbiome is relatively stable it can be changed by long periods of sustained stimuli or factors that produce large perturbations in the gut flora. *(End of excerpt from Hernandez et al 2016).* The functions of the gut microbiome are highly conserved and when disruptions in the microbiome occur, functions are often taken over by other microbiota that can fill that niche.

1.1.1 Experimental Methods Used for Manipulating, Characterizing, and Understanding the Gut Microbiome

A number of techniques in gut microbiome research are used to manipulate the gut microbiome: germ-free living conditions, microbiota transplantation, cohousing, and administration of antibiotics. Animals raised from birth in an environment completely absent of any microbial life are considered "germ-free" and do not have a gut microbiome. Germ-free animals were first utilized in the 1950s [6]. Germ-free mice are an ideal model for understanding in a broad manner if the gut microbiome is involved in a mouse phenotype. For example, a genetic knockout mouse that displays obesity as a result of disturbances in the gut microbiome, no longer displays obesity when raised in germ-free conditions, thus demonstrating the

importance of the microbiome for the development of the phenotype [7]. A major limitation in work with germ-free animals are the numerous physiologic changes and immune deficiencies present in germ-free animals that may influence study outcomes beyond the direct effect of the microbiota [8,9]. Germ-free mice can also be used to receive a transplant of a defined gut microbiota to determine the specific effects of different microbiota populations. Germ-free mice can be colonized with a single microbial species (mono-associated), a specific mix of microbial species (defined microbiota), or an entire gut microbiome (xenografted microbiota) from another host (mouse, human, etc) [10]. Transplantation of gut microbiota into mice normally occurs through the use of a syringe and tube to directly administer the gut microbiota into the stomach [10]. Cohousing is another technique used by the gut microbiome community to transfer the gut microbiome communities between mice [11]. In cohousing, mice of different genotypes or experimental groups are placed in the same cage. Because mice are copraphagic (eat feces), the transfer of gut microbial content occurs between mice over time. Another technique used to manipulate the gut microbiome is the administration of antibiotics. Antibiotics are compounds able to decimate specific microbiota communities. Typically, the broad-spectrum antibiotics used have profound impacts on the overall composition and function of the gut microbiome (*Antibiotics are discussed in greater detail in Section 1.2.2*). Prolonged and continuous treatment with antibiotics for months can be used to cause a shift in the composition of the gut microbiome. Antibiotics allow researchers to selectively modify the gut microbiome to investigate the effects of specific gut microbiome populations. Additionally, antibiotic-treated mice are sometimes used instead of germ-free mice as the recipients of gut microbiota when performing a microbiota transplantation study [12].

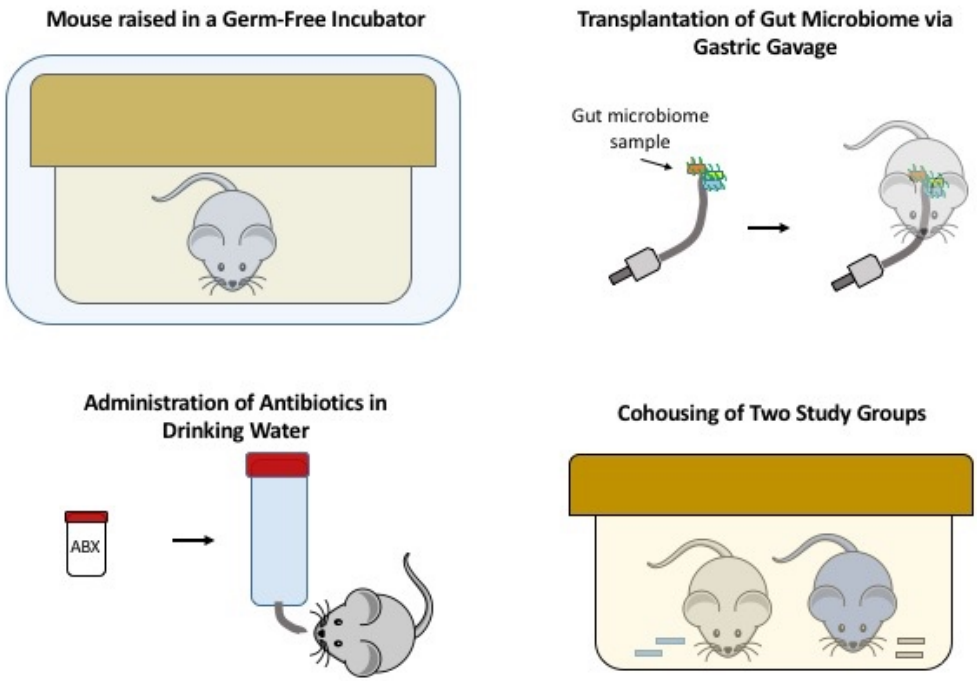

Figure 1.1 Methods for manipulation of the gut microbiome

Next generation sequencing techniques are used to characterize the composition and functions of the gut microbiome. 16s rRNA gene sequencing analyzes a highly conserved 16S rRNA gene to allow for the taxonomic profiling of the gut microbiota [13,14]. Common analyses include determining the total amount of bacteria, the relative abundance of the gut microbiota at each phylogenetic level (species, genus, family, phyla, etc), the overall diversity of the gut microbial community, and the overall phylogenetic tree to illustrate how each microbiota classification is related to one another. Shotgun metagenomics analyzes bacterial DNA to profile the gut microbiome in a similar manner to 16s rRNA sequencing, however it also allows for the identification and quantification of the microbial genes present in order to determine the functional capabilities of the gut microbiome [13-15]. Shotgun metagenomics overall allows for a more specific taxonomic and functional classification of sequences compared to 16s rRNA gene sequencing, although it can be more time consuming and costly. The ability to evaluate the

functional capacity of the microbiome (what the microbes can do) through metagenomics can often be more informative than just identifying the composition (what microbes are present).

1.1.2 Factors that Influence the Gut Microbiome: Emphasis on Diet and Antibiotics

Many factors influence the constituents and function of the gut microbiome throughout life such as diet, treatment with oral antibiotics, environment, physiologic state, pathogen exposure, genetics, age, and probiotics. Diet and antibiotics are explained in further depth as both are most relevant to the thesis.

1.1.2.1 Diet

Diet can have a profound and lasting impact on both the composition and function of the gut microbiome. The host diet is the primary source of energy and nutrients for the gut microbiome. Changes in diet can have rapid effects on the gut microbiome, with detectable differences in the composition of the gut microbiota and the genes expressed in as little as 24 hours [(16)]. A consistent change in diet is able to generate permanent shifts in the composition of the gut microbiota, as the gut microbiota best suited to thrive with the available dietary components establish themselves [(17)]. Changes in diet that last months or years are associated with different gut microbiome profiles [(18)]. In addition to the composition of the diet influencing the gut microbiome, the total food intake, as well as fasting/feeding schedules have been shown to influence the composition and function of the gut microbiome [(19)]. Changes in the gut microbiome resulting from diet can play a large role in the nutrients and energy the host extracts from a diet, as well as overall immune and metabolic function [(20)].

Our understanding of the gut microbiome and diet has focused on diets such as the Western diet and Mediterranean diet. Researchers use rodent chow formulas that are modeled after common human diets. The Western diet, with high levels of animal protein and fat, has been a major focus, as current diet trends are a contributor to the rising levels of obesity and diabetes in the United States [21]. The western diet is modeled in mice by feeding mice high fat diets with various percentages of fat content (35%, 45%, 60%) [22]. Studies in humans and mice have demonstrated that the Western diet reduces bacterial diversity, alters the functions of the gut microbiome [23,24], and leads to other serious health concerns including obesity, insulin resistance, and systemic inflammation that are directly or indirectly linked to the gut microbiome [25,26]. High fat diet is also associated with an increased abundance of the phyla Firmicutes and a decreased abundance of the phyla Bacteroidetes [27]. The Mediterranean diet is a balanced intake of nutrients that includes fatty acids, antioxidants, and a high intake of fiber, and is thus considered far healthier than the Western diet. The Mediterranean diet helps to promote commensal bacteria such as Lactobacillus, Bifidobacterium, and Prevotella, and has been shown to increase the production of short chain fatty acids, as well as decrease obesity and inflammation [28].

Dietary proteins, fats, carbohydrates (starch, sugars, dietary fibers), and polyphenols (commonly found in fruits, seeds, vegetables), influence the composition and function of the gut microbiota [28]. Diets high in protein and animal fat are typically dominated by Bacteroides and those diets high in digestible carbohydrates are dominated by Prevotella [29]. High levels of protein in the diet have also been associated with increased microbial diversity. Digestible carbohydrates have different effects on the gut microbiome depending on the type of sugars. Non-digestible carbohydrates, or dietary fibers, are metabolized by the gut microbiota to help

promote the growth of certain "healthy" microbiota populations. Prebiotics are select dietary fibers that can increase gut microbiome gene richness and commensal organism abundance, and thereby have profound impacts on other aspects of metabolism and inflammation [20,30,31]. Polyphenols have been shown to enrich the gut microbiome with commensal bacteria such as Bifidobacterium and Lactobacillus.

1.1.2.2 Antibiotics

Antibiotics have a profound and lasting impact on the composition and functional profile of the gut microbiome. Antibiotics target key pathways/functions of bacteria to cause cell death or slow cell growth. Each class of antibiotic targets a different key pathway/function of the bacteria. Some of the most common pathways/functions targeted by antibiotics are inhibition of cell wall, protein, DNA, or RNA synthesis. The effects of antibiotic treatment are immediate, but can persist for months to years. Use of antibiotics during critical development windows in childhood can have lasting, detectable impacts into adulthood [32]. Administration of antibiotics that last months or years will generally lead to longer, sustained changes in the gut microbiome than a single dose. The immediate effect of the antibiotics will be a decrease in total bacterial load and diversity, but gradually the gut bacteria not killed by the antibiotics will be able to establish their dominance and achieve the previous bacterial load level. Higher initial doses of antibiotics can have a more profound effect on gut microbiome populations. Additionally, the effect of antibiotics on the gut microbiome depend on the genetics of the host, sex of the host, type of antibiotic dosing (pulsed, intermittent, or continuous), previous exposure to antibiotics, age when administered, and other factors currently being investigated. Antibiotics will not only alter the composition of the gut microbiota, but also change the metagenome and transcriptome

of the gut microbiome [32]. Antibiotics apply a selective pressure to the gut microbiome, and as a result the gut microbiome adapts. Bacteria that are able to resist the effects of the antibiotic are called antibiotic resistant. Antibiotic resistant bacteria have resistance genes that allow them to survive, and to then grow in an uncontrolled manner [33]. Antibiotic resistance genes can be transferred from one species to another. Increased antibiotic use in the United States has become a major concern as the number of antibiotic resistance infections grows.

1.1.2.3 Other Factors

The environment, host genetic background, host age, and probiotics taken by the host are other key factors that can shape the gut microbiome. Environment and geographical location has been shown to affect the gut microbiome [34]. The differences due to geography may be a result of both cultural differences in lifestyle and diet, exposure to microbes specific to certain regions, as well as exposure to environmental pollutants [34,35]. Host genetics can influence the composition of the gut microbiome if the genetic makeup influences any of the pathways or systems involved with the gut microbiome [36]. For example, mice that have immune deficiencies respond differently to the gut microbiome, and develop a distinct microbiome [7]. Aging leads to a great degree of change in the gut microbiome, though it is unclear what the causes for the associations between age and gut microbiome [37,38]. Aging often comes with increased inflammation and it has been hypothesized that the gut microbiome plays a role in this phenomenon. Probiotics are another factor that influences gut microbiota composition and function. Probiotics are live commensal bacterial that provide a beneficial effect on the immune system and metabolic function. The most common bacteria used as probiotics are strains of lactobacillus and Bifidobacterium [39]. Studies have reported promising benefits of probiotic administration, though the area remains controversial topic [40]. For example, the transplant of a

probiotic *Lactobacillus plantarum* strain was able to prevent a malnourished phenotype from developing in germ-free mice with a malnourished gut microbiome [41].

1.1.3 Organ Systems The Gut Microbiome Influences

1.1.3.1 Immune System Function and Development

The gut microbiome is involved in the initial development and continued function of the immune system. The immune system is introduced to the gut microbiome at birth. As the immune system develops it becomes educated as to what microbes are commensal, and what microbes are considered pathogenic. Early in development, the immune system has a blunted inflammatory response to the gut microbiota, as the body is attempting to identify microbiota that are symbiotic and microbiota that are pathogenic [42]. The current hypothesis is that the immune system has evolved alongside the gut microbiome to allow specific symbiotic bacteria to colonize, while still being able to identify and fight off pathogenic bacteria [43]. The gut microbiome eventually reaches a stable equilibrium with both the individual gut microbiota populations, as well as the host immune system. The gut microbiota is crucial for a healthy, well-developed immune system. Rodents raised in a germ-free environment have a severely underdeveloped immune system and are more susceptible to infections [44]. Improper education of the immune system to the gut microbiota has been linked to the development and severity of autoimmune diseases [45].

The gut microbiome is in constant communication with both the innate and adaptive immune system throughout life. The host helps to maintain a homeostasis with the gut microbiome by producing and maintaining a mucosal layer on the gut lining. The mucosal layer helps to minimize any direct contact between gut microbiota and intestinal epithelial cells [42,46].

Intestinal epithelial cells are the cells in closest contact with the gut microbiome on a regular basis. The epithelial cells that line the intestine will produce antimicrobial peptides to help limit direct contact between the gut microbiota and host cells. One of the main methods of communication between the gut microbiome and the host immune system is through the recognition of microbial associated molecular patterns (MAMPs). Pattern recognition receptors are used by host cells to detect the presence of the gut microbiome by detecting MAMPs. Toll-like receptors (TLRs) are one of the main families of pattern recognition receptors. TLRs detect various MAMPs including bacterial products, components on or composing the cell surface, and bacterial DNA or RNA. When TLRs are triggered an intracellular inflammatory cascade begins to help eliminate the microbial presence. Mice deficient in TLRs or TLR downstream signaling have an altered gut microbiota composition and function because the mice are not able to appropriately detect and control the gut microbiota populations [7,47-50].

The innate and adaptive immune system both play a key role in the regulation of a healthy gut microbiome [51]. The antigen presenting cells help to detect for the presence of pathogenic bacteria or bacteria in a location they should not be (i.e. breaching of the intestinal barrier). Antigen presenting cells in the gut and lamina propia use TLRs to detect bacteria and bacterial components. Antigen presenting cells, such as dendritic cells, act as a bridge to the adaptive immune system so they can present the bacterial components to B and T cells. One of the key roles B cells play is in regulation of the gut microbiome through production of antibodies such as IgA. IgA antibodies produced by B cells can help to target bacteria for elimination, change bacterial gene expression, and maintain the integrity of the intestinal barrier [44,51]. The various CD4+T cells secrete cytokines that help to control infections (Th17 cells), protect against intracellular microbiota (Th1 cells), and to even regulate/reduce the immune response when

appropriate (T-regulatory cells) [45]. For the CD4+ T cells to properly differentiate into the major subtypes, the presence of the gut microbiota is required.

1.1.3.2 Metabolism and Nutrition

The gut microbiome offers unique benefits to the host as the gut microbiome is involved in digestion, metabolism, and nutritional intake. The gut microbiome enhances the ability of the host to extract nutrients and energy from the diet that the host cannot extract directly. The gut microbiome collectively has 3.3 million non-redundant genes (~150 times larger than human genome). Many of the genes are devoted to processing foods (largely polysaccharides) and are not included in the host genome [52]. Essentially, the successful operation of many metabolic pathways in the host rely on the combined function of the host and the microbiome [53]. The main site for nutrient and vitamin transfer and absorption is in the intestines. Here, the nutrients, vitamins, and other important metabolites are able to cross the epithelial barrier [53].

The gut microbiome assists with are nutrient absorption and energy extraction. Experiments with germ-free mice have demonstrated the clear importance of the gut microbiome in nutrient and energy extraction from the diet: 1) germ-free mice are underweight with less fat [54].; 2) germ-free mice do not develop diet induced obesity [55,56]. Additionally, gut microbiota transplantation studies with germ-free mice have demonstrated how the gut microbiota alone can lead to malnutrition or obesity depending on the metabolic status of the gut microbiota donor [16,25]. Stool from lean mice has been shown to have more calories remaining compared to stool from obese mice fed the same diet [57].

The gut microbiome has other key functions that help to perform dietary choline metabolism, non-digested fiber fermentation, protein digestion, breakdown of dietary toxins and

carcinogens, absorption of electrolytes and minerals, fat digestion, and bile acid metabolism [57,58]. The processes performed by the gut microbiome lead to the production of neurotransmitters, branched amino acids, short chain fatty acids (acetate, propionate, butyrate), triglycerides, fatty acids, vitamins (K, B group vitamins: biotin, cobalamin, folate, riboflavin, thiamine), and other products as well [58,59]. Short-chain fatty acids have profound impacts on metabolism and immunity that include regulation of T-cells, improving the functioning of tight junction, anti-inflammatory properties, main food source for colonocytes, and even antimicrobial activity [60].

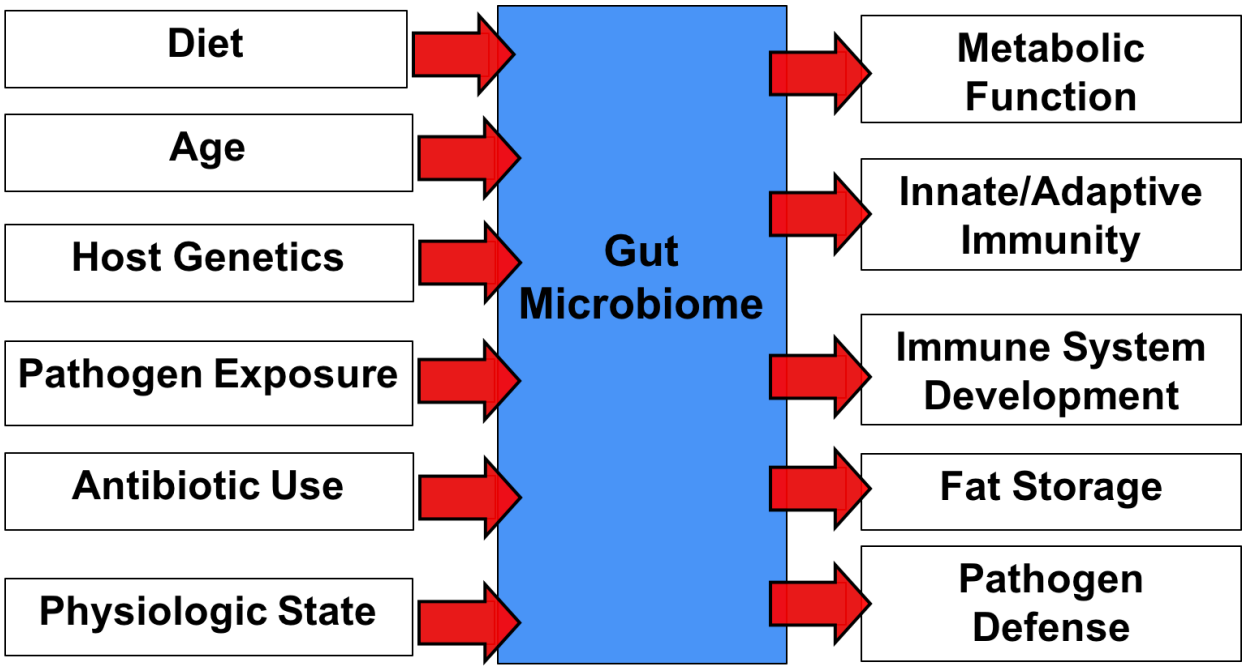

Figure 1.2. Factors affecting the composition and function of the gut microbiome, as well as host functions that are affected by the gut microbiome

1.1.4 Routes the Gut Microbiome Can Influence Bone and Joint

The gut microbiome is capable of influencing bone and joint through three routes: 1) regulation of nutritional absorption; 2) regulation of the mucosal and systemic immune system;

and 3) translocation of bacterial products. Nutritional deficiencies in key vitamins synthesized by the gut microbiome such as vitamin-K, as well as overall malnutrition have been shown to be associated with bone fracture risk in patients [61,62]. Nutrition also plays a role in osteoarthritis as a number of dietary factors are associated with the symptoms and progression of osteoarthritis [63].

The immune system is closely intertwined with bone and joint diseases, as inflammation has been increasingly identified as a contributor to bone and joint disease [64,65]. Interactions between the gut microbiome and the immune system can stimulate pro-inflammatory responses and are associated with systemic inflammatory diseases [66,67]. The gut microbiome has also been implicated in metabolic conditions where chronic low-level inflammation is present such as diabetes, obesity, and metabolic syndrome. Patients with diabetes, obesity, and metabolic syndrome have increased risk of developing osteoarthritis, osteoporosis, or both. Systemic inflammation and overall metabolic status are thought to be a contributors to increased risk in patients with diabetes, obesity, and metabolic syndrome [68-73]. Inflammatory cytokines and related mediators can directly regulate bone remodeling and can negatively impact cartilage health [74-80].

Bacterial products and components able to pass through the gut endothelial barrier and into the systemic circulation are a potential source of inflammation [81-86]. MAMPs including lipopolysaccharide and peptidoglycan are known to influence bone cell function and differentiation [87-91]. TLRs that detect the presence of MAMPs have been implicated in chondrocyte health and osteoarthritis pathology [92-95]. Additionally, the gut microbiome is able to synthesize short chain fatty acids that can have profound effects on inflammation, integrity of the gut barrier, and on health of the gut epithelial cells, thus potentially influencing nutritional

absorption, regulation of the immune system, and release of bacterial products to distant organs [96,97].

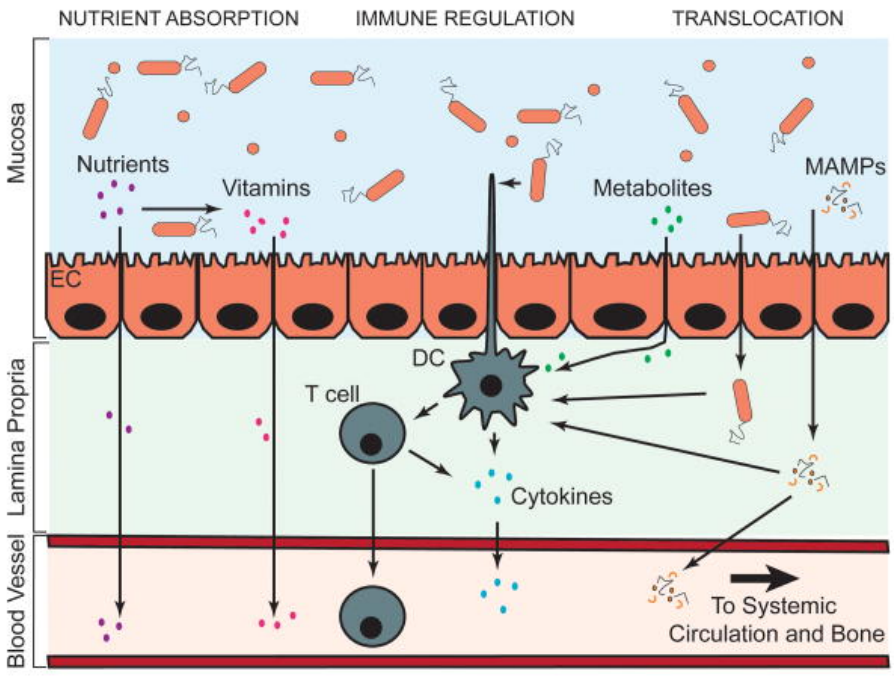

Figure 1.3. Routes the gut microbiome can influence bone and joint.
Figure is reproduced from the article "Links Between the Microbiome and Bone" and is included with permission from Wiley [98]

Chapter 1.2. Introduction to Bone

1.2.1. Osteoporosis and Related Fractures

Osteoporosis is the loss of bone mass and mechanical performance that leads to an increased risk of bone fracture [99] (Fig 1.4). Every year osteoporosis leads to approximately 9 million fractures worldwide [100]. The loss of bone mass begins in early adulthood and continues throughout life. Age is one of the most important risk factors for osteoporosis, as 90% of hip fractures occur in people over the age of 65 [101]. Additionally, other diseases and systemic factors can influence the onset and progression of osteoporosis. For example, women are at

higher risk of osteoporotic fracture (1 in 3 women worldwide experience a fracture) because estrogen depletion after menopause leads to reductions in bone mass. A need for further research to better understand systemic factors, diseases, and other pathways that influence osteoporosis development.

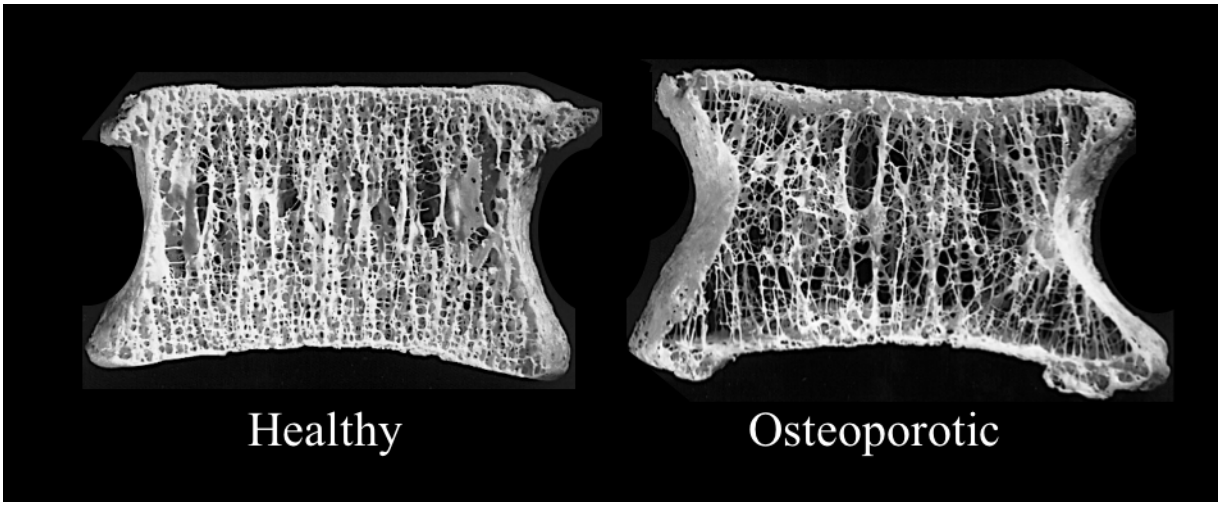

Figure 1.4. Representative image of a human vertebrae in healthy and osteoporotic conditions. Adapted from Mosekilde 1998 [(99)]

1.2.2 Bone Composition and Architecture

Bone is a complex, heterogeneous composite material with different architectures at multiple scales. Bone is composed of both organic and inorganic components. Bone is composed of 65% mineral component and 35% organic matrix [(102)]. The mineral component of bone is composed of hydroxyapatite and can have impurities such as hydrogen phosphate, sodium, magnesium, citrate, carbonate, and potassium [(103)]. The organic phase of bone is composed of primarily type I collagen (~90%), non-collagenous proteins (~5%) such as osteopontin, osteocalcin, osteonectin and matrix GLA protein, lipids (~2%), and water [(104)].

Bone is a hierarchical material with different structures across a range of length scales (Fig 1.5). At the macroscale, bone is divided into two main structures: cortical and cancellous bone. Cortical bone is the dense tissue found primarily in the shafts of long bones as well as the outer shells of bone. Trabecular bone is a porous, spongy structure found at the end of long bones and in the interior of short bones like vertebrae, and is more metabolically active [105]. Cortical bone microstructure can be separated into osteons, composed of cylindrical layers of mineralized collagen (lamellae) formed around a canal [103]. The osteons will typically align with the long axis of the bone. Cancellous bone is comprised of networks of struts called trabeculae. Each trabeculae is composed of lamellae that form parallel to the long axis of the trabeculae [106]. Within each lamellae the mineralized collagen fibers are aligned. Each lamellae has a different orientation than the adjacent lamellae. At the sub-nanostructure level, the three main components of the collagen fiber are collagens, non-collagenous proteins, and apatite crystals [103]. The apatite crystals are positioned between the ends of the aligned collagen molecules. Type I collagen is the primary organic component of bone and is aligned into the collagen fibers. Other, non-collagenous proteins, on the same scale can influence size and orientation of the mineral crystals.

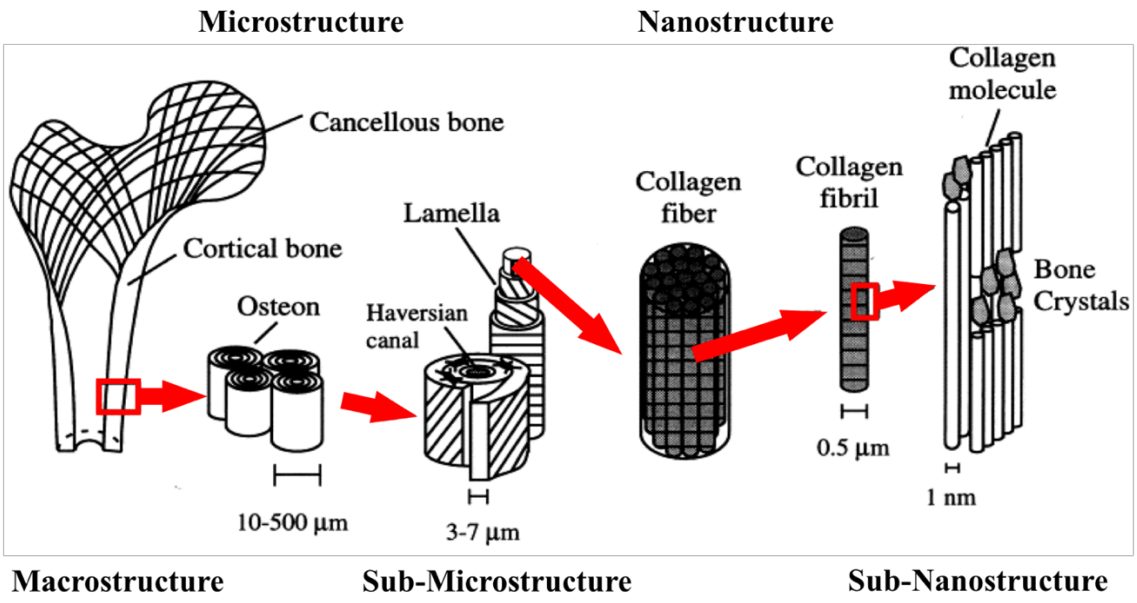

Figure 1.5. The hierarchical structure of bone shown across multiple length scales. Image Adapted from Rho et al 1998 [103]

1.2.3. Bone Characterization

1.2.3.1 Characterization of Bone Structure

The most common technique for imaging the structure of cortical and cancellous bone in animal models is x-ray microcomputed tomography (microCT) [107,108]. MicroCT is a non-invasive imaging modality with high spatial resolution that allows measurement of the 3D morphology of bone. A key factor in processing microCT images is determining the appropriate threshold to properly segment out what in the image is bone from what is not bone [108]. Another key consideration when using microCT in an experiment is the selection of a consistent and appropriate region of interest. A volume of interest, rather than a single 2D image, will often be sampled to get measures more representative of the entire bone or region. Anatomical landmarks and a percentage of total bone length are often used to maintain a consistent volume of interest across specimens.

When assessing cortical bone in mice, commonly the midshaft (diaphysis) of a long bone such as the femur or tibia is used. We are often interested in the midshaft because it is representative of the geometry of the bone during bending tests (*See Whole Bone Mechanical Properties- Three-Point Bend Test*. Characterization of the total area (Fig 1.6), the marrow area, the cortical bone area, average cortical thickness and the ratios amongst these area measurements allow for an understanding of total bone mass and relevant appositional growth patterns (See *Bone Growth and Remodeling*). The length of the whole bone used for analysis of the midshaft is another measure often taken to understand longitudinal growth patterns. Other geometric measurements include the distance from the bending axis of the bone to the periosteal surface (outer surface) and to the endosteal surface (inner surface). The parameters listed above are also often normalized by body mass and/or body length to isolate differences among study groups that are independent of animal body size. Cortical bone tissue mineral density can be approximated by measuring the x-ray attenuation coefficient, as the attenuation coefficient is related to the level of mineral content in the bone.

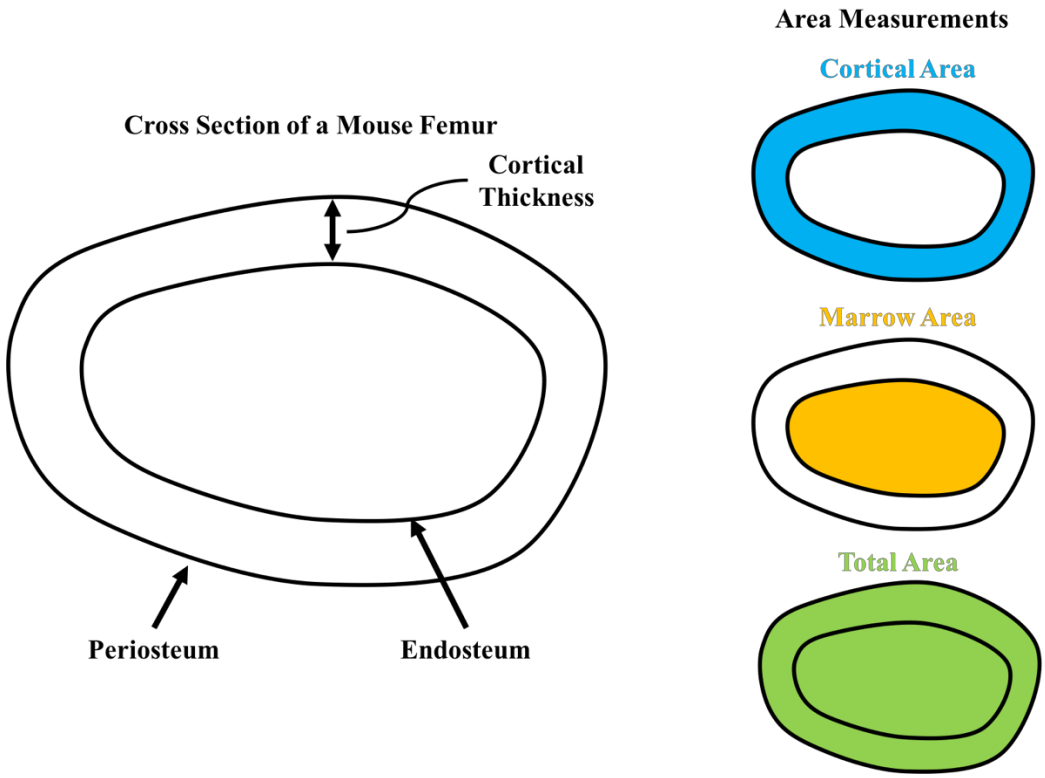

Figure 1.6. Measures made to quantify cortical bone at the midshaft

Trabecular bone is measured with micro-CT as well, but has different measurements to characterize the structure and the amount of bone present. A volume of interest is first selected for characterization. Regions of trabecular are segmented from the rest of the whole bone. The ratio of the volume filled with bone to the rest of the space in the volume represents the bone volume fraction. Bone volume fraction is a key measure for approximating the trabecular bone mass and assessing overall changes in bone mass. Other measures describing the trabecular bone include trabecular thickness, trabecular number (average number of trabeculae per unit length), trabecular separation (mean distance between trabeculae), and the degree of anisotropy (if structure is isotropic or anisotropic) [(108)] . Additionally, trabeculae are classified into either rod-like or plate-like based on the aspect ratio of the trabeculae, and new software is capable of determining the percentage of the structure that consists of rods and plates [(109,110)].

1.2.3.2 Characterization of Cortical Bone Mechanical Properties

The mechanical properties of cortical bone can be determined on both the whole bone and tissue level. Due to the complex hierarchical structure of bone, large changes in the tissue level mechanical properties can influence overall whole bone mechanical properties. Understanding the interplay between the two levels can be crucial for understanding how diseases or other conditions that alter bone can lead to fracture.

1.2.3.2.1 Whole Bone Mechanical Properties- Three-Point Bend Test

The two main contributors to whole bone mechanical performance are: 1) parameters relating to bone structure (including the amount and architecture/shape, see *Characterization of Bone Structure*), and the material composition of the bone. For example, if there are two cortical bone cross-sections that are identical in shape, but one bone is twice as mineralized, we would expect drastically different mechanical performance. Conversely, if the material characterization of the bone demonstrated identical material composition, but one bone had twice the cortical area and thickness, we would expect drastically different whole bone mechanical performance.

A common mechanical test to determine whole bone mechanical properties in mice is the three-point bending (Fig 1.7). In a three-point bend test, a long bone (usually a femur) is placed upon two supports. Next, an indenter located at the mid-diaphysis applies a load to the bone until the bone fractures. During the test, the load applied and the displacement of the femur are recorded (Fig 1.7). Key measurements include: maximum load (the highest load the bone can withstand before fracture, fracture load (the load experienced when fracture occurs), yield load (the load experienced when the bone begins to deform in a non-elastic manner), stiffness (how

much the bone will deform given an applied load), and post-yield displacement (the amount the bone can deform in a non-elastic manner before fracture occurs).

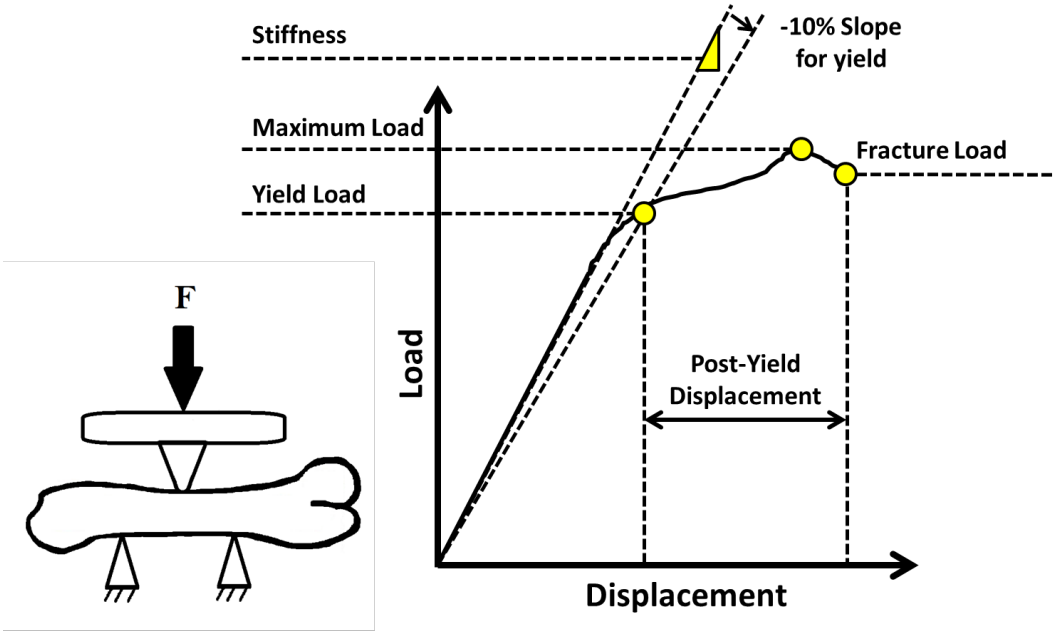

Figure 1.7. Setup and force vs displacement curve for three-point bending test of a mouse femur

A parameter that is measured using microCT and is relevant to the mechanical performance of bone is the moment of inertia. Moment of inertia is a calculated parameter that describes how well the geometry of the bone resists bending. For whole bone testing, moment of inertia is calculated on a region from the mid-diaphysis (same region for cortical bone characterization) as the mid-diaphysis is where fracture occurs. Moment of inertia is strongly correlated with maximum load and stiffness.

1.2.3.2.2 Tissue-Level Mechanical Properties- Nanoindentation

Tissue level properties can be approximated from three-point bending; however, such numerical values are not very reliable due to the heteregenous material composition of bone, and the nonprismatic and irregular geometry of mouse bones. The most common characterization

technique used for tissue-level mechanical properties is nanoindentation. Nanoindentation involves pressing a hard tip at a known force into the surface of the bone (Fig 1.8) [111]. The tip is usually made of diamond. The shape of the tip can vary, but the most commonly used tip is the Berkovich tip (three-sided pyramidal shape) [111,112]. A typical indentation test is broken up into three loading periods: 1) loading ramp where the applied force increases at a constant rate; 2) holding period at a constant load; 3) an unloading ramp (Fig 1.8) [111]. The three loading periods help to avoid the effects of the viscoelastic (load-rate dependent) properties of bone. During the indentation test the displacement (depth of the tip) and load are measured. The loading and unloading protocol can be repeated multiple times per area, as well as for multiple locations per specimen. The thickness of the indented bone specimen must be sufficiently larger than the depth of the indentation so that the stresses within the material are not influenced by nearby boundaries [111]. However, a general rule is to have a sample thickness that is ten times greater than the indentation depth, and a sample roughness that is 10 times less than the indentation depth [112]. Sample preparation for nanoindentation involves polishing of a sample with silicon carbide paper, followed by aluminum oxide slurries to create a surface roughness acceptable for indentation [112].

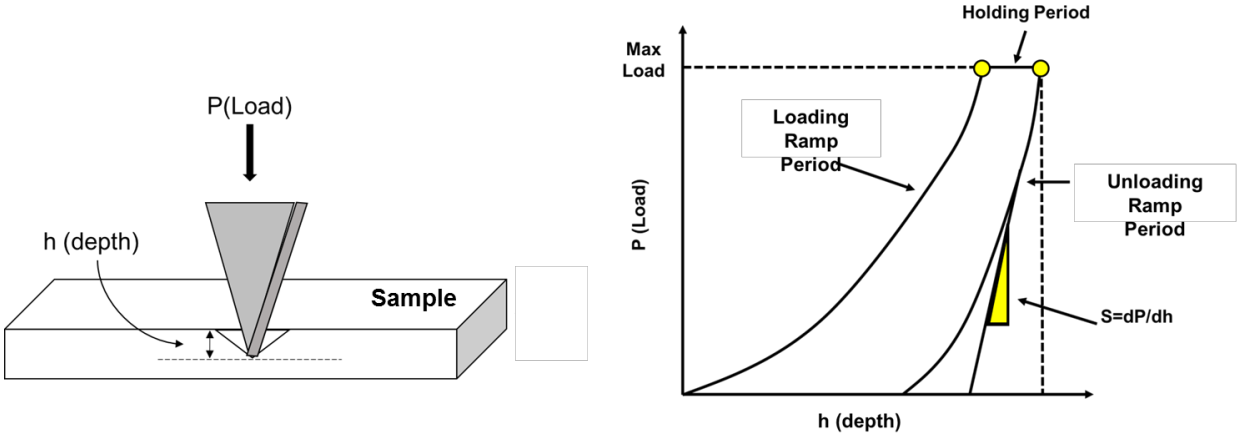

Figure 1.8. Schematic of nanoindentation and an example load vs depth curve.

The two main outcome measures from nano-indentation are reduced modulus and hardness [111]. Reduced modulus is calculated from the unloading curve at the maximum applied load, the contact area of the indenter, a pre-determined constant based on the shape of the tip, and constants relating to the mechanical properties of the tip (elastic modulus and Poisson's ratio) [111]. Hardness is calculated based on the applied force divided by the area of the imprint created by the applied force [111]. The reduced modulus and hardness of bone differ between cortical and trabecular bone, skeletal site, tissue age, and testing parameters [111].

1.2.3.3 Characterization of Material Composition- Raman Spectroscopy

One of the most common techniques for characterizing the material composition of bone is Raman spectroscopy. Raman spectroscopy is a vibrational spectroscopy technique that involves a laser light being focused on a sample [113]. The laser light induces vibrations in the specimen that result in the scattering of a small portion of the laser light at different wavelengths. The shifts in wavelength are measured and reported in terms of wavenumber units (cm^{-1}). The measured shifts can be directly related to chemical composition. Bone has a common spectrum with well-defined band assignments for bone mineral and matrix components (Figure 1.9) [114]. The peak at ~959 cm^{-1} is the phosphate ($\upsilon_1 PO_4^{3-}$) band and is a measure of the mineral content of the bone and is the strongest peak identified in bone [113,114]. The Amide I peak, with characteristic bands at ~1660 cm^{-1} and ~1690 cm^{-1} is the most commonly reported band with regard to collagen content [113,114]. Other peaks used to evaluate collagen content are the Amide III peak with characteristic bands at ~1242 cm^{-1} and ~1272 cm^{-1}, and the proline and hydroxyproline bands at ~853 cm^{-1} and ~876 cm^{-1}. Important considerations when choosing a peak to evaluate collagen and organic matrix components are: 1) Amide peaks can be

polarization dependent; 2) Amide peaks are not collagen specific [114]. The peak at ~1070 cm^{-1} is the most intense carbonate ($v_1 CO_3^{2-}$) band, and can be used to measure the extent of B-type carbonate substitution for phosphate ions in the bone.

The three measures most commonly derived from the characteristic Raman spectra of bone. The mineral:matrix ratio is the ratio of the mineral component of bone to the organic component, and is calculated as the ratio of the $v_1 PO_4^{3-}$peak to one of the peaks used to report collagen content (Amide I, Amide III, Proline+Hydroxyproline). Mineral:matrix is useful to detect changes in mineral content that can occur due to vitamin deficiency, disease, and/or genetic background. Mineral:matrix has been correlated with stiffness and strength on the whole bone level, and with modulus and hardness on the tissue level [114]. The carbonate:phosphate ratio describes the degree to which carbonate ions have been substituted for phosphate ions in the mineral apatite, and is calculated as the ratio of the $v_1 PO_4^{3-}$peak to the $v_1 CO_3^{2-}$ peak. Carbonate to phosphate can vary with bone architecture, age, and mineral crystallinity [113]. The carbonate to phosphate ratio has been associated with tissue and whole bone mechanical performance [114]. Crystallinity is related to the size, shape, and perfection of the bone mineral crystals, and is calculated as the inverse of the full-width-half-max of the $v_1 PO_4^{3-}$peak [115]. Crystallinity has been correlated with stiffness, bending modulus, and yield stress on the whole-bone level [116,117], and strength, stiffness, modulus, and yield stress on the tissue-level [115]. Mineral:Matrix, carbonate:phosphate, and crystallinity increase with tissue age [113]. Recently, the ratio between the 1660 cm^{-1} and 1690 cm^{-1} bands in the Amide I peak has been shown to be indicative of the maturity of the collagen cross-links [118]. Raman spectra are expressed as ratios between peaks to avoid variation associated with spectra acquisition settings. Tissue heterogeneity is a measure used to characterize the variability of a parameter (mineral:matrix, carbonate:phosphate,

crystallinity, etc) over a specified area. Tissue heterogeneity is calculated by determining the full-width-half-max of the Gaussian distribution of all the measured spectra parameter values. Tissue heterogeneity is thought to play a role in the mechanical performance of bone, specifically influencing crack propagation and stress concentrations [119].

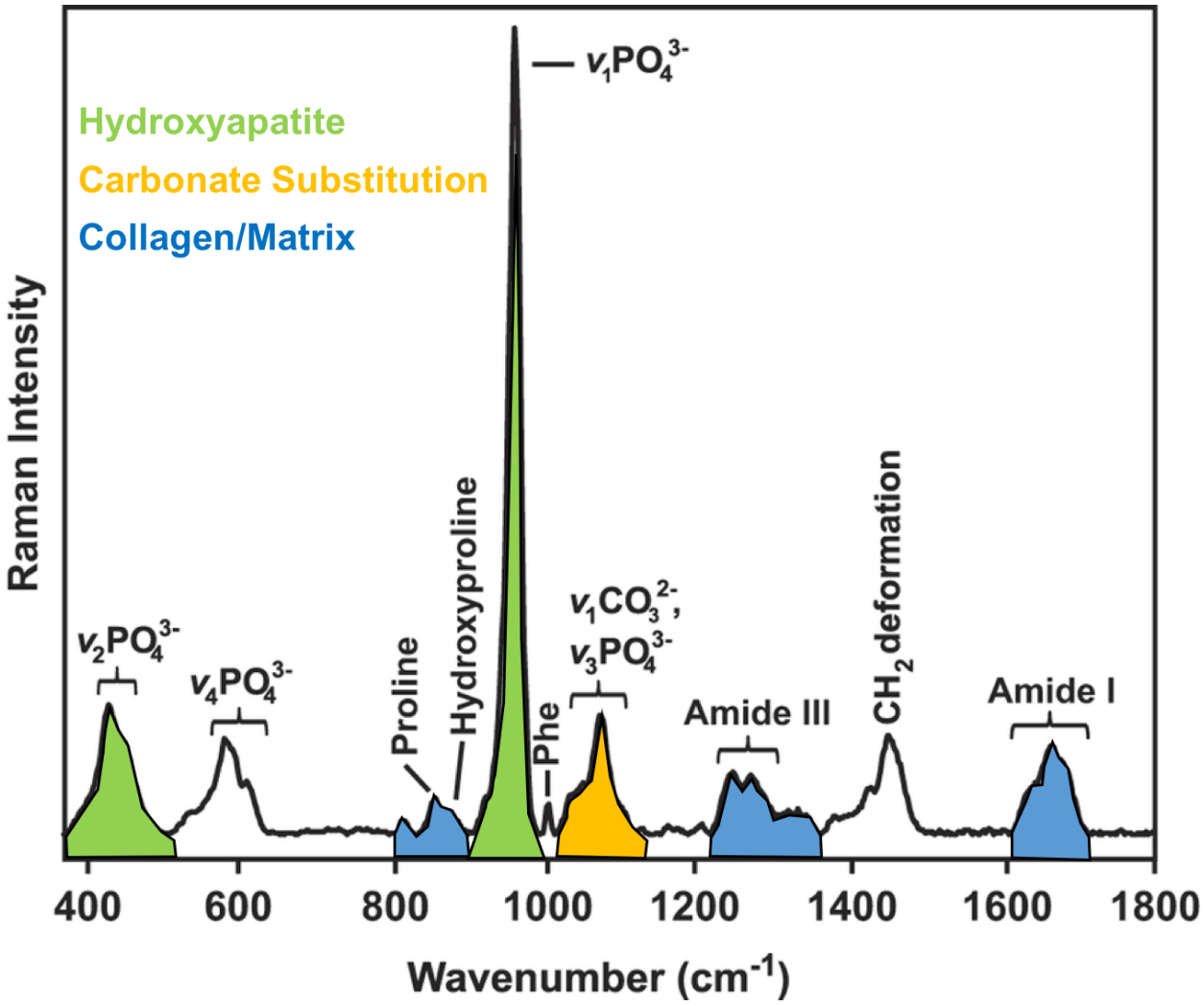

Figure 1.9. Example spectra of bone with important peaks highlighted.
Adapted from Mandair et al 2015 [114]

Multiple processing steps are required to obtain relevant measures from the acquired spectra. The following processing steps are required in the following order for a sample of bone embedded in PMMA: 1) normalization of sample spectra and PMMA spectra to the PMMA peak

at ~813 cm^{-1}. This step helps to eliminate any effects of inter-test variability of the Raman systems; 2) subtraction of the PMMA contribution from the measured sample spectra to eliminate any potential contributions of the PMMA to the measured spectra; 3) baselining of each peak to ensure only contributions from each specific peak are used for the calculation of Raman outcome parameters and to eliminate any effects of background flourescence.

1.2.3.4 Bone Growth, Modeling, and Remodeling

Three main types of bone cells are involved in the development and functioning of the skeleton (Figure 1.10). Osteoblasts are the cells that help to form new bone by first depositing osteoid (mixture of collagen and other proteins). Osteoblasts then deposit calcium and other minerals into the osteoid to make bone. Osteoclasts are the cells that resorb bone. Osteoblasts and osteoclasts are found on the surfaces of bones. Osteocytes are former osteoblasts that have become embedded inside the bone tissue. Osteocytes help to maintain mineral balance, communicate with osteoblasts and osteoclasts to trigger resorption and formation, and play a key role in sensing mechanical stimuli in bone.

The two types of bone growth are appositional and endochondral. Appositional bone growth occurs when bone tissue is added to the outer circumference (periosteum) by osteoblasts to increase the size and modify the shape of the bone. Endochondral bone growth occurs at regions called growth plates to extend the length of bones. Bone cannot directly be added to the end of bones, as the end regions are in direct contact with each other and are moving at the joints. Instead, bone is added at the growth plate in the epiphysis. Chondrocytes at the growth plate will first produce cartilage, and then over time the osteoblasts will deposit bone matrix and mineral to eventually form hard mineralized bone.

Bone modeling occurs to adapt the bone structure to mechanical loading, increase bone size, and to maintain overall mechanical performance of the bone [120]. Bone modeling primarily occurs during growth but continues throughout life [121]. During bone modeling, the processes of bone formation or bone resorption are not coupled. The action of osteoblasts to deposit new bone and osteoclasts to resorb bone are independent of one another. An example of bone modeling is bone formation on the periosteal surface to increase bone size and shape.

In contrast, in bone remodeling, the action of the osteoblasts and osteoclasts are coordinated [120]. As bone becomes old or damaged, repair of the old and damaged bone in necessary to maintain the integrity of the skeleton. This process is called bone remodeling. Osteoclasts first initiate the process by resorbing the old or damaged bone. Osteoblasts then move into the area to fill the resorbed area with new bone. Osteocytes are thought to direct the initiation of bone remodeling. Bone remodeling at a healthy rate is beneficial for the skeleton and helps to maintain its mechanical performance. However, in pathological conditions, an imbalance between osteoclastic resorption and osteoblastic formation leads to a deteriorated skeleton and increased fracture risk.

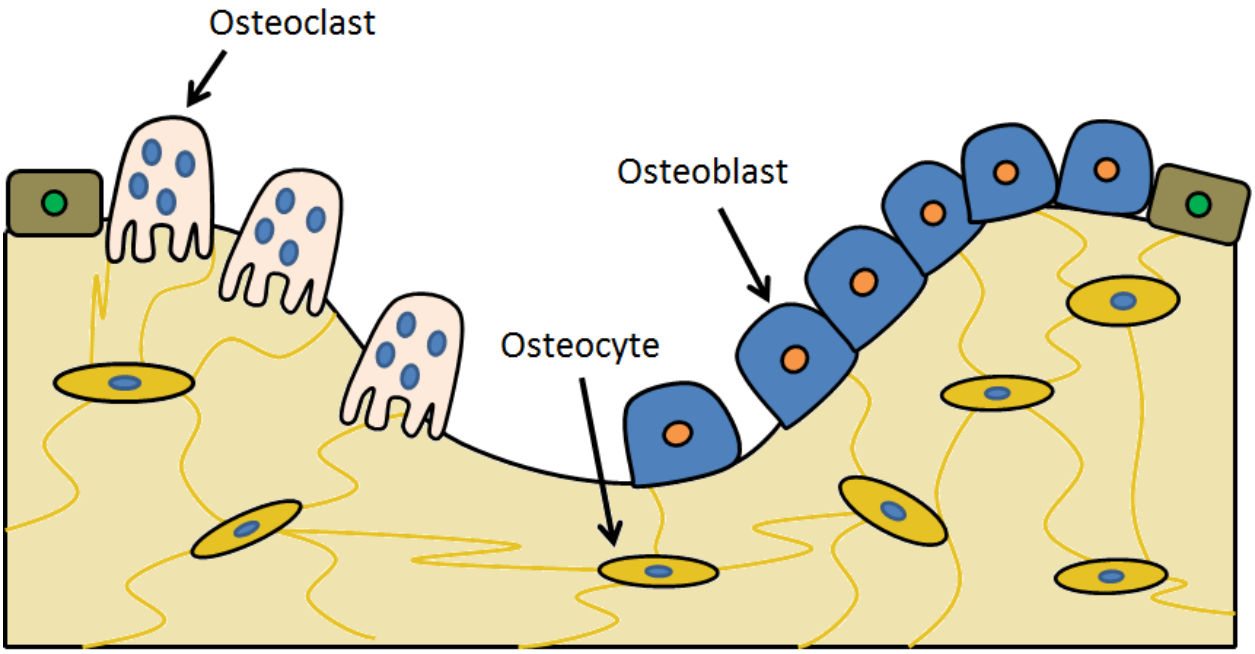

Figure 1.10. The three key cells involved in bone growth, modeling, and remodeling.

Chapter 1.3. Introduction to Cartilage and Osteoarthritis

Chapter 1.3.1 The Burden of Osteoarthritis

Osteoarthritis is the most common cause of joint disability for adults in the world. Osteoarthritis is a joint disorder that involves mechanical wear and tear of the joint leading to degeneration of both bone and cartilage. Common symptoms of osteoarthritis include pain, swelling, and loss of joint function/range of motion. The total number of people with osteoarthritis is expected to increase drastically in the coming years as life expectancy increases. Currently, there are no preventive treatments for osteoarthritis and there are only limited treatments that work to slow the progression of osteoarthritis or reduce symptoms such as pain. Knees are the most common joint to experience osteoarthritis due to the large load-bearing responsibility during activities of daily living. The most common outcome for severe knee osteoarthritis is complete joint replacement, where the diseased joint is surgically removed and

an implant inserted. Joint replacements have lengthy recovery times, risk of infection, and are costly. There is an urgent need to better understand both the pathogenesis of osteoarthritis so that improved therapies can be created and the burden of osteoarthritis reduced.

Chapter 1.3.2 Changes to an Osteoarthritic Joint

A joint is the location where two bones intersect and motion can occur. The two main components of a joint are the articular cartilage (on the surface of the bone to allow for articulation of the joint, and the subchondral bone (bone directly underneath the cartilage) (Fig 1.11). Cartilage is responsible for lubrication between two bones and to allow for smooth movement. The subchondral bone helps to provide overall structural stability for the joint. The knee joint also includes the synovial membrane that contains synovial fluid that acts a source of nutrients and lubrication, the meniscus to provide additional lubrication and load-bearing ability, and ligaments to stabilize the joint and prevent excessive movement in certain planes of motion. In an osteoarthritic joint, severe pathophysiologic changes are observed that include cartilage loss, changes to subchondral bone morphology, osteophyte formation, and inflammation (Fig 1.11). Clinically, osteoarthritis is detected using radiographic evidence, as well as swelling and reports of pain and limited mobility.

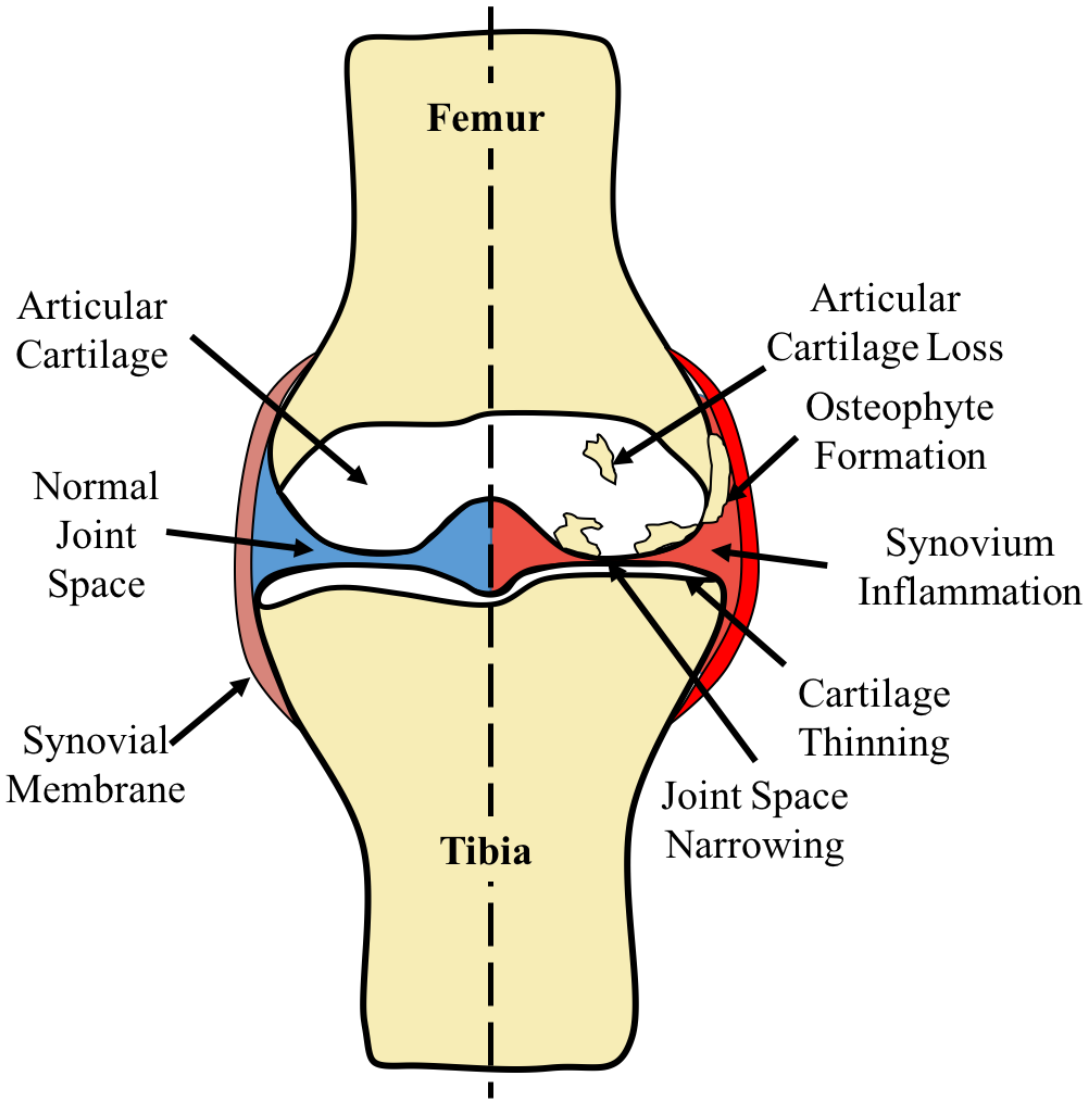

Figure 1.11. Changes in a healthy joint and an osteoarthritic joint.

Chapter 1.3.2.1 Articular Cartilage in Healthy and Osteoarthritis Conditions

Cartilage is composed of chondrocytes as well as the surrounding extracellular matrix. The extracellular matrix is composed of water, collagen, proteoglycans, and non-collagenous proteins. Cartilage is avascular in nature, and as a result, has a very limited ability to repair itself. Articular cartilage can be divided into three zonal layers each with specific morphological characteristics (Fig 1.12): superficial, middle, and deep zones. The structure of the superficial

zone is tightly packed collagen fibers that are aligned with the articular surface. Chondrocytes in this zone are flatter in shape [122]. As the superficial layer becomes damaged, the deeper zones become more susceptible to damage. The middle zone consists of thicker collagen fibrils arranged in an oblique orientation. Chondrocytes in the middle zone are more spherical in shape [122]. The deep zone has the thickest collagen fibrils aligned perpendicular to the articular surface. Chondrocytes in the deep zone are aligned in a column-like orientation [122]. The tidemark separates the deep zone from the calcified cartilage zone. The calcified cartilage zone secures the collagen fibrils to the subchondral bone beneath to ensure the cartilage remains in place.

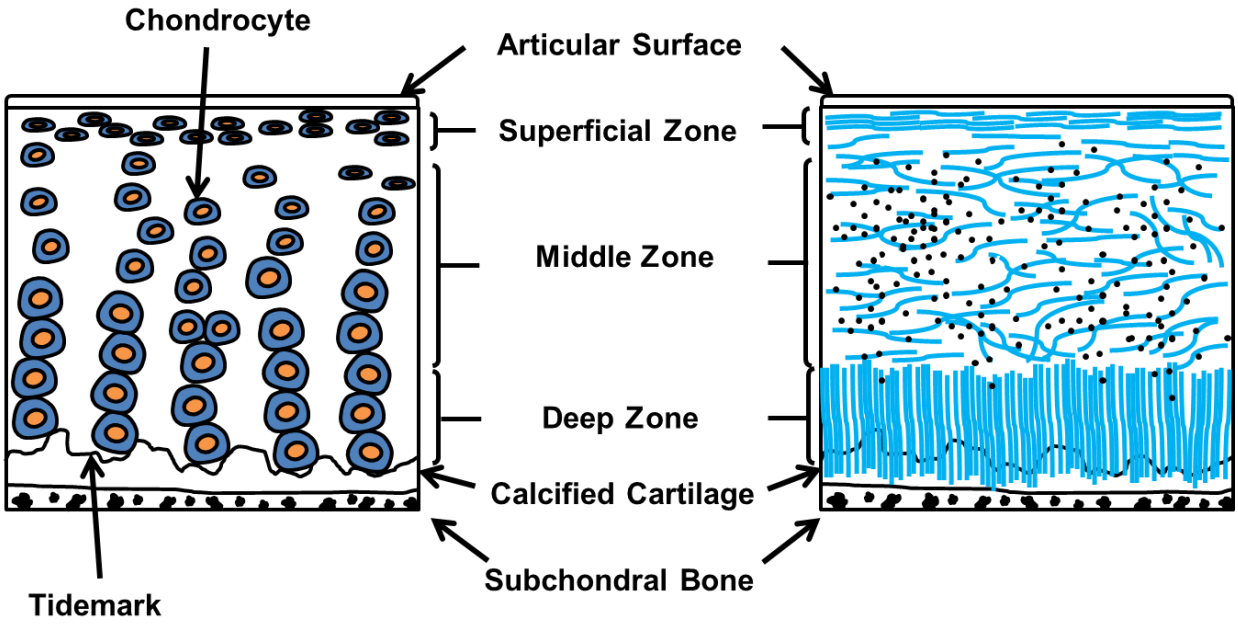

Figure 1.12. The three different zones of cartilage and the related structures. Adapted from Fox et al 2009 [122]

Under osteoarthritic conditions, erosion of the cartilage surface is common. During the early stages of osteoarthritis development chondrocytes that were previously inactive will become active and begin cloning themselves to form clusters. The superficial zone is the first region to experience any erosion. Typically, small fibrillations in the cartilage surface occur first (Fig

1.13) [122]. Increased cartilage calcification with also occur in the earlier stages of osteoarthritis development. Cartilage calcification can be detected by the progression of the tidemark towards the articular surface. During early osteoarthritis there is an up-regulation of proteinases that degrade cartilage. Matrix metalloproteinases (MMP's) degrade the surrounding extracellular matrix and are thought to be a potential therapeutic target for osteoarthritis [122]. Reductions in the health and integrity of cartilage can be detected by observing the overall loss of proteoglycans in the cartilage observed in histology slides. The more substantial the loss of stain and the deeper into the cartilage the loss of proteoglycans, the more severe the cartilage health. Once the cartilage matrix has been degraded it is not possible for the cartilage matrix to be repaired to its original state. In the most severe osteoarthritis conditions, the entire articular cartilage has worn away, and in the joint there is bone on bone contact, resulting in severe pain, swelling, and further degeneration of the joint.

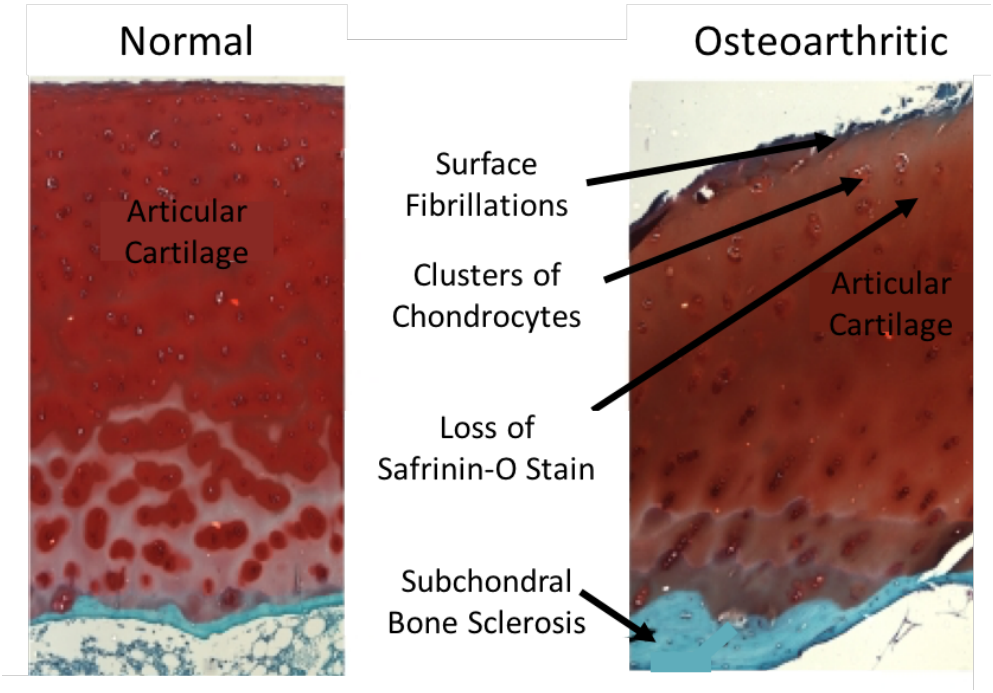

Figure 1.13. Signs of osteoarthritis in articular cartilage.
Adapted from Goldring 2012 [123]

Chapter 1.3.2.2 Subchondral Bone in Healthy and Osteoarthritis Conditions

The subchondral bone provides stability to the joint as it is the tissue that can withstand the highest loads in the joint. The subchondral bone can be divided into the subchondral cortical bone plate, and the distal epiphyseal cancellous bone region (Fig 1.14.) As osteoarthritis progresses, we see changes that occur to both the cortical and cancellous subchondral bone (Fig 1.14) [124]. During early stages of osteoarthritis, both the subchondral cortical bone and the cancellous bone plate experience thinning due to an increased bone remodeling rate [125]. As the subchondral bone plate thins, there is an expansion of the calcified cartilage region, leaving multiple tidemarks. In later stages of osteoarthritis, the rate of bone resorption slows and the bone formation rate remains unchanged, leading to subchondral bone plate thickening. Clinically, subchondral bone thickening is a radiographic hallmark of osteoarthritis.

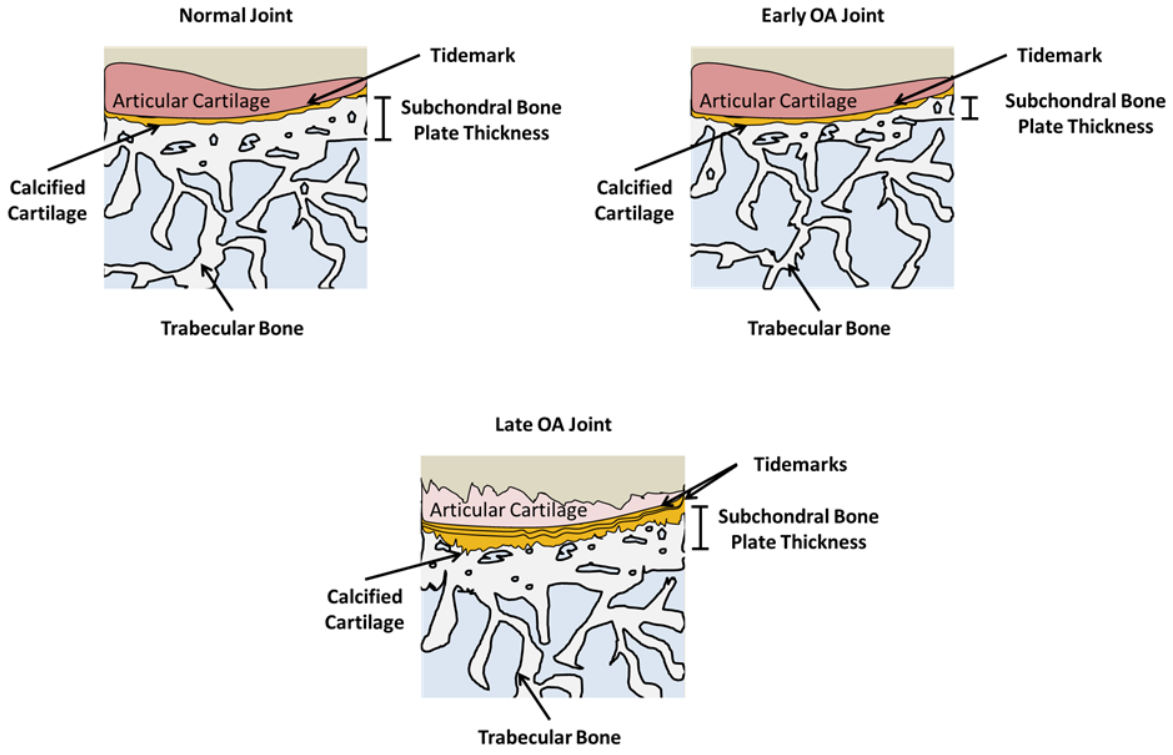

Figure 1.14. Changes to subchondral bone in early and late stages of osteoarthritis.

Chapter 1.3.2.3 Osteophyte Formation

Osteophytes are another hallmark of osteoarthritis. An osteophyte is a bony outgrowth that develops from the periosteum at the junction between cartilage and bone in the joint (Fig 1.15) [126]. Osteophytes are thought to develop during OA to help stabilize the joint and to redistribute mechanical loads appropriately. Osteophytes can form in early stages of osteoarthritis and are not always detectable clinically. Osteophytes first begin to form when cells in the synovial lining begin to proliferate. Cells begin to deposit additional matrix, and then in later stages endochondral ossification occurs. The final osteophyte is integrated with the subchondral bone.

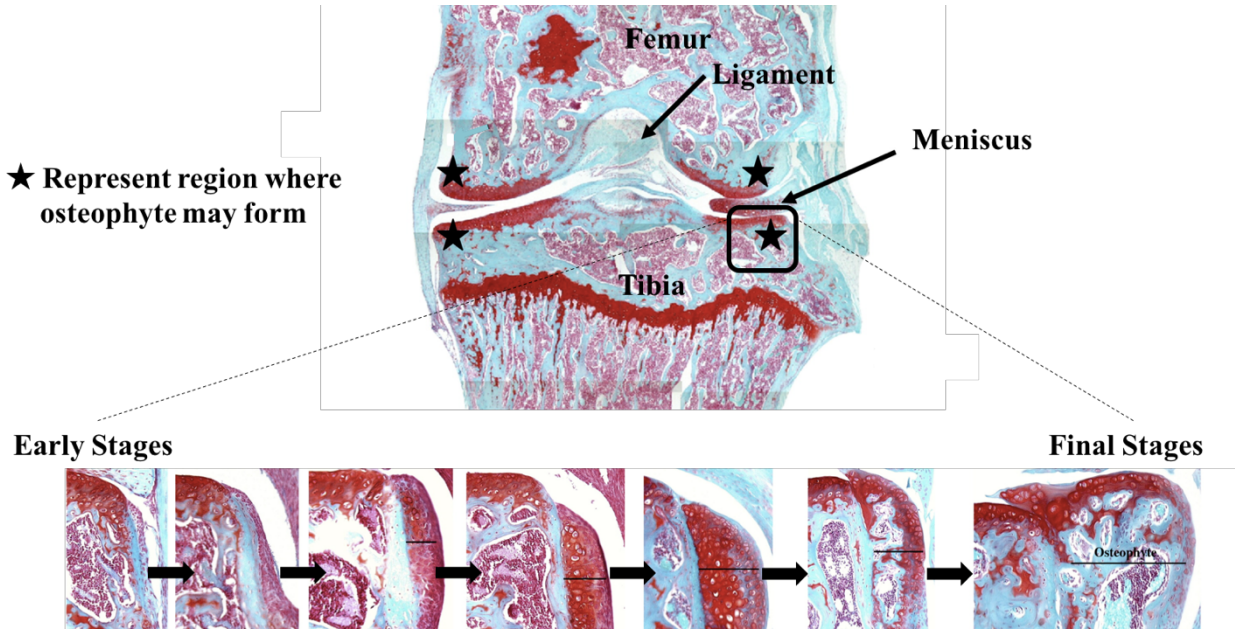

Figure 1.15. Changes to subchondral bone in early and late stages of osteoarthritis. Adapted from van der Kraan 2007 [126]

Chapter 1.3.3 In-Vivo Rodent Models of Osteoarthritis

To better understand osteoarthritis, several models have been developed that create osteoarthritis-like pathology in rodents. The models fall into four different categories [127]: 1) Mechanical- a noninvasive mechanical load is applied to the joint of the animal to induce the

development of osteoarthritis like changes in the joint; 2) Surgical: a destabilization of the joint is created by surgically removing ligaments. The altered joint mechanics leads to cartilage damage and advanced signs of osteoarthritis; 3) Spontaneous and genetic: Mice develop osteoarthritis pathology due to age. Different strains of mice, as well as specific knock-out, knock-in, and transgenic mice are more susceptible to the development of osteoarthritis with age; 4) Chemical: chemicals are injected into the joint to induce inflammation, and to degrade chondrocyte health and extracellular matrix components leading to osteoarthritis development.

The two main types of mechanical load-induced models are cyclic compression and a traumatic injury [(128)]. In the traumatic injury models, a single large force is applied to the joint that results in an acute traumatic injury such as a fracture [(129)] or a rupture of a ligament [(130)]. The in-vivo cyclic tibial compression models apply a load through the ankle and knee joint. After a sustained period of loading (1-6 week depending on the model) both cartilage damage and changes to the subchondral bone occur. The thesis will focus on the cyclic compressive in-vivo loading model developed by the van der Meulen lab [(131)]. In the van der Meulen model, cyclic compression leads to changes in articular cartilage that include decreased cartilage thickness, loss of proteoglycans, surface fibrillations, vertical clefts past the superficial zone, and erosion of the cartilage surface. Cyclic compression leads to changes in bone that include subchondral bone plate thickening, subchondral trabecular bone loss in the epiphysis, and osteophyte formation. Longer durations of loading (1, 2, or 6 weeks), as well as the higher load magnitudes (4.5N or 9N), lead to an increased amount of cartilage damage and subchondral bone changes.

Chapter 1.4 Thesis Aims

Osteoporosis and osteoarthritis affect millions of people worldwide every year. Osteoporosis related fractures totaled 8.9 million worldwide annually [(132)] and osteoarthritis

affects over 30 million people in the US alone. Recently, the gut microbiome has been identified as a factor that can influence chronic conditions associated with bone and joint disease such as obesity, diabetes, metabolic syndrome, inflammatory bowel diseases, and malnutrition. Therefore, the aims of this dissertation are: 1) Determine the effects of altering the gut microbiome on bone phenotype and bone mechanical performance; 2) Determine the effects of altering the gut microbiome on the chemical composition of cortical bone; 3) Determine the effects of the gut microbiome on the development and severity of in-vivo non-invasive load induced osteoarthritis.

Chapter 1.4.1 Aim 1- Determine the effects of altering the gut microbiome on bone phenotype and bone mechanical performance.

The gut microbiome is associated with chronic conditions that are associated with increased fracture risk. Recent evidence suggests that the gut microbiome can influence bone mass, however no studies have determined if the mechanical performance of the bone is influenced by the gut microbiome. Additionally, previous studies have not evaluated mice at skeletal maturity. In this aim, alterations to the gut microbiome are caused by genotypic alteration and chronic treatment with antibiotics. Cortical and trabecular bone morphology is analyzed by micro-computed tomography (microCT). Three-point bending is performed on the femur to investigate the mechanical performance of cortical bone in mice with an altered gut microbiome. The composition of the gut microbiome is characterized using 16S rRNA sequencing. The results of this aim were presented at American Society for Bone and Mineral Research annual meeting and published in the Journal of Bone and Mineral Research [(133)].

Chapter 1.4.2 Aim 2- Determine the effects of altering the gut microbiome on the chemical composition of cortical bone

In Aim 1 we found that modifications to the gut microbiome led to alterations in the the mechanical performance, suggesting impaired bone tissue material properties. Raman spectroscopy is used to determine the chemical composition of cortical bone sections from the tibial metaphysis. To further understand how the gut microbiome can influence bone tissue material properties we perform shotgun metagenomics to evaluate the functional capacity of the microbiome. The results from shotgun metagenomics are used to explore the three potential routes the gut microbiome can influence bone: regulation of nutritional absorption, translocation of bacterial products, and regulation of the immune system [(98)]. The results of this aim were presented at the 2018 World Congress of Biomechanics Conference, the 2018 American Society for Bone and Mineral Research meeting and are prepared for submission to the Journal of Bone and Mineral Research.

Chapter 1.4.3 Aim 3- Determine the effects of the gut microbiome on the development and severity of in vivo non-invasive load induced osteoarthritis

Metabolic syndrome is characterized by obesity, hyperglycemia, and insulin resistance, and recently a close relationship to the gut microbiome has been established. Metabolic syndrome is also associated with increased risk of developing osteoarthritis (OA), but it is unclear if the association is attributable to increased mechanical loading on joints caused by obesity or other aspects of the metabolic syndrome. Here we examined the effects of metabolic syndrome, obesity, and the gut microbiome on osteoarthritis by using an in vivo non-invasive loading model to induce osteoarthritis in mice. We use a mouse model of metabolic syndrome dependent on the gut microbiome for the phenotype to develop, as well as a mouse model of severe obesity/diabetes induced by feeding of a high fat diet. 16S rRNA gene sequencing was performed to evaluate the compositional differences in the gut microbiome. The results of this

aim have been presented at the Orthopedic Research Society Upstate NY and Northeast Regional Meeting, the Orthopedic Research Society annual meeting, the Cartilage Repair Symposium, and has been accepted for publication in Osteoarthritis and Cartilage.

Chapter 2- Alterations to the Gut Microbiome and Bone Phenotype

This chapter was published in the Journal of Bone and Mineral Research in 2017 in Volume 32, Issue 6. The article is titled "Alterations to the Gut Microbiome Impair Bone Strength and Tissue Material Properties" and is reprinted here with permission of Wiley [133].

Chapter 2.1 Abstract

Alterations in the gut microbiome have been associated with changes in bone mass and microstructure, but the effects of the microbiome on bone biomechanical properties are not known. Here we examined bone strength under two conditions of altered microbiota: 1) an inbred mouse strain known to develop an altered gut microbiome due to deficits in the immune system (the toll-like receptor 5 deficient mouse, TLR5KO); and 2) disruption of the gut microbiota (ΔMicrobiota) through chronic treatment with selected antibiotics (ampicillin and neomycin). The bone phenotypes of TLR5KO and WT (C57Bl/6) mice were examined following disruption of the microbiota from 4 weeks to 16 weeks of age as well as without treatment (n = 7-16/group, 39 animals total). Femur bending strength was less in ΔMicrobiota mice than in untreated animals and the reduction in strength was not fully explained by differences in bone cross-sectional geometry, implicating impaired bone tissue material properties. Small differences in whole bone bending strength were observed between WT and TLR5KO mice after accounting for differences in bone morphology. No differences in trabecular bone volume fraction were associated with genotype or disruption of gut microbiota. Treatment altered the gut microbiota

by depleting organisms from the phyla Bacteroidetes and enriching for Proteobacteria, as determined from sequencing of fecal 16S rRNA genes. Differences in splenic immune cell populations were also observed; B and T cell populations were depleted in TLR5KO mice and in ΔMicrobiota mice ($p < 0.001$), suggesting an association between alterations in bone tissue material properties and immune cell populations. We conclude that alterations in the gut microbiota for extended periods during growth may lead to impaired whole bone mechanical properties in ways that are not explained by bone geometry.

Chapter 2.2 Introduction

The microbes that inhabit the gastrointestinal tract are known collectively as the gut microbiota. Alterations in the gut microbiota are associated with a number of conditions that cause bone loss or increase fracture risk including malnutrition [134,135], inflammatory bowel disease [136-138], obesity [71,139], and metabolic disease [140-142]. The gut microbiota, therefore, have the potential to influence bone and contribute to differences in fracture risk among patient populations.

The gut microbiome is initially obtained at birth [143] and subsequently shaped by factors such as environment [144] and diet [4,23]. Exposure to the gut microbiome is necessary for the proper education and development of the innate and adaptive immune systems [145]. Dendritic cells, macrophages, granulocytes, T and B cells, and intestinal epithelial cells directly interact with the gut microbiome [145]. Toll-like receptors are one set of receptors on immune cells that recognize the components of the gut microbiome and facilitate communication between the gut microbiome and the immune system [146]. Alterations in the gut microbiota or improper

communication between the immune system and gut microbiota can lead to chronic immune responses and disease [147].

The effects of the microbiome on bone structure and density have been studied in mice using two standard tools for manipulating the microbiome: germ-free animals and oral antibiotic treatments [10,12]. The changes in bone following these manipulations of the gut flora differ considerably among studies. Germ-free mice (raised in the absence of live microbes) have been reported to display reduced bone mass[41], as well as increased bone mass [148] as compared to mice raised in conventional environments. Alterations in the gut microbiota through treatment with oral antibiotics have been reported to affect bone density in mice, but the findings have been mixed, possibly due to differences in animal age, sex, antibiotic used, dosing schedule and mouse genotype [149-152].

Genetic models are another tool for studying the effects of the microbiome on animal physiology. The Toll-like receptor 5 deficient mouse (TLR5KO) is a congenic mouse strain that has been used to study the effects of the gut microbiome on animal physiology and disease. Toll-like receptor 5 (TLR5) is the innate immune receptor for flagellin and does not have an endogenous ligand [153]. Hence, phenotypic traits of the TLR5KO mouse are primarily due to alterations in host-microbe interactions [47]. Failure of the TLR5KO mouse to respond to flagellin is associated with changes in the gut microbiome that lead to increases in intestinal and systemic inflammation and a metabolic syndrome-like phenotype characterized by mild obesity, insulin resistance, increased blood pressure and increased blood glucose [7,47]. The metabolic syndrome-like phenotype of the TLR5KO mouse does not develop in mice raised in a germ-free environment and can be transferred to wild-type mice through transplantation of the gut microbiota, demonstrating that the phenotype depends on the gut flora [7].

While prior work has shown that the disruption or absence of the microbiome can influence bone, interpreting conflicting findings among studies is challenging because many prior studies use young animals of different ages (less than 12 weeks of age) or low resolution imaging techniques (mouse DXA). Comparing bone phenotypes in such young animals is not recommended because bone is changing rapidly during growth [154]. Additionally, none of the previous studies have examined the effect of alterations in the gut microbiota on bone mechanical performance. In the present study, we tested the hypothesis that alterations in the gut microbiota can have an effect on whole bone biomechanical performance. Specifically, we determined changes in bone structure and strength associated with alterations in the gut microbiota caused by 1) genotypic alterations (the TLR5KO mouse) and 2) chronic treatment with antibiotics that target the gut microbiota.

Chapter 2.3 Materials and Methods

Chapter 2.3.1 Study Design

Animal procedures were approved by Cornell University's Institutional Animal Care and Use Committee. Mice from the C57BL/6J inbred strain and the B6.129S1-Tlr5tm1Flv/J (TLR5KO) congenic strain were acquired from the Jackson Laboratory (Bar Harbor, ME) and each bred separately in conventional housing in our animal facility. C57BL/6J is the recommended control strain for TLR5KO [7,155]. Animals were housed in plastic cages filled with 1/4-inch corn cob bedding (The Andersons' Lab Bedding, Ohio), fed with standard laboratory chow (Teklad LM-485 Mouse/Rat Sterilizable Diet) and water ad libitum, and provided a cardboard refuge environmental enrichment hut (Ketchum Manufacturing; Brockville, Ontario). Male mice were divided into four groups: two groups treated to disrupt the gut microbiota

(C57BL/6J: n=7, TLR5KO: n=8) and two untreated groups (C57BL/6J: n=12, TLR5KO: n=16). Mice with disrupted microbiota are referred to as "ΔMicrobiota." Mice were housed in cages with other animals from the same genetic background/treatment group. Treated groups received broad-spectrum antibiotics (1.0 g/L ampicillin, 0.5 g/L neomycin) in their drinking water from weaning at 4 weeks of age until skeletal maturity (16 weeks of age) [7]. Chronic antibiotics used in this manner causes consistent disruptions to the gut microbiota over a prolonged time period [11]. Ampicillin and neomycin have poor bioavailability, thereby limiting extra-intestinal effects of treatment [7,156]. Additionally, neomycin and ampicillin have never been associated with impaired bone growth. Animals were euthanized at 16 weeks of age. Femora, tibiae, epididymal fat pads, and spleen were collected immediately after euthanasia. Fecal pellets were collected one day prior to euthanasia to allow analysis of the microbiota.

Chapter 2.3.2 Cortical Bone Mechanical Testing

The right femora were harvested, wrapped in PBS-soaked gauze, and stored at -20°C prior to analysis. Femur length was measured from the greater trochanter to the lateral condyle using digital calipers. Images of the femoral diaphyseal cross-section were obtained by micro-CT with a voxel size of 25 μm (GE eXplore CT 120; 80 kVp, 32 μA, 100 ms integration time). Images were processed using a Gaussian filter to remove noise and a global threshold for each group was used to segment mineralized tissue from surrounding non-mineralized tissue. Femoral cross-sectional geometry was determined using a volume of interest extending 2.5% of total bone length and centered midway between the greater trochanter and lateral condyle (BoneJ, bonej.org, version 1.3.3) [157]. Measurements included total area, cortical cross-sectional area, cortical thickness, marrow area, and moment of inertia about the medial-lateral axis.

Femora were thawed to room temperature and maintained hydrated during mechanical testing. Right femora were loaded to failure in three-point bending in the anterior-posterior direction at a rate of 0.1 mm/s using a span length of 6 mm between outer loading pins (858 Mini Bionix; MTS, Eden Prairie, MN, USA). Force and displacement were measured using a 10 lb. load cell (Transducer Techniques, SSM-100, Temecula, CA) and a linear variable differential transducer at a 100 Hz sampling rate. Bending stiffness was calculated as the slope of the linear portion of the force-displacement curve [154]. Peak bending moment was calculated as half the peak load multiplied by half the span length [154]. The peak bending moment is related to bone tissue material properties and bone midshaft geometry by the following equation [158]:

$$M = \sigma_b \cdot \frac{I}{c}$$

where M is peak bending moment, σ_b is bone tissue material strength, I is the moment of inertia, and c is the distance from the neutral axis to bone surface. The term $\frac{I}{c}$ incorporates all geometrical properties that can influence peak bending moment. Differences in peak bending moment that are not explained by $\frac{I}{c}$ are caused by alterations in tissue material properties. Due to irregularities in force versus displacement data associated with motion some specimens were excluded from the biomechanical analysis (4 WT, 1 WT ΔMicrobiota, 3 TLR5KO).

Chapter 2.3.3 Trabecular Bone Morphology

Images of the tibiae were collected using micro-computed tomography with 6 μm voxels (μCT35; Scanco Medical AG, Switzerland; 55 kVp, 145 μA, 600 ms integration time). The trabecular bone microarchitecture of the proximal tibial metaphysis was examined in a region extending from the growth plate to 10% of total bone length. Measurements included bone

volume fraction (BV/TV), trabecular thickness (Tb.Th), trabecular separation (Tb.Sp), and cortical tissue mineral density (ct. TMD). A global threshold for each group was used to segment mineralized tissue from surrounding non-mineralized tissue. A randomized subset (n=8) was selected for analysis of trabecular bone morphology for the TLR5KO mice.

Chapter 2.3.4 Gut Microbiome Analysis

Chapter 2.3.4.1 DNA Extraction

Gut microbiota analysis was performed on six samples per group. Isolation of DNA from feces was performed by using PowerSoil DNA Isolation Kit (MO BIO Laboratory Inc., Carlsbad, CA) according to manufacturers' instructions. DNA concentration and purity were then evaluated using a NanoDrop ND-1000 spectrophotometer (NanoDrop Technologies, Rockland, DE) at wavelengths of 230, 260, and 280 nm.

Chapter 2.3.4.2 Quantitative PCR

The total bacterial load of fecal samples was determined using quantitative PCR (qPCR) as previously described [159]. The total bacterial load was defined as the total number of 16S rRNA gene copies. Briefly, quantification of the 16S rRNA target DNA was achieved by using the forward: 5'-TGG AGC ATG TGG TTT AAT TCG A-3', and reverse: 5'-TGC GGG ACT TAA CCC AAC A-3') [160,161] Unibac primers, and 10-fold serial dilutions ranging from 10^0 to 10^7 plasmid copies of a plasmid DNA standard which was cloned in-house[159]. Plasmid standards and feces samples were run in duplicates. The average of the cycle threshold value was used for calculation of the total bacterial load.

Chapter 2.3.4.3 Next-Generation Sequencing and Bioinformatics

Amplification of the 16S rRNA gene, library construction and bioinformatics were executed according to previously described methods [159]. Briefly, for amplification of the V4 hypervariable region of the bacterial/archaeal 16S rRNA gene, primers 515F and 806R were used [162]. The 5'-barcoded amplicons were generated in triplicate using 12-300 ng of template DNA, 2 X EconoTaq® Plus Green Master Mix (Lucigen®, Middleton, WI) and 10 μM of each primer. Replicate amplicons were pooled and purified using the Gel PCR DNA Fragment Extraction kit (IBI Scientific, Peosta, IA) and visualized by electrophoresis through 1.2% (weight/volume) agarose gel stained with 0.5 mg/ml ethidium bromide. Blank controls in which no DNA was added to the reaction were performed. Purified amplicon DNA was quantified using fluorometry (Quant-iT™ PicoGreen® from Life Technologies Corporation, Carlsbad, CA, USA).

Standardization of feces amplicon sample aliquots was performed to the same concentration and then pooled into one run according to individual barcode primers for the 16S rRNA gene. Final equimolar libraries were sequenced using the MiSeq reagent kit v2 (300 cycles) on the MiSeq platform (Illumina, Inc., San Diego, CA, USA).

Raw 16S rRNA gene sequences generated were demultiplexed using the open source software pipeline Quantitative Insights Into Microbial Ecology (QIIME, version 1.7.0-dev) [163]. Sequences were filtered for quality using established guidelines [164]. Taxonomy was assigned using UCLUST (www.drive5.com) consensus taxonomy assigner, against the Greengenes reference database[165]. Low-abundance clusters were filtered, and chimeric sequences were removed using USEARCH [166]. Additionally, we generated a species-level OTU table using the MiSeq Reporter Metagenomics Workflow. The MiSeq Reporter classification is based on the

Greengenes database (http://greengenes.lbl.gov/), and the output of this workflow is a classification of reads at multiple taxonomic levels: kingdom, phylum, class, order, family, genus and species.

Shannon diversity index was performed (QIIME, version 1.7.0-dev). Before estimating the Shannon diversity index, all sample libraries were rarefied to an equal depth of 10,000 sequences (QIIME, version 1.7.0-dev).

Chapter 2.3.5 Colon Histology

To evaluate gut inflammation, colons were collected at euthanasia and fixed in 10% neutral buffered formalin for 48 hours. Colons were embedded in paraffin, sectioned, and scored by the Cornell Animal Health Diagnostic Center. Each sample was scored based on 4 assays: lymphoid aggregate size, lymphoid aggregate density, apoptotic cells per high powered field, and presence of inflammation.

Chapter 2.3.6 Flow Cytometry

Splenocytes were harvested from the spleen of three mice from each group immediately after euthanasia as described previously [167,168]. The splenocytes were subsequently stained by incubation in 50 μL of FACS containing antibodies (1:500 dilution) for an hour. For analyzing B cells, *Anti-CD20* antibody conjugated to *Phycoerythrin (PE)* (BD Pharmagen) was used and for T cells *Anti-CD3* antibody conjugated to *PE* (BD Pharmagen) was used. The stained cells were rinsed twice with FACS buffer and re-suspended in 50 μL FACS buffer to be analyzed by BD Accuri C6 flow cytometer. The flow cytometer results were analyzed using FlowJo software (FlowJo LLC, Ashland, Oregon). Gut microbiota interact with and can be regulated by B and T

cell populations [145,169]. Therefore, we examined the relative percentages of B and T cells in spleens of these mice.

Chapter 2.3.7 Statistical Analyses

Measures of bone were adjusted for body mass (unadjusted values are provided in Supplemental Table b) [154]. Homogenous variance was tested using Levene's test and normality tested using the Shapiro-Wilk Test. If parametric assumptions were met, a one-way ANOVA followed by post-hoc Holm correction for multiple comparisons was performed to test for differences between groups. If parametric assumptions were violated, either data was submitted to a log transform to achieve homogenous variance and normality or a non-parametric ranked Dunn's test followed by post-hoc Bonferroni adjustment for multiple comparisons was used.

To determine if genotype or treatment influenced whole bone strength in ways that were not explained by cross-sectional geometry, we performed an ANCOVA, implemented with a GLM model using $\frac{I}{c}$ as the covariate with genotype and treatment as fixed effects. Statistical tests were conducted using JMP Pro (v.9, 2013, SAS Institute Inc., Cary, NC, USA).

Chapter 2.4 Results

Chapter 2.4.1 Body Mass and TLR5KO Phenotypes

The TLR5KO mice showed a mild obesity phenotype with an average body mass 10.4% greater than WT ($p < 0.05$; Fig 2.1A) and an average epididymal fat pad mass 52.0% greater than WT ($p < 0.05$; Fig 2.1B). Body mass and fat pad mass in TLR5KO mice with disrupted microbiota and WT mice with disrupted microbiota were similar, as demonstrated in prior work [7]. No differences in colon histological scoring were observed among groups. One TLR5KO

mouse had elevated colon histological scores suggesting mild colitis, but did not display gross differences in bone morphology or body mass and was not excluded from the study [155].

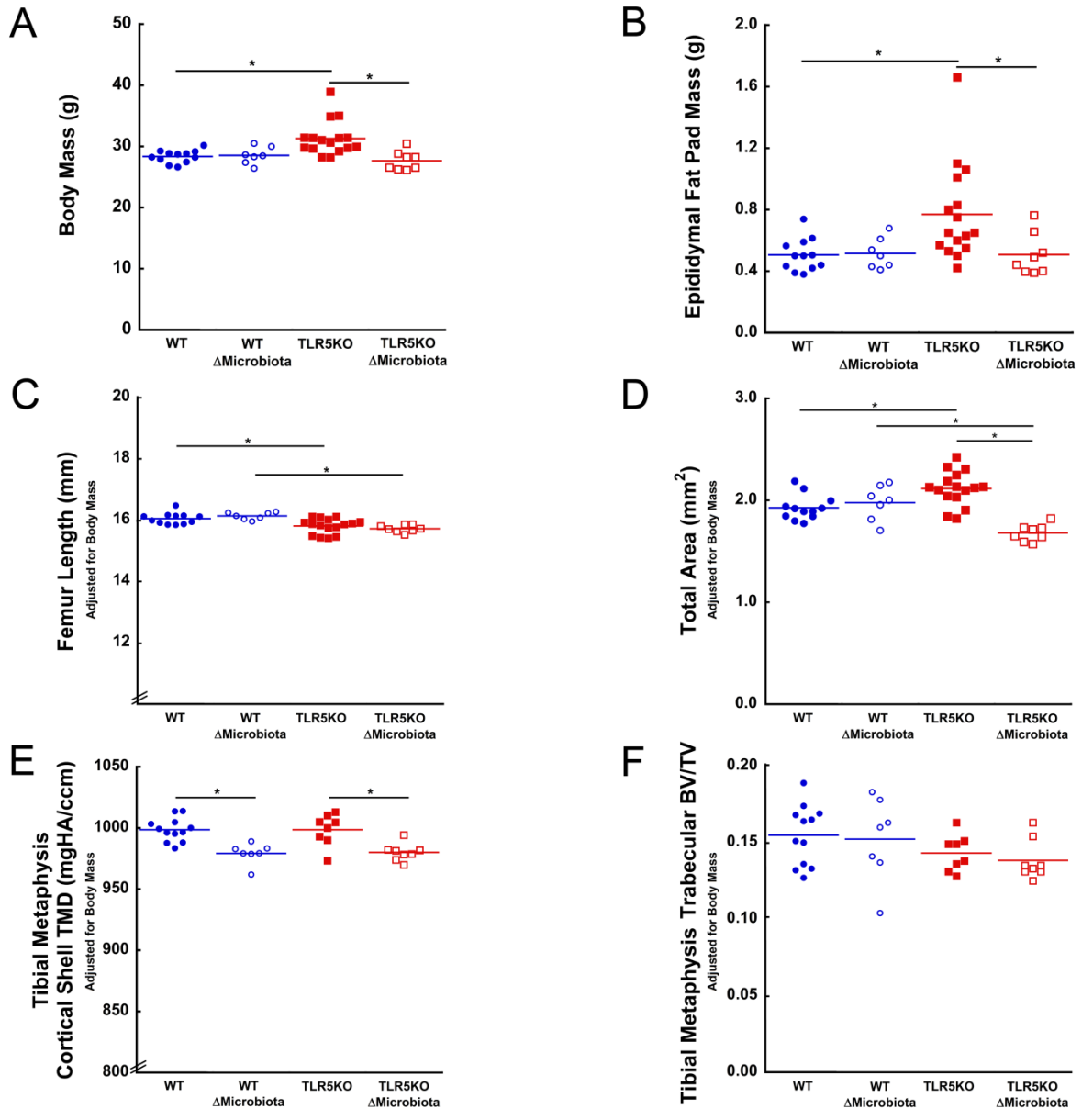

Figure 2.1. Metabolic and bone phenotype of mice with an altered gut microbiome.

TLR5KO mice had greater body and fat pad mass. Disruption of the gut microbiota in TLR5KO mice prevented the development of increased body and fat pad mass. Disruption of the gut microbiota in WT mice had no effect on (A) body mass or (B) epididymal fat pad mass. (C) TLR5KO mice femur length was less than WT in both untreated and treated groups (D) Total area was increased in untreated TLR5KO mice compared to untreated WT mice. Disruption of

gut microbiota led to a reduced total area in TLR5KO ΔMicrobiota mice. (E) Disruption of the gut microbiota in both genotypes was associated with a reduced tibial metaphysis cortical TMD. (F) No differences in tibial metaphysis BV/TV were observed between any groups. Solid colored lines on dot plots represent mean. Measures in Fig 2.1C, 2.1D, 2.1E, 2.1F are adjusted for body mass. * $p < 0.05$.

Chapter 2.4.2 Femoral Whole-Bone Bending Strength and Geometry in TLR5KO Mice

Bone morphology in TLR5KO mice differed from WT mice. Total cross-sectional area was larger in TLR5KO mice compared to WT mice ($p < 0.05$, Fig 2.1D). Marrow area, cortical area, and cortical thickness (Table a) in TLR5KO mice were similar to that in WT mice. TLR5KO mice had a larger moment of inertia compared to WT mice ($p < 0.05$, Fig 2.2A). Femoral bone length was 1.5% smaller in TLR5KO mice compared to WT mice ($p < 0.05$, Fig 2.1C, Table a).

The peak bending moment in untreated TLR5KO mice was similar to that in WT mice (Fig 2.2B), but the moment of inertia in TLR5KO mice was larger than in WT mice. Whole bone strength in TLR5KO mice was less than that in WT mice after accounting for differences in cross-sectional femoral geometry (ANCOVA, effect of genotype, $p<0.0001$, Fig 2.2C). No differences in post yield displacement (Table a) or bending stiffness (Fig 2.2D) were observed between WT and TLR5KO mice.

Table a Micro-computed tomography measures of cancellous and cortical bone and whole bone mechanical testing measures after adjustments for body mass are shown.

		Wild Type		TLR5KO	
	Body Mass Adjusted Measure	Untreated	ΔMicrobiota	Untreated	ΔMicrobiota
Proximal Tibia	Bone Volume Fraction	0.15 ± 0.02	0.15 ± 0.03	0.14 ± 0.01	0.14 ± 0.01
	Trabecular Thickness (μm)	0.045 ± 0.002	0.043 ± 0.005	0.041 ± 0.003 [a]	0.038 ± 0.002[$]
	Trabecular Separation (μm)	0.197 ± 0.014	0.192 ± 0.008	0.187 ± 0.007	0.178 ± 0.007[$]
	Cortical TMD (mg HA/cm^3)	999 ± 10	979 ± 8[*]	999 ± 13	980 ± 7[#]
	Growth Plate Thickness (μm)	558 ± 46	562 ± 41	550 ± 54	528 ± 21
Femoral Diaphysis	Cortical Area (mm^2)	0.87 ± 0.07	0.81 ± 0.09[*]	0.94 ± 0.07	0.69 ± 0.04[#]
	Marrow Area (mm^2)	1.05 ± 0.06	1.17 ± 0.10[*]	1.17 ± 0.15	1.00 ± 0.08[#]
	Total Area (mm^2)	1.93 ± 0.12	1.98 ± 0.17	2.12 ± 0.17 [a]	1.68 ± 0.08[#,$]
	Cortical Thickness (μm)	210 ± 10	189 ± 15[*]	216 ± 13	172 ± 12[#,$]
	Moment of Inertia (mm^4)	0.15 ± 0.02	0.14 ± 0.02	0.17 ± 0.03 [a]	0.10 ± 0.01[#,$]
	Moment of Inertia/ c (mm^3)	0.22 ± 0.03	0.22 ± 0.03	0.25 ± 0.03	0.17 ± 0.01[#,$]
Whole Femur	Length (mm)	16.04 ± 0.18	16.13 ± 0.12	15.80 ± 0.24[a]	15.71 ± 0.12[$]
	Peak Bending Moment (N∗mm)	40.79 ± 2.71	37.18 ± 2.35[*]	38.75 ± 2.37	30.22 ± 1.76[#,$]
	Bending Stiffness (N/mm)	193 ± 26	177 ± 21	175 ± 33	152 ± 7
	Post Yield Displacement (mm)	0.20 ± 0.17	0.35 ± 0.09	0.29 ± 0.11	0.42 ± 0.07

Values are mean ± SD. TMD=Tissue mineral density
[*]WT-ΔMicrobiota v. WT-untreated, $p<0.05$
[#]TLR5KO-ΔMicrobiota v. TLR5KO-untreated, $p<0.05$
[a]TL5KO-untreated v. WT-untreated, $p<0.05$

[$]TLR5KO-ΔMicrobiota v. WT-ΔMicrobiota, p<0.05

Chapter 2.4.3 Femoral Whole-Bone Bending Strength and Geometry in Mice With a Disrupted Microbiota

Disruption of the gut microbiota resulted in differences in geometry in TLR5KO mice and in WT mice. Disruption of the gut microbiota in WT mice resulted in increased marrow area, decreased cortical area, and decreased cortical thickness compared to untreated WT mice ($p < 0.05$, Table a). Disruption of the gut microbiota did not result in changes in total area, moment of inertia, or femoral length in WT mice (Fig 2.1C, Fig 2.1D, 2.2A, Table a). Disruption of the gut microbiota in TLR5KO mice resulted in decreased total area, marrow area, cortical area, cortical thickness, and moment of inertia as compared to untreated TLR5KO mice ($p < 0.05$, Fig 5.1D, Fig 2.2A, Table a). Disruption of the gut microbiota did not influence femoral length in TLR5KO mice (Fig 2.1C, Table a). Femoral length was 2.6% smaller in TLR5KO ΔMicrobiota mice compared to WT ΔMicrobiota mice ($p < 0.05$, Fig 2.1C, Table a).

Disruption of the gut microbiota was associated with reduced peak bending moment. Disruption of the gut microbiota in WT mice resulted in an average peak bending moment 9% less than in untreated WT mice ($p < 0.05$, Fig 2.2B). Disruption of the gut microbiota in TLR5KO mice led to a peak bending moment 22% less than in untreated TLR5KO mice ($p < 0.05$, Fig 2.2B). After accounting for differences in cross-sectional geometry, peak bending moment in mice with a disrupted microbiota was less than that in untreated mice (ANCOVA, effect of ΔMicrobiota, $p < 0.0001$, Fig 2.2C). The effect of disruption of the gut microbiota on bone tissue material properties appeared to differ between WT and TLR5KO mice (ANCOVA, ΔMicrobiota x genotype, $p=0.09$, Fig 2.2C). Disruption of the gut microbiota in both WT and TLR5KO mice showed a trend suggesting reduced whole bone femoral bending stiffness ($p < 0.15$, Fig 2.2D, Table a). Disruption of the gut microbiota was not associated with differences in

post yield displacement (Table a).

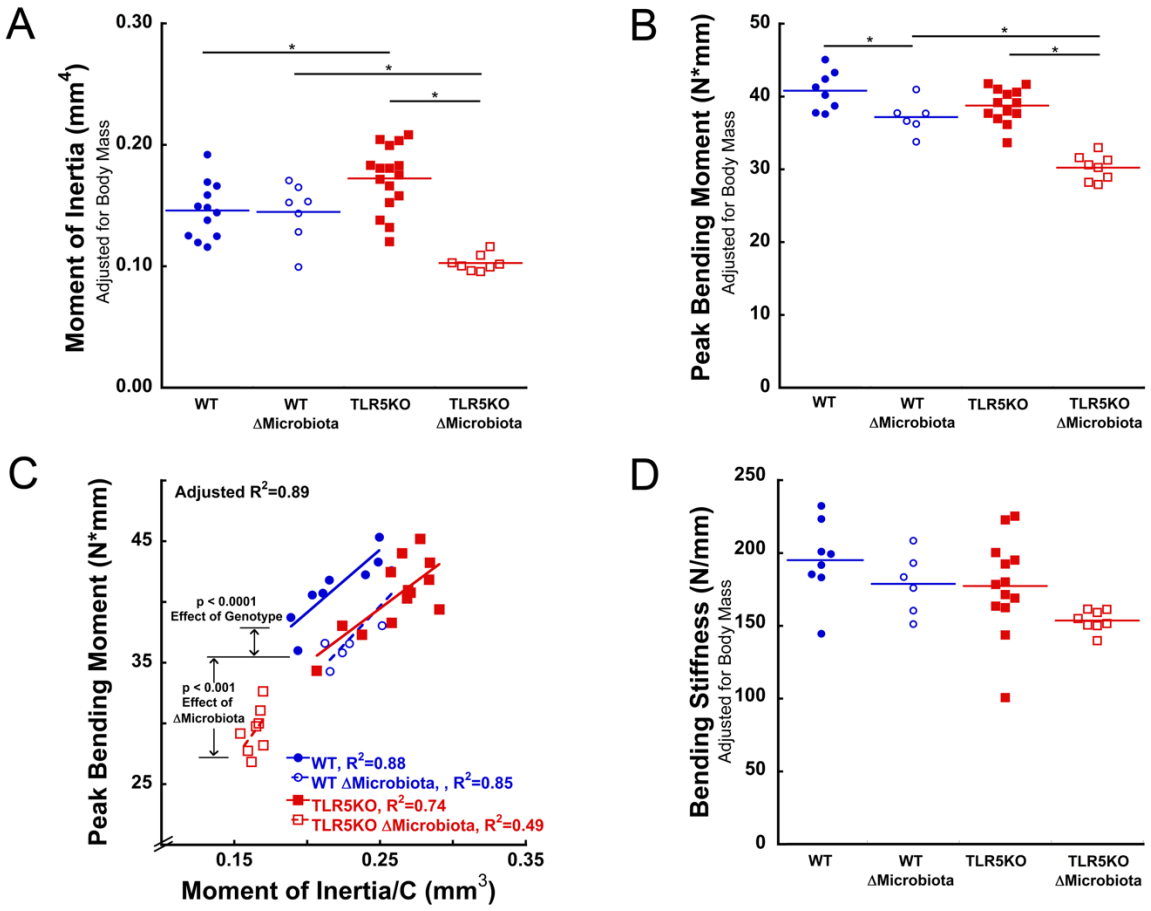

Figure 2.2. The effects of altering the gut microbiome on moment of inertia and whole bone strength.

Whole bone bending strength in mice with altered microbiota was less than would be expected from differences in cross-sectional geometry.(A) The moment of inertia was larger in TLR5KO mice. (B) Whole bone bending strength (peak bending moment) was less in ΔMicrobiota mice than in untreated animals. The peak bending moment in TLR5KO mice did not differ from that of WT mice. (C) Whole bone bending strength in TLR5KO mice was less than in WT mice after accounting for I/c (difference between solid red and blue lines). Bending strength in ΔMicrobiota mice was less than that in untreated animals (difference between dotted and solid lines indicates results of ANCOVA). (D). Disruption of the gut microbiota in both WT and TLR5KO mice showed a trend suggesting reduced whole bone femoral bending stiffness. Solid colored lines on dot plots represent mean. Measures in Fig 2.2A, 2.2B, and 2.2D are adjusted for body mass. * $p < 0.05$

Chapter 2.4.4 Tibial Trabecular Microarchitecture and tissue mineral density

Cancellous bone volume fraction in the proximal tibia did not differ among groups (Fig 2.1F). No differences in tibial cortical bone tissue mineral density were observed between untreated WT and TLR5KO mice. Disruption of the gut microbiota was associated with reductions in cortical bone tissue mineral density in both strains of mice ($p < 0.05$, Fig 2.1F). The thickness of the growth plate in the proximal tibia did not differ among groups (Table a).

Chapter 2.4.5 Microbiome Analysis

Sequences from feces microbiome assays were filtered for size, quality, and for the presence of chimeras and the total post-quality control number of sequences used in this study were 2,465,448. The average coverage was 102,727 ± 32,103 (mean ± SD) reads per sample. No differences in the mean number of reads for each group were observed (WT: 112,309 ± 11,935; WT ΔMicrobiota: 88,325 ± 18,501; TLR5KO: 101,706 ± 39,625, and TLR5KO ΔMicrobiota: 108,568 ± 47,800) ($p = 0.612$).

Although the total bacterial load did not differ among the four groups (Fig 2.3D), profound changes in the gut microbiota were observed. The gut microbiota composition at the phyla level differed among groups (Fig 2.3A). The gut microbiota in WT and TLR5KO mice was dominated by the Bacteroidetes phylum (Fig 2.3A, 2.3C). The gut microbiota in ΔMicrobiota mice was dominated by the Proteobacteria phylum (Fig 2.3A, 2.3B). Proteobacteria abundance was greater in TLR5KO ΔMicrobiota mice compared to WT ΔMicrobiota mice ($p < 0.05$, Fig 2.3B). The diversity of the gut microbiota, as measured by the Shannon Diversity Index, was reduced in groups with a disrupted gut microbiota (TLR5KO: 4.8 ± 0.5; TLR5KO ΔMicrobiota: 1.7 ± 0.2; WT: 4.7 ± 0.4; WT ΔMicrobiota: 2.5 ± 0.3) ($p < 0.05$, Fig 2.3E). Compared to untreated animals from the same genetic background, reductions in gut microbiota

diversity in TLR5KO ΔMicrobiota mice were greater than those in WT ΔMicrobiota mice ($p < 0.05$, Fig 2.3E). One sample from the WT ΔMicrobiota mice was determined to be an outlier and removed (Fig 2.3E).

Chapter 2.4.6 Splenocyte Populations

The total percentage of CD20+ B cell splenocytes was reduced in TLR5KO mice and WT ΔMicrobiota mice compared to untreated WT mice ($p < 0.05$, Fig 2.3F). The percentage of CD3+ T cells in the spleen was reduced in TLR5KO and WT ΔMicrobiota mice compared to untreated WT mice ($p < 0.05$, Fig 2.3G). Splenocytes from TLR5KO ΔMicrobiota mice were not obtained due to user error.

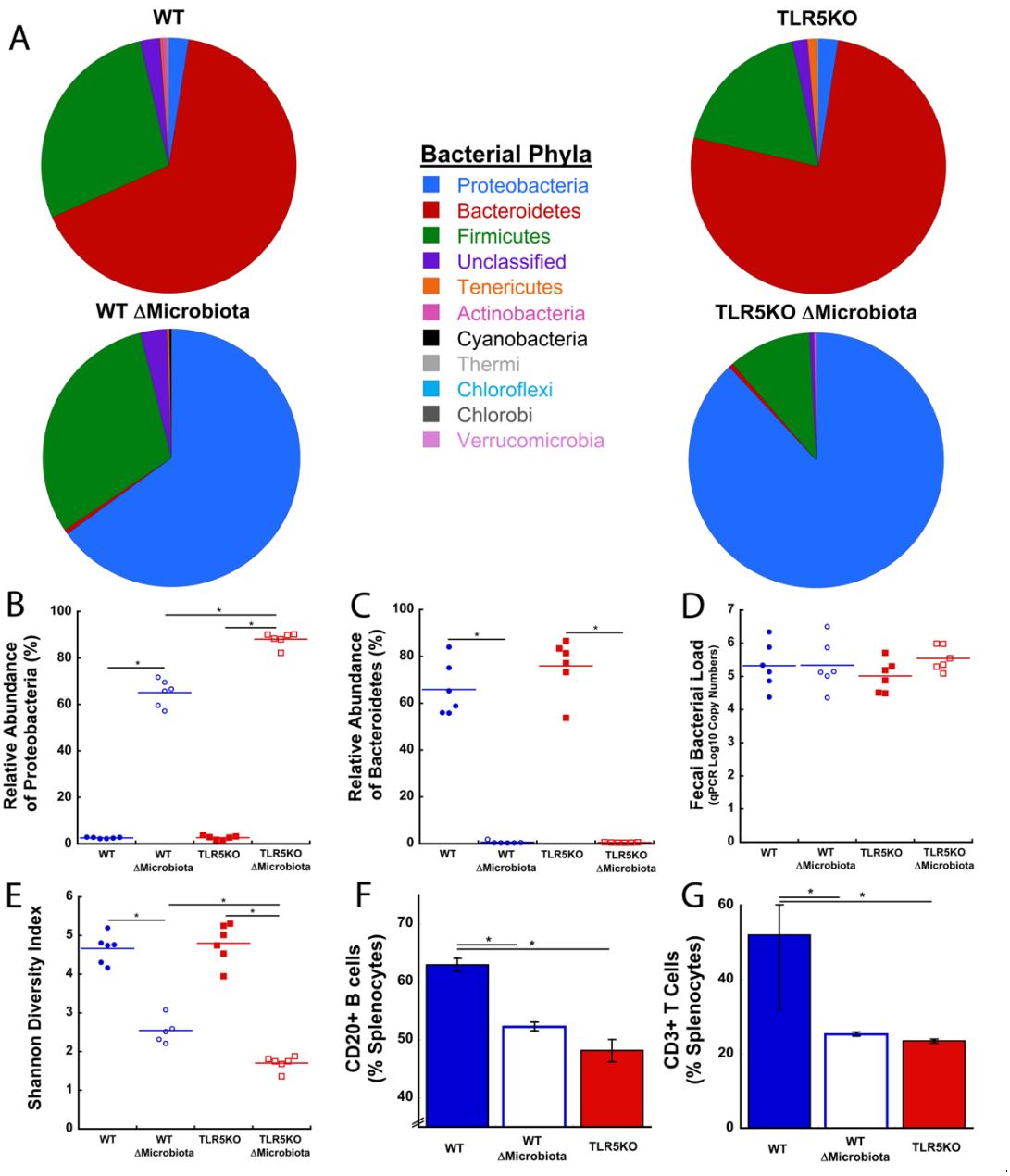

Figure 2.3. Gut microbiota composition and immune system profile in TLR5KO mice and ΔMicrobiota mice.

Disruption of the gut microbiota with antibiotics did not alter total bacterial load, but had dramatic effects on gut microbiota composition and bacterial diversity, and immune cell count.(A) The relative composition of bacterial phyla shifted from a Bacteroidetes dominated phyla in untreated mice to one dominated by Proteobacteria in ΔMicrobiota mice (n=6/group). (B) Proteobacteria is enriched in ΔMicrobiota mice, especially in TLR5KO ΔMicrobiota mice (Bonferroni correction). (C) Bacteroidetes dominates gut microbiota composition in untreated WT and TLR5KO. (D) Total bacterial load was unaffected by antibiotic treatment. (E) Bacterial diversity was dramatically reduced in ΔMicrobiota mice. (F) The percentage of splenic CD20+ B

cells was reduced in ΔMicrobiota mice and untreated TLR5KO mice (n=3/group). (G) The percentage of splenic CD3+ T cells in the spleen was reduced in ΔMicrobiota mice and untreated TLR5KO mice (n=3/group). Solid colored lines on dot plots represent mean. * $p < 0.05$ after adjusting for multiple comparisons.

Chapter 2.5 Discussion

Here we report the effects of an altered gut microbiota on bone mechanical properties in WT and TLR5KO mice. Disruption of the gut microbiota through long-term exposure to antibiotics led to reductions in whole bone bending strength that exceeded what could be explained by the associated changes in cross-sectional geometry, suggesting impairment of bone tissue material properties. Small differences in whole bone bending strength were observed between WT and TLR5KO mice after accounting for differences in bone morphology.

Together the differences in whole bone strength, cross-sectional geometry and tissue mineral density suggest that alterations in the gut microbiota changed the mechanical properties of the bone tissue itself. Whole bone strength in bending is determined by both cross-sectional geometry and tissue material properties. In bending, the ratio $\frac{I}{c}$ is the geometric measure that describes the entire effect of cross-sectional geometry on bending strength and is directly proportional to the maximum load an object can sustain in bending. Consistent with this relationship, the ratio $\frac{I}{c}$ was the single best predictor of whole bone strength, accounting for 71% of the variation in peak bending moment across groups. However, differences in the regression lines (Fig 2.2C) indicated that the ratio $\frac{I}{c}$ did not completely explain differences in strength among the four groups, a situation that implies alteration in bone tissue mechanical properties. Tissue mineral density (TMD) is a material property that can influence bone strength [(170)]. TMD in the tibial metaphysis of mice with a disrupted microbiota was less than that of untreated mice.

Although we did not measure TMD at the femoral midshaft directly, our findings in the tibia suggest that TMD may partially explain the reductions in femoral bone strength. Other factors such as collagen quality and non-collagenous proteins may also explain the reductions in femoral bone strength.

TLR5KO mice had larger total area than WT mice, but similar marrow area and cortical area. Increased total area without differences in marrow or cortical area at skeletal maturity has been associated with more rapid periosteal expansion during growth [154]. The increased periosteal expansion in TLR5KO mice may be a mechanism employed by the skeleton to maintain whole bone strength despite impaired bone tissue material properties [171].

Disruption of the gut microbiota resulted in decreased cortical bone at the femoral diaphysis in both WT mice and TLR5KO mice. Disruption of the gut microbiota in WT mice was not associated with alterations in total area, but was associated with decreased cortical area and cortical thickness. Disruption of the gut microbiota in TLR5KO mice prevented the more rapid periosteal expansion that occurred in untreated TLR5KO mice, and resulted in smaller cortical area, marrow area, and cortical thickness. Though marrow area was smaller in TLR5KO ΔMicrobiota mice, marrow area was larger than would be expected from the associated changes in total area. Decreased cortical area and cortical thickness is often attributed to decreased accumulation of bone mass during growth [154].

Treatment with antibiotics had a larger effect on bone morphology and whole bone strength in TLR5KO mice than in WT mice. This observation has many potential explanations: First, disruption of the gut microbiota prevented the development of the mild obesity phenotype in TLR5KO mice. Obesity is associated with differences in bone morphology and mechanical performance[172] . The bones in treated TLR5KO mice, therefore, not only have the effect of an

impaired microbiota, but also reduced adiposity. Second, disruption of the gut microbiota in TLR5KO mice had a larger effect on the relative abundance of Proteobacteria and microbial diversity (the Shannon diversity index) than in WT mice, which could help explain the larger effect on the bone phenotype. Third, the immune system and immune responses are impaired in TLR5KO mice, leading to altered gene expression and activity by the gut microbiota [47].

The composition of gut microbiota in untreated and treated mice was consistent with prior work. The total bacterial load in fecal samples did not differ between antibiotic treated and untreated groups, consistent with previous reports that oral antibiotic treatment can cause a large initial reduction in a bacterial population that recovers over time to a newly stabilized population [150,173,174]. The dominant phylum in untreated mice was Bacteroidetes, consistent with reports that Bacteroidetes are the predominant phylum throughout a healthy mouse's lifespan [175]. Disruption of the gut microbiota by chronic antibiotic treatment led to a gut microbiota population enriched by the phylum Proteobacteria (a minor component of the untreated mouse gut microbiota). The high relative abundance of Proteobacteria observed in mice with a disrupted microbiota at 16 weeks of age was similar to the immature and unstable gut microbiota typical of newborn mice [169]. As a mouse matures, its immune system begins to regulate gut microbiota composition via B cell production of IgA antibodies that target Proteobacteria [169]. The antibiotic treatment in the current study may have prevented the shift from Proteobacteria to Bacteroidetes that normally occurs in mice after weaning. Furthermore, the reduced splenic B cell count in mice with a disrupted microbiota is also consistent with the increased presence of Proteobacteria. The prevalence of members of the Proteobacteria phylum has been associated with increased incidence of microbial dysbiosis, metabolic disease, and inflammation, all factors known to influence host physiology and the immune system [146,176].

To understand the mechanisms linking changes in the microbiota to impaired bone tissue material properties it is useful to consider the three primary mechanisms through which the microbiome can influence organs distant from the gut: regulation of the immune system, regulation of nutrient absorption, and translocation of bacterial products across the epithelial barrier [98].

We consider the effects of the microbiota on the immune system to be a likely explanation for the differences in bone tissue material properties in the current study. Disruption of the gut microbiota with antibiotics reduced CD20+ B and CD3+ T cell populations and was correlated with reduced whole bone strength. Similarly, untreated TLR5KO mice also had reduced CD20+ B and CD3+ T cell populations. B and T cell populations have the potential to cause profound changes in bone remodeling and bone turnover [177-181]. However, it is not yet clear how alterations in B and T cell populations would lead to changes in bone tissue material properties.

While we cannot ignore the possibility that alterations in nutritional absorption influenced our findings, we consider this explanation unlikely for several reasons: First, body mass and fat pad mass in the mice were all similar or greater than that in untreated wild type animals, suggesting an acceptable caloric intake. Second, trabecular bone volume fraction was not different among the groups, and femoral length only had small differences. Trabecular bone volume fraction and whole bone length are typically severely reduced in situations of nutritional deficiency [41,182]. Trabecular bone is extremely responsive to impaired nutrition; animals submitted to short-term severe calcium and vitamin D deficiencies showed reductions in trabecular bone volume fraction of 24-58% [183,184], yet we did not observe reductions in trabecular bone volume fraction. Third, the reduction in peak bending moment seen in mice with

a disrupted microbiota is not fully explained by changes in bone geometry or bone mass, whereas in animal models of reduced dietary calcium and vitamin D, reductions in whole bone strength are usually well described by changes in bone geometry, mass, and tissue mineral density [183,184]. Lastly, examination of colon histology did not indicate intestinal inflammation in any of our groups, suggesting that treatment with antibiotics to disrupt the gut microbiota did not lead to increased gut inflammation that can impair nutritional absorption [185,186]. Animal models with extensive intestinal inflammation commonly develop reduced body mass and dramatic trabecular bone loss, which, again, was not present in any of our treatment groups [187,188].

Translocation of bacterial products (or even live bacteria) across the gut endothelial barrier is another potential mechanism for gut microbiota to influence bone. Microbial products such as lipopolysaccharide and flagellin are capable of traveling through the bloodstream to distant organs and causing localized inflammation [189]. Translocation of bacteria across the endothelial barrier is one of the mechanisms that explains the TLR5KO metabolic syndrome phenotype, so translocation may be involved in the observed differences in bone [47]. While bone cells can respond to lipopolysaccharide and flagellin [98], how such a response would lead to changes in bone tissue mechanical properties is not clear.

A number of strengths of the current study are worth noting. First, the study is unique in examining the effect of alterations in the gut microbiome on whole bone mechanical performance. Previous studies in which the microbiota was modified focused solely on bone structure or bone mass and did not examine mechanical performance. Second, the current study examined the effects of prolonged disruption of the gut microbiota during growth on the bone phenotype achieved at skeletal maturity. Most of the prior studies of bone in mice under conditions of altered gut microbiota examined bone from young, rapidly growing animals (7-9

weeks of age)[98], and did not evaluate the bone phenotype at skeletally maturity. Differences in bone phenotype in growing animals sometimes indicate differences in growth rate and do not always imply changes in bone phenotype at skeletal maturity [154,190,191]. As we only looked at skeletally mature mice, we could not assess differences in bone growth and acquisition, although differences in cross-sectional geometry such as total area suggest differences in rates of periosteal expansion (see above). Third, the current study provided both a detailed analysis of bone along with a full analysis of the constituents of the gut microbiome as determined using 16S rRNA sequencing and therefore provides differences in phyla, bacterial diversity, and total bacterial load along with a detailed bone morphological and biomechanical analysis. We are aware of only one prior study that provides both a detailed analysis of bone morphology and a detailed analysis of the microbiome [192].

Despite the novelty of the current study, some limitations must be considered when interpreting the results. The contents of the gut microbiota are dynamic and robust to external stimuli; short-term treatments (~1-2 weeks) with antibiotics generate a transient change in the gut microbiota that mostly returns to baseline when treatment was suspended [173]. To examine a condition of sustained alterations in the gut microbiota during growth we treated mice with chronic antibiotics from the age of weaning until skeletal maturity. Although chronic antibiotic treatment is rarely applied to humans throughout growth and development, less drastic changes in the human gut microbiota do occur for prolonged periods of time as a result of diet or metabolic status [173]. The study is further limited by not directly performing a compositional assessment of bone tissue. Direct measures of bone tissue material properties can help explain the mechanical phenotypes but more direct assays of mouse bone tissue mechanical properties than those performed here have additional limitations, especially in determination of tissue

strength (see Supplementary Material from Jespen et al 2015 [154]). The current study does not include assessment of bone turnover. Recent findings, however, suggest that the relationship between the microbiota and bone remodeling is complex and dynamic. For example, mice treated with an antibiotic cocktail of ampicillin, vancomycin, metronidazole, and neomycin show changes to serum turnover markers after one week of treatment, but no detectable differences from untreated animals after one month of treatment [149]. Understanding the effects of manipulation of the microbiome on bone remodeling would therefore require examination at many points during growth/treatment. Lastly, the current study uses the C57BL/6J as a control strain for the TLR5KO strain, despite the TLR5KO mice containing minor remnants of B6.129S1 genetics. However, the TLR5KO congenic strain is backcrossed for 11 generations to the C57BL/6J background to ensure the two strains are over 99.9% genetically identical, thus limiting potential effects of B6.129S1 genetics.

Despite the limitations of our study, our observations regarding changes in bone tissue mechanical properties suggest a new explanation to a long-standing clinical question. Fracture risk in some patient populations is much greater than expected from bone mineral density, a situation commonly attributed to impaired "bone quality"[193]. Although the term bone quality encompasses many different characteristics of bone [194], impaired bone tissue mechanical properties are a well-recognized component. Changes in bone tissue mechanical properties are often cited as a contributor to fracture risk that exceeds what is explained by BMD in patients with obesity, diabetes, and inflammatory bowel disease – three chronic clinical conditions that are also associated with drastic changes in the gut microbiome. Our findings in mice suggest an intriguing possibility that alterations in gut microbiota may contribute to alterations in clinical fracture risk by regulating bone tissue mechanical properties, although further studies are

required to confirm this hypothesis.

Chapter 2.6 Conclusion

We conclude that alterations in the gut microbiota throughout growth can lead to changes in whole bone strength that are greater than expected from whole bone size or shape. These findings suggest that alterations in the gut microbiota can influence bone tissue mechanical properties.

Chapter 2.7 Acknowledgements

This publication was supported in part by the National Institute of Arthritis and Musculoskeletal and Skin Diseases of the National Institutes of Health (U.S) under Award Number AR068061 and by the Office of the Assistant Secretary of Defense for Health Affairs through the office of the Congressionally Directed Medical Research Programs (CDMRP) under Award No. W81XWH-15-1-0239. The content of the work is solely the responsibility of the authors and does not necessarily represent the official views of the National Institutes of Health or the Department of Defense. We thank Adrian Alepuz for his help in analyzing mechanical testing data.

Authors' roles: Conceived and designed the experiments: JDG, REL, MCHM, SRG, CJH. Performed the experiments: JDG, MWH, FFF, TNS, ML, FA, SFL. Analyzed data: JDG, CJH, FA, AS, RCB, SFL. Wrote and Revised Manuscript: JDG, CJH, SFL. Critical revision and final approval of the manuscript: All authors.

Chapter 2.8 Supplementary Material

Table b Micro-computed tomography measures of cancellous and cortical bone and whole bone mechanical testing measures are shown.

		Wild Type		TLR5KO	
	Measure	Untreated	ΔMicrobiota	Untreated	ΔMicrobiota
Proximal Tibia	Bone Volume Fraction	0.15 ± 0.02	0.15 ± 0.03	0.15 ± 0.01	0.13 ± 0.01
	Trabecular Thickness (μm)	44.70 ± 1.98	43.30 ± 5.63	41.30 ± 2.66	36.40 ± 2.13$^{\#,\$}$
	Trabecular Separation (μm)	197 ± 14	191 ± 11	187 ± 7	176 ± 7$^{\$}$
	Cortical TMD (mg HA/cm^3)	999 ± 10	979 ± 8*	997 ± 13	981 ± 7$^{\#}$
	Growth Plate Thickness (μm)	558 ± 46	562 ± 41	550 ± 54	526 ± 21
Femoral Diaphysis	Cortical Area (mm^2)	0.87 ± 0.07	0.82 ± 0.10	0.96 ± 0.07^{a}	0.67 ± 0.05$^{\#,\$}$
	Marrow Area (mm^2)	1.06 ± 0.07	1.17 ± 0.10	1.17 ± 0.15	0.99 ± 0.08$^{\#,\$}$
	Total Area (mm^2)	1.93 ± 0.13	1.98 ± 0.18	2.13 ± 0.17^{a}	1.66 ± 0.08$^{\#,\$}$
	Cortical Thickness (μm)	210 ± 10	189 ± 17*	220 ± 14^{a}	170 ± 12$^{\#,\$}$
	Moment of Inertia (mm^4)	0.15 ± 0.02	0.15 ± 0.03	0.18 ± 0.03^{a}	0.10 ± 0.01$^{\#,\$}$
	Minimum Moment of Inertia/ c (mm^3)	0.22 ± 0.03	0.22 ± 0.03	0.25 ± 0.03^{a}	0.16 ± 0.01$^{\#,\$}$
Whole Femur	Length (mm)	16.05 ± 0.21	16.15 ± 0.24	15.88 ± 0.26	15.61 ± 0.14$^{\#,\$}$
	Peak Bending Moment (N∗mm)	41.09 ± 2.84	37.32 ± 2.86*	40.47 ± 3.00	29.43 ± 1.87$^{\#,\$}$
	Bending Stiffness (N/mm)	194 ± 18	177 ± 21	195 ± 38	143 ± 10$^{\#}$
	Post Yield Displacement (mm)	0.31 ± 0.12	0.32 ± 0.08	0.27 ± 0.11	0.34 ± 0.10

Values are mean ± SD. TMD=Tissue mineral density
*WT-ΔMicrobiota v. WT-untreated, $p<0.05$
$^{\#}$TLR5KO-ΔMicrobiota v. TLR5KO-untreated, $p<0.05$
^{a}TL5KO-untreated v. WT-untreated, $p<0.05$
$^{\$}$TLR5KO-ΔMicrobiota v. WT-ΔMicrobiota, $p<0.05$

Chapter 3- Alterations to the Gut Microbiome and Bone Tissue Composition

This chapter is in preparation for submission to the *Journal of Bone and Mineral Research*. The manuscript is titled "Alterations in the gut microbiome change bone tissue composition"

Chapter 3.1 Abstract

The gut microbiome has been shown to alter whole bone strength by modifying bone tissue material properties. Here we report a metagenomic analysis of the fecal microbiome to identify changes in the functional capacity of the gut microbiome in situations where bone quality is impaired. Male C57Bl/6 mice (WT) and Toll-like receptor 5 deficient mice (TLR5KO, a strain with altered gut microbial function) were subjected to disruption of the gut microbiota (ΔMicrobiome) using oral antibiotics (starting at 4 weeks of age) or remained untreated (n=7-8/group). Prior work has indicated that ΔMicrobiome impaired bone tissue strength in WT mice but did not modify tissue strength in TLR5KO mice. Disruption of the gut microbiome in the two mouse strains led to differential modifications to the abundance of microbial genes responsible for the synthesis of vitamins (K and B); bacterial cell wall and capsule; and carbohydrate production. Raman spectroscopy of bone from these mice indicated that in WT mice, disruption of the gut microbiome resulted in reduced bone mineral crystallinity while in TLR5KO mice, ΔMicrobiome was associated with increased bone mineral crystallinity ($p<0.05$). Supplementary biochemical analysis focused on vitamin K, a factor secreted by gut microbes that has previously been associated with bone health. Vitamin K content in the cecum, liver and kidneys was dominated by microbe-derived forms and differences among groups mirrored changes in crystallinity (decreased by ΔMicrobiome in WT mice, increased in TLR5KO mice) and bone matrix osteocalcin content. Together these findings suggest that disruption of the gut microbiome

may impair bone tissue strength in WT mice by causing deficiencies in bone matrix composition while in TLR5KO mice, disruption of the gut flora led to adequate (or even increased) amounts of components of bone matrix and hence no modifications in bone tissue material properties. This study illustrates the use of metagenomic analysis to link the microbiome to bone phenotypes and implicates microbially synthesized vitamin-K as a regulator of bone matrix quality.

Chapter 3.2 Introduction

Bone mineral density is the primary clinical measure used to estimate the risk of osteoporosis-related fracture. However, in many clinical studies bone mineral density does not fully explain fracture risk, suggesting that aspects of bone other than density/mass influence fracture risk [195,196]. The term "bone quality" is used to refer to characteristics of bone other than bone mineral density that influence bone strength and fracture risk [197]. Recently, the gut microbiome has been identified as a factor that can influence bone quality by modifying bone tissue composition and material properties [133].

The gut microbiome consists of the genomic components, products, and microorganisms in the gastrointestinal tract. Changes in the constituents of the microbiome have been associated with a number of chronic diseases including arthritis and cardiovascular disease. Recent studies have indicated that the gut microbiome can influence bone mass: mice raised from birth in an environment completely absent of microbial life (germ-free) have altered long bone length and trabecular and cortical bone mass [41,148,149]. Disruption of the gut microbiome using oral antibiotics can lead to changes in trabecular and cortical bone mass and femoral geometry in mice [133,150-152,198]. We recently demonstrated that disruption of the gut microbiome with oral antibiotics led to reductions in femoral whole bone strength that could not be explained by changes in bone mass and geometry, implicating impaired bone tissue quality (Fig 3.1) [133].

Specifically, we examined C57Bl/6 mice (WT) as well as a mouse strain known to develop an altered gut microbiota (the Toll-like receptor 5 deficient mouse, TLR5KO). We found that disruption of the gut microbiome alters bone tissue strength in WT (C57Bl/6) mice (shift in regression line in Fig. 1) but did not alter bone tissue strength in the Toll-like receptor 5 deficient mouse (single shared regression line in Fig 3.1).

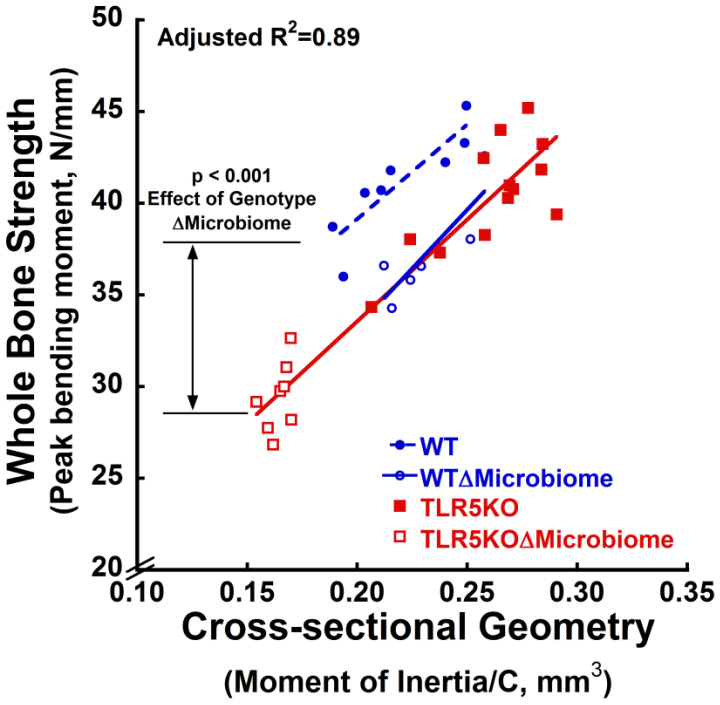

Figure 3.1. Disruption of the gut microbiome leads to changes in whole bone mechanical performance

Disruption of the gut microbiome in WT mice is associated with reductions in whole bone strength greater than can be explained by differences in femoral geometry (differences in regression lines), while in TLR5KO mice, disruption of the gut microbiota did not modify the relationship between bone geometry and whole bone strength (adapted from Guss et al. 2017) [133].

Studies demonstrating an effect of the microbiome on bone have included analysis of the composition of the gut flora using sequencing of the bacterial 16S rRNA gene to determine the relative abundance of microbial taxa based on phylogeny (phylum, class, order, etc.) [41,133,192,198].

While bacterial phylogeny is useful for understanding the microbial community, more detailed sequencing often is required to identify molecular pathways that link the microbiome to host phenotype. Metagenomic analysis sequences the entire microbial genome, and provides information on the functional capacity of the gut microbiome (i.e. which genes are present) [15,199]. Metagenomic analysis is useful because many interactions between the microbiota and the host are a result of microbial function rather than microbial taxonomy. To our knowledge, metagenomic analysis of the microbiome has not yet been used to understand the effects of the microbiome on bone.

The gut microbiome may influence bone tissue through three general mechanisms: 1) regulation of nutrient absorption and microbe-derived vitamins; 2) regulation of the immune system; and 3) translocation of inflammatory bacterial products across the gut barrier [98]. While regulation of the immune system and inflammatory molecules released by bacteria can lead to changes in bone resorption, bone formation and bone mass [200], these mechanisms only regulate bone matrix quality by modifying tissue age, a factor that does not vary much in mice. In contrast, vitamins produced by the gut microbiota can influence bone tissue. In particular, vitamin K is produced by the gut microbiota and has long been associated with bone health [201,202].

Changes in the composition and structure of the organic or mineral composition of bone can lead to changes in both tissue-scale and whole bone mechanical performance [114,203,204]. Bone tissue chemical composition can be assessed using Raman spectroscopy to determine: crystallinity (the size and stochiometrric perfection of the hydroxyapatite crystal lattice), mineral-to-matrix ratio (the extent of collagen mineralization and mineral content), and the carbonate-to-phosphate ratio (the extent of carbonate substitution into hydroxyapatite crystals).

Additionally, nanoindentation can characterize the mechanical properties (hardness and reduced modulus) at the tissue-scale [203]. Although multiple studies report modifications in bone composition and nanomechanical properties in the context of bone quality and fracture risk [114,203,205-207], no previous studies have evaluated changes in bone tissue composition associated with changes in the gut microbiome.

The goal of this line of investigation is to determine how modifications to the gut microbiome can influence bone tissue quality. Using samples from a previously reported study including microbiome-induced changes in bone strength (Fig. 3.1), we performed metagenomic analysis of fecal microbiota as well as microscale chemical analysis of bone tissue. Specifically, we determined the changes in the fecal metagenome and bone tissue chemical composition and nanomechanical properties following alterations to the gut microbiome caused by (1) genotypic alterations (Toll-like receptor 5 deficient mouse) and (2) chronic treatment with antibiotics to disrupt the gut microbiome.

Chapter 3.3 Materials and Methods

Chapter 3.3.1 Study Design

Animal procedures were approved by Cornell University's Institutional Animal Care and Use Committee. Mice from the C57BL/6J inbred strain and the B6.129S1-Tlr5tm1Flv/J (TLR5KO) congenic strain were acquired (Jackson Laboratory, Bar Harbor, ME), and each strain bred separately in conventional housing in our animal facility. C57BL/6J is the recommended control strain for TLR5KO [7,15,155,199]. Animals were housed in plastic cages filled with 1/4-inch corn cob bedding (The Andersons' Lab Bedding, Maumee, Ohio), fed with standard laboratory chow (Teklad LM-485 Mouse/Rat Sterilizable Diet) and water *ad libitum*, and provided a cardboard refuge environmental enrichment hut (Ketchum Manufacturing,

Brockville, Ontario). The study examined male C57BL6/J (WT) and Toll-like receptor 5 deficient (TLR5KO) male mice either treated to modify the gut microbiome or untreated. Treated groups received broad-spectrum antibiotics (1.0 g/L ampicillin, 0.5 g/L neomycin) in their drinking water from weaning at 4 weeks of age until skeletal maturity (16 weeks of age) [7]. Chronic antibiotics cause disruptions to the gut microbiome that are maintained over a prolonged time period [11]. Ampicillin and neomycin have poor oral bioavailability, thereby limiting extra-intestinal effects of treatment [7,156]. Additionally, neomycin and ampicillin have never been associated with impaired bone growth, do not influence bone length, body mass or gut inflammation [133] and do not cause noticeable changes in serum calcium or vitamin D (Supplemental Fig 3.7). Mice treated to disrupt the microbiome are referred to as "ΔMicrobiome." Mice were housed in cages with other animals from the same genetic background/treatment group. Animals were euthanized at 16 weeks of age. The right tibia, cecum, liver, kidney, and fecal samples were collected. Kidney and liver were stored at -20°C freezer and cecum and fecal samples were stored at -80°C freezer.

The study was performed using two cohorts of animals. One cohort of animals, described in a prior study (Fig. 3.1 [133]), was used for metagenomic analysis and tissue chemical, nanomechanics and biochemistry (ΔMicrobiome C57BL/6J: n=7, TLR5KO: n=8; untreated WT, C57BL/6J: n=11, TLR5KO: n=8). A second cohort of animals was used for follow-up biochemical analysis of tissue biochemistry (ΔMicrobiome TLR5KO: n=6; untreated WT, C57BL/6J: n=6, TLR5KO: n=6).

Chapter 3.3.2 Metagenomic Analysis

Fecal samples collected one day prior to euthanasia were used for metagenomics analysis. Metagenomic analysis was performed on six samples per group (2 animals per cage). DNA was extracted (DNeasy PowerSoil DNA Isolation Kit, MO BIO Laboratories Inc., Carlsbad, CA) following manufacturer's recommendations. The fecal pellet was added to the PowerBead tubes (Qiagen, Germantown, MD) and followed by a 10-minute vortex step. Following addition of Solution C1, to enhance cell lysis, samples were incubated at 70 C for 10 minutes and then subjected to a vortex step for 15 minutes using the MO BIO Vortex Adapter tube holder. Isolated DNA was quantified (Qubit dsDNA Broad Range Assay Kit, Life Technologies, Carlsbad, CA). Aliquots of DNA were normalized to the same concentration of 0.2 ng/ul of DNA per sample. A sequence library was prepared (Nextera XT DNA Library Preparation Kit, Illumina, San Diego, CA) to yield an average library size of 500 bp. Final equimolar libraries were sequenced (MiSeq reagent kit v3 on the MiSeq platform, Illumina, San Diego, CA) to generate 300 bp paired-end reads [159].

Metagenomic analyses were performed using MG-RAST (Metagenome Rapid Annotation using Subsystem Technology version 4.0.3). In the MG-RAST analysis, the fragments of DNA in a sample are compared to protein, RNA, and subsystem databases. Functional annotation of sequences in the current study used the SEED subsystem [208]. The functional abundance analysis was performed using a "Representative Hit Classification" approach with a maximum e-value of 1×10^{-5}, minimum identity of 60%, and a minimum alignment length of 15 measured in amino acids for proteins and base pairs for RNA databases. The subsystems are grouped into hierarchical classifications ranging from the broadest functional category at "Level 1", to more specific functional roles at "Level 2" and "Level 3", and then to the most detailed category of "Function". The data underwent a normalization and

standardization process (within MG-RAST) to reduce inter-sample variability and to allow data to be more easily comparable. The normalized counts were calculated as: $normalized_i = log2(raw_{counts_i} + 1)$. The standardized counts were calculated as: $standardized_i = (normalized_i - mean(normalized_i))/stdev(normalized_i)$. Normalized counts are used as a measure of the abundance of genes that match a functional category.

Principal coordinate analysis (PCoA) of the functional hierarchy based on the Bray-Curtis distance was performed to investigate overall functional diversity amongst samples. Principal coordinate analysis reduces the dimensionality of a complex dataset with thousands of variables to a smaller number so the diversity between samples can be easily visualized in a two- or three-dimensional scatterplot [209]. Each principal coordinate explains a percentage of the variation in the data set, with the first two principal components accounting for the most variation. PCoA was performed at subsystem Level 1, Level 2, and Level 3 hierarchies.

Chapter 3.3.3 Raman Spectroscopy and Nanoindentation

The right tibiae were harvested and fixed in 10% neutral buffered formalin for 48 hours. Tibiae were then embedded undecalcified in methyl methacrylate and a single 2-mm-thick transverse section from the proximal metaphysis was collected using a diamond wafering saw (Buehler, Lake Bluff, Illinois). All sections were polished anhydrously on a Multiprep automatic polishing system (Allied High Tech, Rancho Dominguez, CA) at 30 RPM with a 200g sample load. Samples were polished with increasing grit silicon carbide polishing paper (800, 1200 grit) using ethylene glycol as a lubricant, and followed by a series of slurries of aluminum oxide powder (particle size of 3 μm, 1μm, and 0.1 μm) in ethylene glycol [210]. The final root mean square (RMS) roughness of the surface was determined to be ~35nm by measurement of ten 5

x5-μm^2 scans per sample with a surface profilometer (VKX Laser-Scanning Microscope; Keyence, Inc.).

A Raman imaging system (InVia Confocal Raman Microscope; Reinshaw Inc.) was used to collect spectra of the tibial cross sections using two different sampling strategies: 1) Analysis of regions throughout the cross section (n=4/group); and 2) High-density spatially-resolved mapping analysis of one quadrant (n=7-10/group). For analysis throughout the cross section, 20 individual point spectra were collected across four quadrants of the cross section corresponding to 25%, and 75% of the cortical thickness with an additional three points collected 50 microns away from the midline of the cortex (forming a '+' sign). The five spectra were averaged to determine a single representative measure per quadrant per sample. Spectra were collected over the range 720-1,820 cm^{-1} with a 785nm laser and a 50x long-working-distance objective (N.A.=0.55) collecting for 30s at 50% power with cosmic ray correction. Spectra first were normalized to the absorbance of PMMA at 813 cm^{-1} (MATLAB, MathWorks). Last, spectra were baseline-corrected to account for background fluorescence. The following Raman bands were evaluated: phosphate (PO_4^{3-}) ν_1PO_4 (integration area ~930-980 cm-^{1}) [211], amide III (integration area ~1215-1300 cm-^{1}) [211], and carbonate (CO_3^{2-}) CO_3 (integration area ~1050-1100 cm-^{1}) [211]. From each spectrum the following measures were calculated: mineral-to-matrix ratio (determined as the area ratio of phosphate ν_1PO_4 and amide III); carbonate substitution (measured as the area ratio of carbonate to phosphate ν_1PO_4); and mineral crystallinity (measured as the inverse of the full-width-half-max of a Gaussian fit of the phosphate ν_1PO_4 peak) [212]. For the high-density spatially-resolved mapping, spectra were acquired every 4 μm over a 40 μm x 40 μm area in the posterior region, centered between the periosteum and endosteum to avoid recently formed bone tissue, for 121 total spectra [213]. The center of the cortex was selected to

characterize mature bone. The high data density (121 spectra) was used to determine mean values as well as compositional heterogeneity, measured by the full width at half maximum of a Gaussian function fit of the distribution of each Raman measure.

Nanoindentation was performed on the same sections and regions analyzed by Raman spectroscopy. Nanoindentation arrays were performed using a Berkovich indenter tip (TI-900 Triboindenter, Bruker, Eden Prairie, MN) calibrated to a silica glass standard. Each array consisted of a 4 x 4 grid of indentations with a 30 second ramp load to P_{max} = 2500 μN, a 30 second hold to reach equilibrium, and a five-second elastic unloading. Indents were placed 15 μm away from each other to avoid mechanical interactions among indentations.

Hardness (H) and reduced modulus (E_r) were determined from the force vs. displacement curves of each indentation [214] using the following relations:

$$H = \frac{P_{max}}{A_c} \quad , \quad E_r = \frac{S\sqrt{\pi}}{2\sqrt{A_c}},$$

for which S is the contact stiffness (the slope of the load-displacement curve upon initial unloading) and A_c is the projected contact area of the indentation. The nominal contact depth of the indents in the bone samples was 260 nm.

Chapter 3.3.4 Biochemical Analysis

Biochemical analyses of tissues were performed after receiving the results of the metagenomics analysis as a means of testing the functional significance of modifications to the microbial metagenome (n=6/group). Based on the metagenomics findings, the biochemical analysis focused on vitamin K. Vitamin K is a class of fat-soluble vitamers consisting of phylloquinone (vitamin K_1 in older literature) and the menaquinones (vitamin K_2 in older literature). Menaquinones exist in 10 known forms, identified by the length of the isoprenoid

side chain of the molecule (MK4-MK13) [215]. Phylloquinone and MK-4 are derived from the diet. The remaining nine known forms of menaquinone are synthesized primarily by bacteria in the gut, although some bacterially-derived forms of vitamin K are found in fermented or cured food products [215]. The cecum is an important site for microbial production of vitamin K [216]. The liver and kidney are distant organs where vitamin K accumulates [217]. Phylloquinone (PK) and menaquinones (MK-4-13) concentrations in the cecum, liver and kidney were measured by liquid chromatography/mass spectroscopy (LC/MS) [218]. Procedures for vitamin K extraction and sample purification are described elsewhere [218]. The LC/MS system consists of an Agilent 6130 Quadrupole MSD with an atmospheric pressure chemical ionization (APCI) source connected to an Agilent series 1260 HPLC instrument (Agilent Technologies, Santa Clara, CA). Separations were completed using a reversed-phase C18 analytical column (Kinetex 2.6 μm, 150 mm x 3.0 mm; Phenomenex, Inc., Torrance, CA).

A major function of vitamin K in bone is carboxylation of Gla-containing proteins during bone formation. Osteocalcin is a Gla-containing protein and the most abundant non-collagenous protein in bone. Mouse humeri were dissected and wrapped in PBS soaked gauze. The tested mouse humeri were homogenized in 600 μl of extraction buffer containing 0.05M EDTA, 4M guanidine chloride and 30mM Tris-HCl (Omni BeadRuptor 24, Omni International, Atlanta, GA). After homogenization, the solution was centrifuged at 13000 rpm for 15 minutes to eliminate remaining mineral debris from the supernatant. The supernatant was dialyzed against 1x PBS and 5mM EDTA for two days to eliminate denaturant. Extracted bone protein concentrations of the dialyzed solutions were assessed using a Pierce™ Coomassie Plus (Bradford) Assay Kit. The extracts then were serially diluted 1000-fold in PBS for use with the LSBio Mouse OC ELISA kit, which has a working range of 0.156-10 ng/mL. The OC

quantification ELISA was performed as per manufacturer protocol. Osteocalcin content was assessed in 4-6 animals per group.

Chapter 3.3.5 Statistical Treatment

Group differences between Raman mapping measures, nanoindentation measures, metagenome sequence abundances, vitamin K levels, and osteocalcin content were determined using a one-way ANOVA with group as the factor followed by the Holm correction for multiple comparisons with ✔=0.05 (JMP Pro 9.0.0). The effect of genotype, treatment, genotype x treatment, and quadrant on Raman measures was detected using a 2-factor repeated measures ANOVA and included individual as a random effect to account for repeated measures within each animal (JMP Pro 9.0.0). Post-hoc comparisons using least squared mean student t-tests with Holm correction for multiple comparisons were performed when interaction effects were significant.

Chapter 3.4 Results

Chapter 3.4.1 Metagenomic Functional Analysis

The functional capacities of the gut microbiome differed among groups (Fig 3.2A). Principal coordinate analysis based on Bray-Curtis dissimilarity showed that the overall functional capacity of untreated WT and TLR5KO mice were similar (two groups clustered together, Fig 3.2B). Disruption of the gut microbiome caused drastic changes in the functional capacity of the gut microbiome that differed between the two genotypes, as indicated by distinct clusters in the principal coordinate analysis (Fig 3.2B).

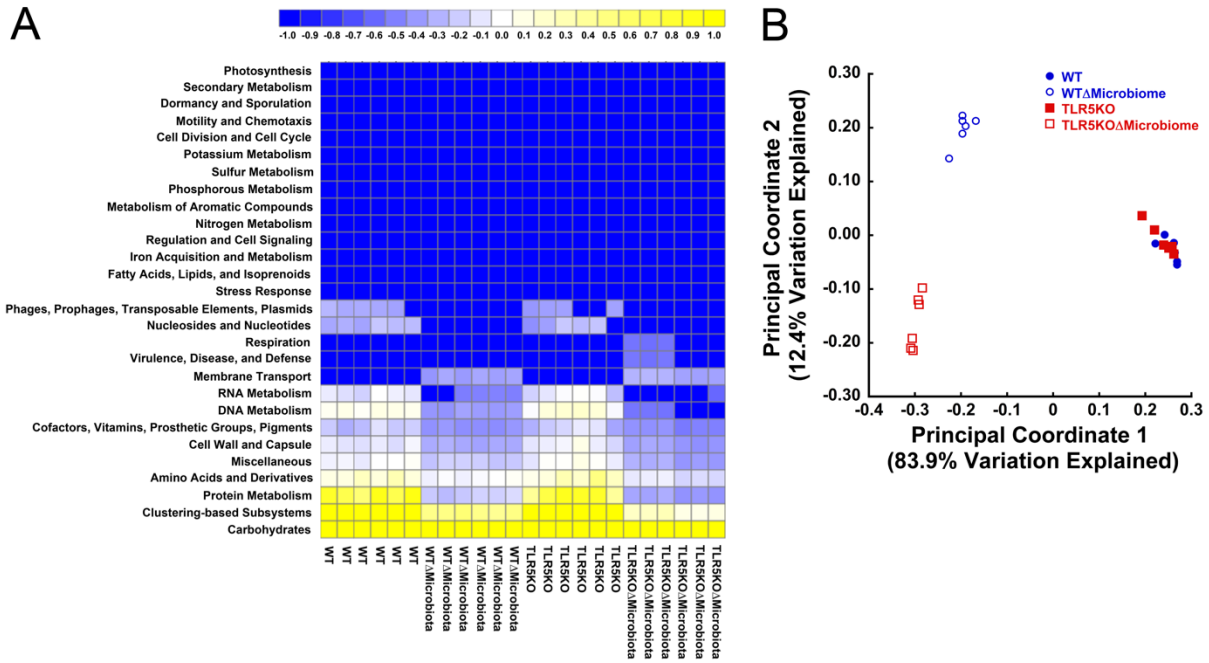

Figure 3.2. Disruption of the gut microbiome leads to large changes in the functional capacity of the gut flora

Disruption of the gut microbiota led to large changes in the functional capacity of the gut flora. (A) The abundance of genes from multiple functional categories were differentially modified in the gut flora of ΔMicrobiome mice. (B) Principal coordinate analysis showed that the overall functional capacity of ΔMicrobiome mice was distinct from that of untreated WT and TLR5KO mice. Furthermore, the functional capacity of WTΔMicrobiome and TLR5KOΔMicrobiome were distinct from one another.

The metagenomics findings identified differences in vitamin biosynthesis in ΔMicrobiome mice. Pathways related to the synthesis of vitamin B and vitamin K were altered by disruption of the gut microbiome. Mice with a disrupted gut microbiome had lower normalized counts for genes associated with the synthesis of vitamin B2, B6, and B7 compared to untreated mice (Fig 3.3A), but had greater normalized counts for genes involved in the synthesis of vitamin B9 and K. Principal coordinate analysis at SEED subsystems level 2 hierarchy revealed that the overall functional capacity of genes for vitamin B and K biosynthesis was dramatically different between untreated mice and mice with disrupted gut microbiota

(Supplemental Figure 3.8A). Further investigation identified differential presence of multiple genes involved in menaquinone biosynthesis (Fig 3.3B, Supplemental Fig 3.8B): normalized counts for MenH, MenF, and MenE genes are greater in ΔMicrobiome mice (Fig 3.3B) and the abundance of MenB genes was less in ΔMicrobiome mice than in untreated WT and TLR5KO mice.

The overall functional capacity and the abundance of genes for six of eight carbohydrate functional categories were altered by ΔMicrobiome in both WT and TLR5KO mice (Fig 3.3C, Supplemental Fig 3.8C). The functional capacity of genes for carbohydrates in WTΔMicrobiome and TLR5KOΔMicrobiome were distinct from each other (Supplemental Fig 3.8C). No differences in the overall abundance of fermentation genes were detected. However, principal coordinate analysis at SEED subsystems level 3 hierarchy revealed that the overall functional capacity of genes for fermentation were dramatically different following disruption of the gut microbiome (Supplemental Fig 3.8D).

The abundance of genes related to the cell wall and cell capsule differed among groups (Fig 3.3D). Normalized counts for genes for capsular and extracellular polysaccharides were less abundant in mice with a disrupted gut microbiome than in untreated mice. Disruption of the gut microbiome led to increased abundance of genes associated with Gram-negative cell wall components, particularly in the TLR5KOΔMicrobiome. Normalized counts for genes for Gram-positive cell wall components were less abundant in untreated TLR5KO mice compared to WT mice. Genes for Gram-positive cell wall components were less abundant in TLR5KOΔMicrobiome mice compared to untreated TLR5KO mice and compared to WTΔMicrobiome mice. Principal coordinate analysis at SEED subsystems level 2 hierarchy revealed that the overall functional capacity of genes for cell wall and cell capsule were

drastically changed due to disruption of the gut microbiome (Supplemental Fig 2E). The functional capacity of genes relating to Gram negative cell wall components differed between ΔMicrobiome mice and untreated mice (Supplemental Fig 3.8F).

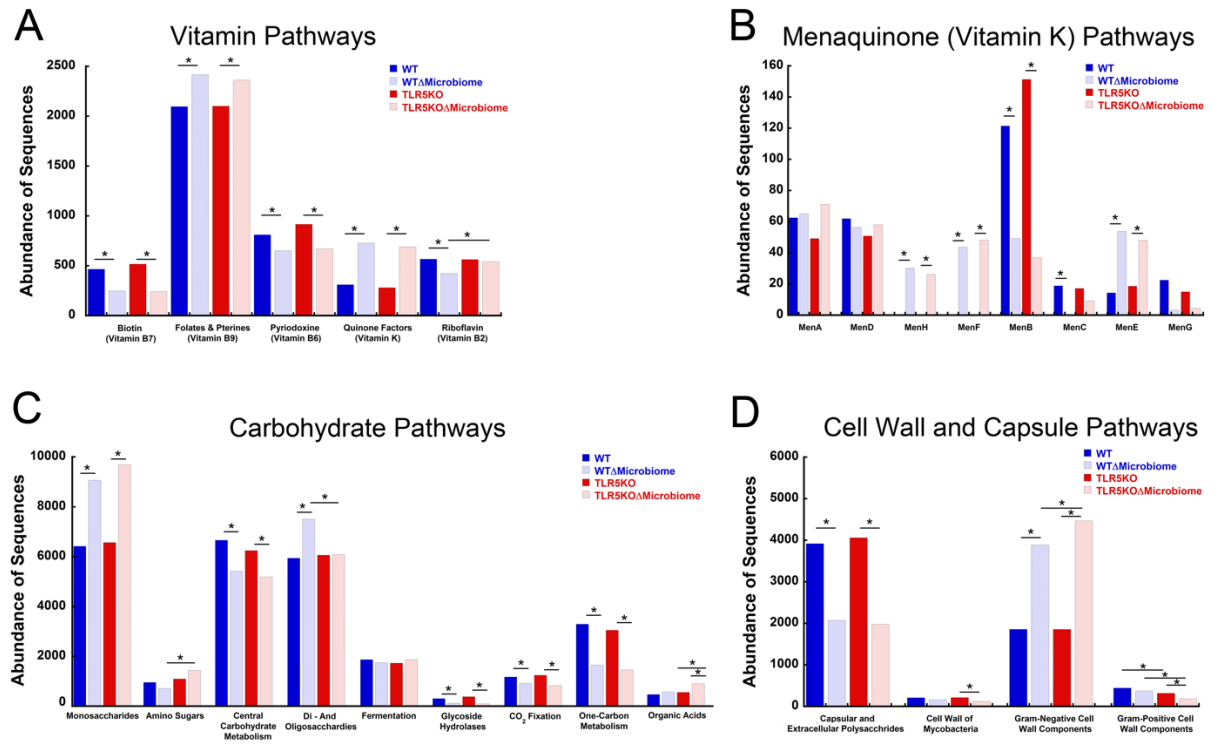

Figure 3.3. Key pathways for vitamin synthesis, carbohydrates, and bacterial cell wall and capsule components are disrupted in ΔMicrobiome mice**.**

Key pathways are disrupted in ΔMicrobiome mice. (A) The abundance of genes involved in Vitamin B and K synthesis were altered. (B) Several gene pathways for menaquinone biosynthesis were disrupted in ΔMicrobiome mice, while some were similar compared to untreated controls. (C) Carbohydrate pathways were affected by disruption of the gut microbiome. The abundance of genes for six of eight carbohydrate functional categories were altered by ΔMicrobiome in both WT and TLR5KO mice. (D) Pathways relevant for bacterial cell wall and capsule components were altered in mice with a disrupted gut microbiome. Disruption of the gut microbiome led to increased abundance of genes associated with Gram-negative cell wall components, particularly in the TLR5KOΔMicrobiome mice. Normalized counts for genes for Gram-positive cell wall components were less abundant in untreated TLR5KO mice compared to WT mice. Genes for gram-positive cell wall components were less abundant in TLR5KOΔMicrobiome mice compared to untreated TLR5KO mice and compared to WTΔMicrobiome mice.

Chapter 3.4.2 Raman Spectroscopy and Nanoindentation

In the analysis across the tibial cross-section (Fig 3.4A), disruption of the gut microbiome resulted in changes in bone tissue crystallinity and carbonate substitution. In WT mice, disruption of the gut microbiome led to decreased crystallinity, increased carbonate substitution and no detectable differences in mineral:matrix (two-way ANOVA, Fig. 3.4A-D). However, in TLR5KO mice, disruption of the gut microbiome led to increased crystallinity without detectable changes in carbonate substitution or mineral:matrix (two-way ANOVA, Fig. 3.4A-D). Among untreated animals, crystallinity was, on average lower in TLR5KO mice than in WT mice and there were no detectable differences between carbonate substitution and mineral:matrix. Carbonate substitution was less in TLR5KOΔMicrobiome mice compared to untreated TLR5KO mice.

High density mapping of the posterior tibia revealed changes in Raman parameters consistent with those found in the cross sectional analysis (Fig 3.4E). Disruption of the gut microbiome resulted in differences in crystallinity among groups ($p<0.001$, ANOVA). Post-hoc analysis showed increased crystallinity in the TLR5KO mice following disruption of the gut flora and trends suggesting decreased crystallinity in the WTΔMicrobiome mice (Fig 3.4F). No differences in crystallinity were observed among WT and TLR5KO mice with unmodified gut flora. No differences in mineral:matrix or carbonate substitution were observed among the groups (Fig. 3.4E-H). No differences in tissue heterogeneity (distribution width) in mineral:matrix, carbonate substitution, or crystallinity were detected among groups (Supplemental Fig 3.9A-C).

Reduced modulus measured using nanoindentation was similar among groups (Supplemental Fig 3.10A; WT: 30.8 GPa ± 1.06; WTΔMicrobiome: 30.4 GPa ± 1.20; TLR5KO: 31.0 GPa ± 1.62, and TLR5KOΔMicrobiome: 31.4 GPa ± 1.41, mean ± SD). Hardness was

similar among groups (Supplemental Fig 3.10B; WT: 1.08 GPa ± 0.07; WTΔMicrobiome: 1.09 GPa ± 0.04; TLR5KO: 1.08 GPa ± 0.06, and TLR5KOΔMicrobiome: 1.11 GPa ± 0.03).

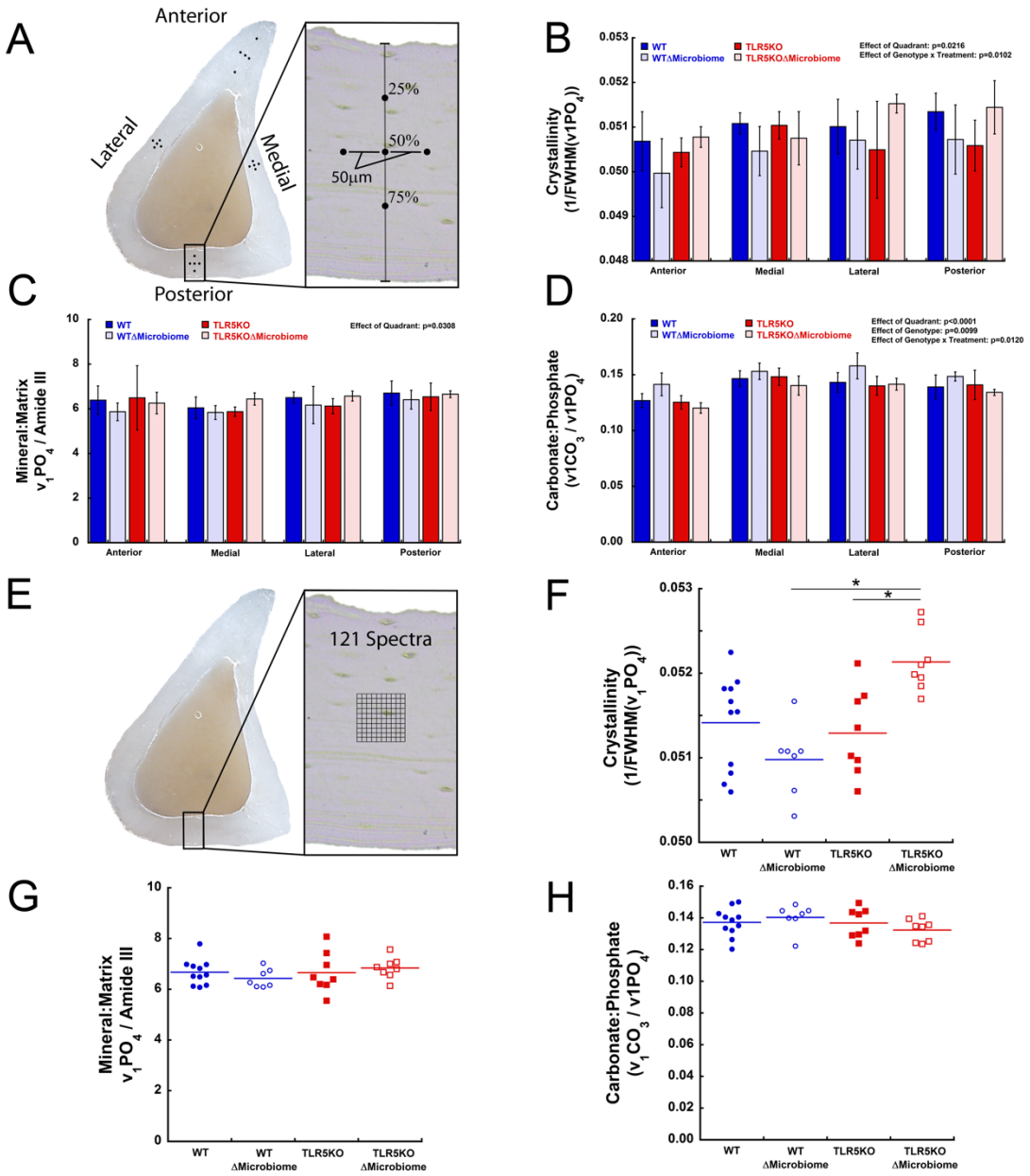

Figure 3.4. Disruption of the gut microbiome leads to changes in bone tissue composition.

Disruption of the gut microbiome led to changes in bone mineral crystallinity. (A) Five Raman point spectra were collected in each of the four anatomical quadrants of a tibial diaphysis cross section (n=4/group). (B) Crystallinity was decreased in WTΔMicrobiome mice compared to untreated WT, whereas crystallinity was increased in TLR5KOΔMicrobiome compared to untreated TLR5KO. (C) Mineral:matrix ratio was not affected by genotype or ΔMicrobiome. (D)

Carbonate substitution was increased in WTΔMicrobiome mice compared to untreated WT, but decreased in TLR5KOΔMicrobiome mice compared to untreated TLR5KO. (E) High density spatially-resolved mapping analysis was also performed with Raman spectroscopy on the posterior region of a tibial diaphysis cross section (n=7-10/group). The mapping results were consistent with the cross sectional analysis. (F) Bone mineral crystallinity was greater in TLR5KOΔMicrobiome mice compared to TLR5KO. A trend toward decreased crystallinity in WTΔMicrobiome mice was observed. (G) Mineral:matrix ratio was similar among groups. (H) Mean carbonate:phosphate was similar among groups. Lines indicate $p < 0.05$ in pairwise comparisons.

Chapter 3.4.3 Biochemical Analysis

Vitamin K content in the cecum, liver, and kidney primarily consisted of microbe-derived menaquinones; on average, the microbe-derived menaquinones (MK5-13) accounted for 83.3% to 99.9% of the total vitamin K content (Fig 3.5A-C). Total cecal vitamin K content was lower in WTΔMicrobiome mice compared to untreated WT mice (Fig 3.5A). Cecal vitamin K content was greater in TLR5KOΔMicrobiome compared to untreated TLR5KO mice. TLR5KO mice had greater cecal vitamin K content compared to WT mice. Total liver vitamin K content was lower in WTΔMicrobiome compared to untreated WT mice (Fig 3.5B). TLR5KOΔMicrobiome mice had greater liver vitamin K content compared to WTΔMicrobiome mice. Kidney vitamin K content demonstrated similar trends of decreased content in WTΔMicrobiome and increased content in TLR5KOΔMicrobiome (Fig 3.5C). Mean matrix-bound osteocalcin concentration did not differ significantly among groups in this cohort ($p = 0.13$, ANOVA, Fig. 3.6) although trends demonstrated a decrease in matrix-bound osteocalcin content level in WT mice with a disrupted gut microbiome, and an increase in TLR5KO mice with a disrupted gut microbiome.

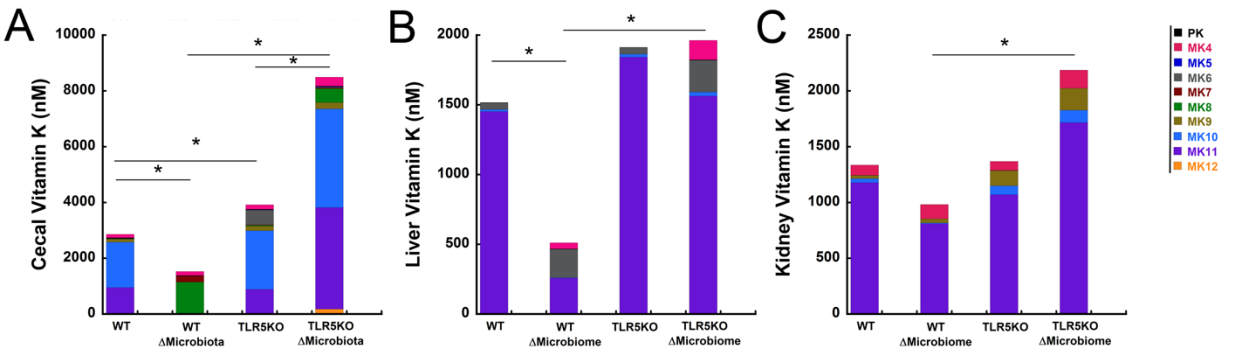

Figure 3.5. Vitamin K content is altered by disruption of the gut microbiome.

Vitamin K content was altered by disruption of the gut microbiome. (A) Cecal vitamin K content was decreased in the WTΔMicrobiome mice compared to untreated WT mice. However, vitamin K content was increased in TLR5KOΔMicrobiome mice. Similar patterns were seen in (B) liver vitamin K content and (C) kidney. * indicates $p < 0.05$ using the Holm posthoc test.

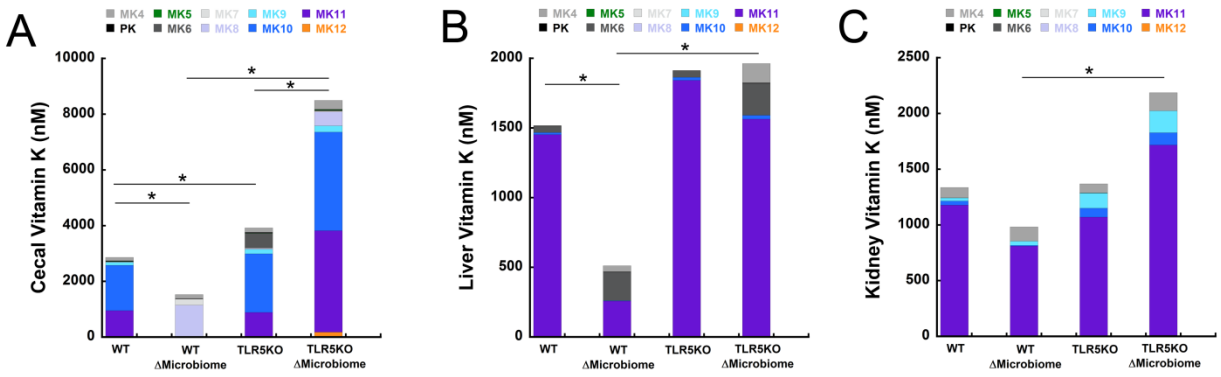

Figure 3.6. Osteocalcin content in the humerus of mice.

Osteocalcin content in the humerus of mice displayed trends similar to those seen in Raman spectra (Fig. 3.4) and tissue vitamin K concentrations (Fig. 3.5). $p = 0.13$ with ANOVA.

Chapter 3.5 Discussion

We demonstrate for the first use of a metagenomic analysis of the fecal microbiota to identify causes for modifications in bone tissue material properties. We found that the functional capacity of the gut microbiome was differentially regulated by oral antibiotics in WT and TLR5KO mice, and that the abundance of genes associated with vitamin-K production in the gut microbiota were altered. Differences in the metagenome were associated with changes in bone tissue crystallinity and the concentrations of vitamin K in the cecum and internal organs. We interpret these findings to suggest that modifications to the functional capacity of the gut microbiome in WT mice can lead to modifications in vitamin K secreted by the gut flora that are associated with insufficiencies in bone tissue matrix composition and quality.

The changes in bone tissue chemistry observed here are consistent with modifications in whole bone mechanical performance reported previously for this cohort (Fig. 3.1). Crystallinity has previously been correlated with bone tissue strength and/or stiffness in humans and animals [115,116,219]. The reduction in matrix crystallinity in WTΔMicrobiome mice is consistent with the reductions in whole bone strength that are not explained by geometry in WT mice (Fig. 3.1, blue lines). In contrast, in the TLR5KO mice, disruption of the gut microbiome is associated with increased matrix crystallinity, yet there was no noticeable change in the relationship between whole bone strength and geometry (Fig. 3.1, red line). We interpret these findings as suggesting that ΔMicrobiome led to a deficiency in matrix quality in WT mice but did not cause such deficiencies in TLR5KO mice. In contrast, nanoindentation measures did not differ among groups, a fact we attribute to the fact that mechanical failure under three-point bending is due to excessive tensile stresses, while nanoindentation assesses the matrix mechanical performance under compressive stresses.

Although the metagenomic analysis identified differences among groups in the overall functional capacity of the gut microbiome, and specifically the abundance of genes related to vitamin synthesis, cell wall and capsule synthesis, and carbohydrate synthesis, the current study focused on vitamin synthesis as the factor most likely to influence bone tissue quality (as opposed to bone quantity). While components of the cell wall and capsule can migrate to the bone and influence bone remodeling and likely bone volume or density [98], no mechanism linking microbial cell wall/capsule components to altered bone tissue constituents has been proposed. Additionally, our prior taxonomic analysis of the gut flora this cohort [133] suggests that the differences in functional capacity of the bacterial cell wall and capsule in the current study may simply reflect differences in taxonomy. Specifically, ΔMicrobiome was associated with increases in the abundance of genes associated with production of Gram negative cell capsule components and our prior 16S rRNA analysis indicated increases in the abundance of organisms from the Gram negative phyla *Proteobacteria*. Similarly, ΔMicrobiome was associated with reductions in abundance of genes associated with Gram positive cell capsule components while our prior report showed reductions in the abundance of organisms from the Gram positive phyla *Firmicutes*. Second, although carbohydrate synthesis can influence the production of molecules such as short chain fatty acids that have been associated with changes in bone formation and remodeling [149], a mechanism through which short chain fatty acids lead to altered bone tissue quality has not yet been proposed.

The observed differences in the abundance of genes associated with vitamin synthesis led to follow up biochemical analyses focused on vitamin K. Vitamin K has long been associated with bone health [201,202]. Concentrations of vitamin K in the cecum and kidney varied among groups in patterns mimicking variation in matrix crystallinity, supporting the idea that reductions

in microbe-derived vitamin K is correlated with impaired bone tissue mechanical performance. Microbe-derived forms of vitamin K (menaquinones 5-13) dominated the total amount of vitamin K and differences among groups, further suggesting a microbiome-based modulation of vitamin K as a potential factor that can influence whole bone strength.

Although vitamin K may influence bone tissue quality in multiple ways, the best understood mechanism is γ carboxylation of gamma-carboxyglutamic (Gla-) containing proteins [220]. The body contains many vitamin K-dependent proteins, however, the vitamin K-dependent protein osteocalcin is the most abundant non-collagenous protein in bone tissue and is known to influence bone tissue mechanical properties [221,222]. Vitamin K-dependent γ carboxylation of osteocalcin is required for proper binding of osteocalcin to bone tissue [220,223]. Interestingly, our preliminary biochemical analysis of bone tissue shows trends suggesting variation in matrix-bound osteocalcin among groups that are similar to those seen in matrix crystallinity and cecal and kidney vitamin K concentrations (decreased in WTΔMicrobiome and increased in TLR5KOΔMicrobiome, Fig. 3.6). Furthermore, the variation in crystallinity measured by Raman spectroscopy in the study is also consistent with modifications to the concentration of non-collagenous proteins such as osteocalcin. Crystallinity is descriptive of the size, perfection, and maturity of hydroxyapatite crystals [115]. Non-collagenous proteins such as osteocalcin, matrix Gla protein, and osteopontin can regulate and direct the formation and size of collagen fibrils, as well as mineralization and crystal nucleation, leading to changes in crystallinity [224-229]. Indeed, osteocalcin-deficient mice have altered bone mineral crystal size and decreased crystallinity, similar to the response to WTΔMicrobiome mice [230]. Although limited samples were used for the biochemical analysis of osteocalcin, when viewed in the context of biomechanical findings in this cohort (Fig. 3.1), the metagenomics findings, Raman spectroscopy, cecal and tissue vitamin

K concentrations, the current study provides preliminary evidence that the microbiota may regulate bone tissue quality through the synthesis of vitamin K (Supplemental Fig 3.11). These findings illustrate how metagenomics analysis of the microbiota can be used to generate hypotheses regarding the underlying mechanisms of altered bone strength.

We previously measured a small but significance difference in bone tissue quality between untreated WT and TLR5KO mice (Fig 3.1). Differences in mechanical function of bones between the two mouse strains may be a result of other differences in the composition and functional capacity of the gut microbiome between the two mouse strains (Fig 3.2A-B, Fig 3.3A-D, Supplemental Fig 3.8A-D) or potentially due to systemic inflammation and metabolic syndrome seen in untreated TLR5KO mice. Previous studies have found obesity and the metabolic syndrome to impair bone mass and bone strength in mice, although the findings are mixed and depend on methods of inducing inflammation/obesity [231-234]. Lastly, it is possible that the impaired immune system and/or effects of microbial products such as short chain fatty acids or microbe associate molecular patterns are influencing bone quality, although a mechanism for these factors to influence bone tissue quality (as opposed to quantity) has not yet been proposed.

Several strengths in the study are worth noting. To our knowledge the current study is the first to associate changes in the gut flora metagenomic profiles with bone phenotypes. Previous studies have reported changes in phylogenetic profile using 16S rRNA sequencing [41,133,149,192]. Because many different microbes have the same functional capacity, a shift in the phylogenetic population in the gut microbiota may not represent differences in the functions of the microbiota that influence the host. Metagenomic analysis, therefore, provides more information about potential links between the microbiome and bone. Second, to our knowledge, the current study is

the first to evaluate how alterations to the gut microbiome can influence bone tissue composition and material properties. Most previous studies have focused on how the gut microbiome can influence bone microstructure and bone remodeling, but have not reported bone mechanical performance, a trait that is more directly related to fracture risk. Lastly, the vitamin K assays allowed for the differentiation between dietary and microbe-derived forms of vitamin K. Previous studies evaluating vitamin K and bone phenotype in rodents have been restricted to phylloquinone or only one menquinone [235-237].

Despite the strengths of the current study, a few limitations must be considered when interpreting the findings. First, as with many metagenomic analyses, the current study was hypothesis-generating and, as molecules of interest were not known a priori, it was not possible to design the study with statistical power for all follow up biochemical assays (matrix osteocalcin in particular, Fig 3.6). Despite this limitation, the trends in osteocalcin, cecal and kidney vitamin K and bone tissue crystallinity were all consistent with one another, supporting a potential microbiome – vitamin K - matrix osteocalcin mechanism. However, the effects of vitamin K may be a result of other vitamin K-dependent molecules in bone tissue (matrix Gla protein, etc.) or other ligands of vitamin K in the body (the pregnane X receptor, for example [238]). Additionally, although Raman spectroscopy is useful for examining chemical composition, other modifications in tissue composition may not be detectable through Raman spectroscopy, especially because the technique examines only a small region of each specimen. However, the current study provided more spectra per bone sample than many studies investigating bone tissue composition in mice using Raman spectroscopy [219,239-241]. Third, the biochemical analysis focused only on vitamin K in the cecum, liver, and kidney. Future studies will require a more comprehensive testing of other

key potential factors such as vitamin B, circulating MAMPs such as LPS, and intestinal short-chain fatty acids.

In conclusion, we find that disruption of the gut microbiome leads to drastic shifts in the overall functional capacity of the gut microbiome that can differ among mouse strains. We observed shifts in functional capacity of the gut microbiota that were associated with changes in bone mineral crystallinity, the degree of carbonate substitution, and concentrations of microbially-derived forms of vitamin K in the body. Together our findings support the use of metagenomics for a microbiome analysis, and provide preliminary evidence for a mechanism in which production of vitamin K by the gut flora may influence downstream pathways responsible for bone tissue composition and structure.

Chapter 3.6 Acknowledgements

This publication was supported in part by the National Institute of Arthritis and Musculoskeletal and Skin Diseases of the National Institutes of Health (U.S) under Award Number AR068061 and by the Department of Defense Congressionally Directed Medical Research Programs under Award Number W81XWH-15-1-0239. The content of the work is solely the responsibility of the authors and does not necessarily represent the official views of the National Institutes of Health or the Department of Defense. Additional funding was obtained from the USDA ARS Cooperative Agreement 58 -1950 - 7 -707. Any opinions, findings, or conclusion expressed in this publication are those of the authors and do not necessarily reflect the view of the US Department of Agriculture.

Authors' roles: Conceived and designed the experiments: JDG, CJH, RCB, SLB, MKS, DV, SPB, ED. Performed the experiments: JDG, SR, ZR, CHH, CJT, MKS. Analyzed data:

JDG, CJH, ET. Wrote and Revised Manuscript: JDG, CJH. Critical revision and final approval of the manuscript: All authors.

Chapter 3.7 Supplemental Material

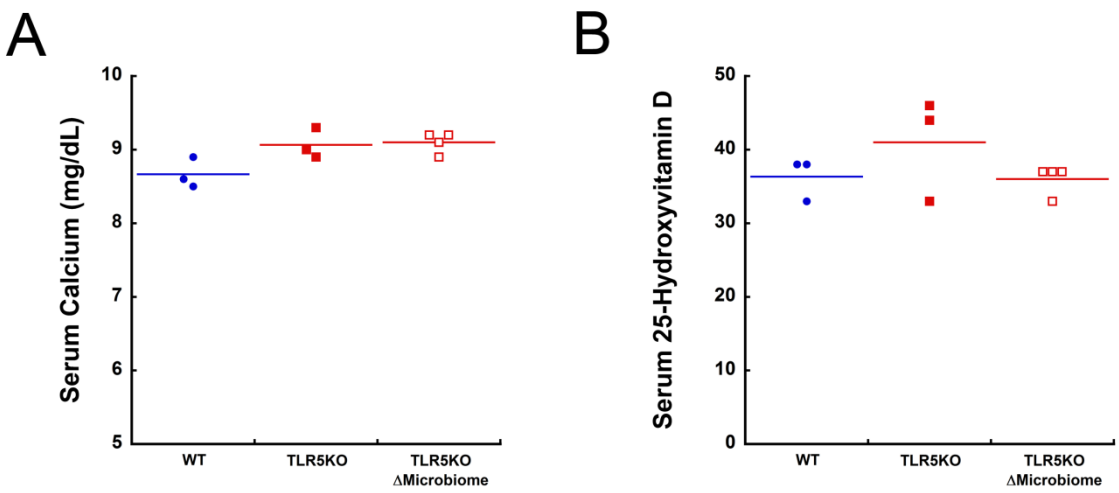

Figure 3.7. Serum calcium and serum 25-hydroxyvitamin D are similar in a small subset of animals

Serum calcium and serum 25-hydroxyvitamin D in a small subset of animals. Serum measures were taken from a small subset of animals. (A) Serum calcium and (B) serum 25-hydroxyvitamin D were similar among groups. Serum total 25(OH)D was measured using LC/MS/MS (Waters Acquity UPLC with TQD triple quadrupole mass spectrometer) and NIST standards for assay calibration. Serum calcium was measured on an automated clinical chemistry analyzer (Olympus AU400; Olympus America Inc., Melville, NY, USA).

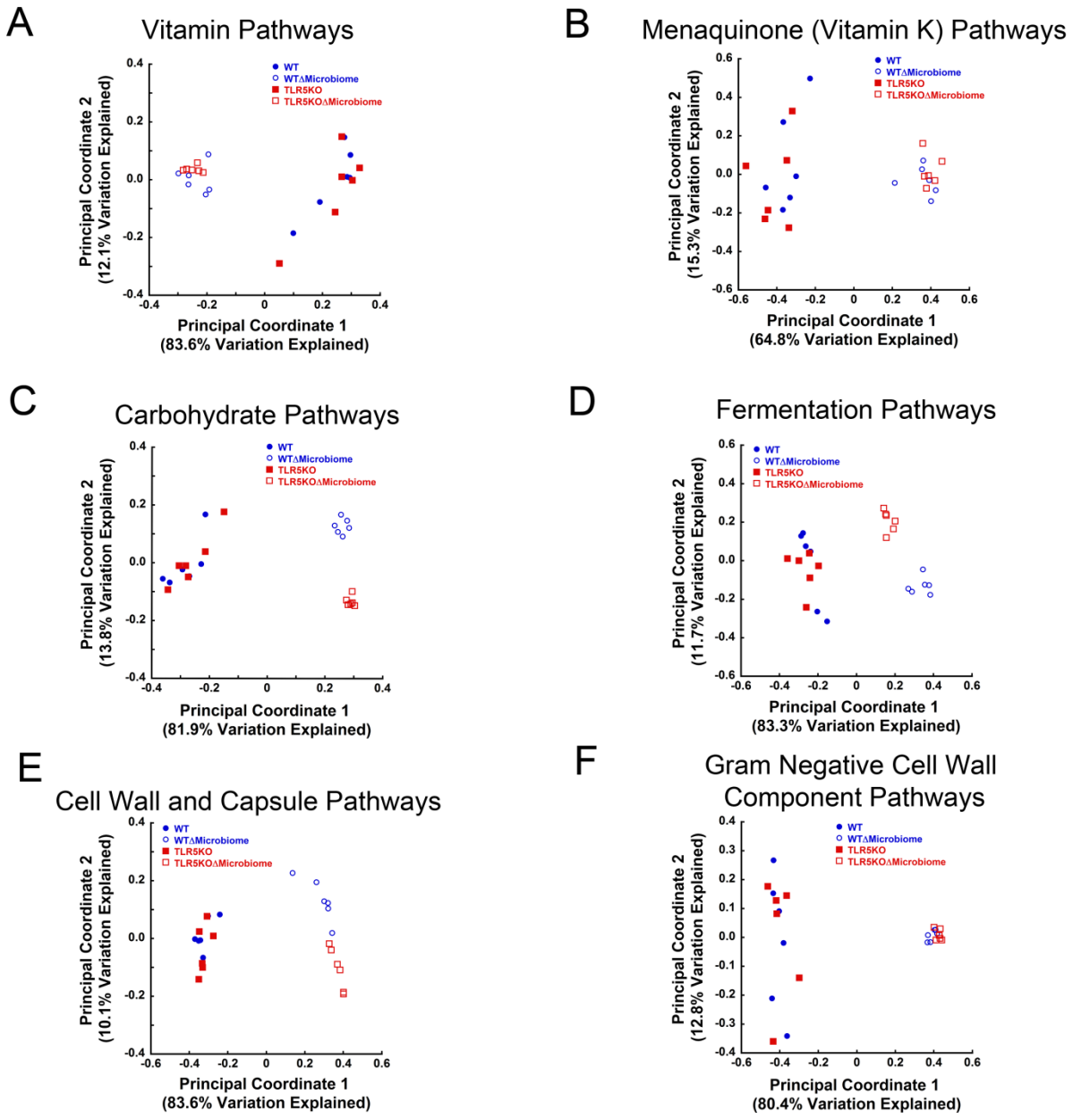

Figure 3.8. Principle coordinate analysis of key pathways demonstrate the effects of disruption of the gut microbiome

Principal coordinate analysis of key pathways demonstrated the effects of disruption of the gut microbiome. Disruption of the gut microbiome led to drastic changes in the overall functional

capacity of genes for (A) Vitamin synthesis, (B) Menaquinone (Vitamin K-2) synthesis, (C) carbohydrate pathways, (D) fermentation, (E) bacterial cell wall and capsule components, (F) Gram negative cell wall components (such as LPS).

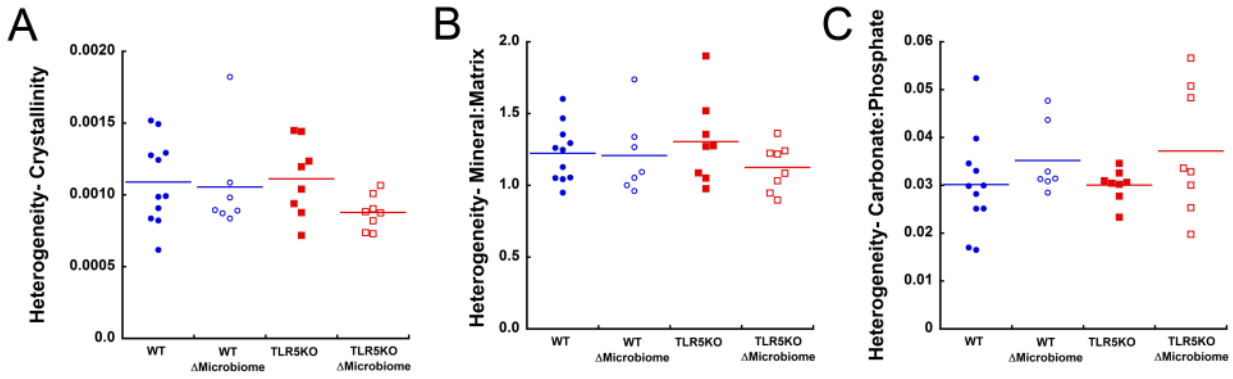

Figure 3.9. Heterogeneity in Raman measurements were similar among groups.

High density spatially resolved maps of 121 spectra were taken with Raman spectroscopy on the posterior region of a tibial diaphysis cross section (n=7-10/group). The heterogeneity per sample was calculated from the full-width-half-max of a Gaussian fit of the distribution of each Raman measure. The heterogeneity of (A) crystallinity, (B) mineral:matrix, and (C) carbonate:phosphate were similar among groups.

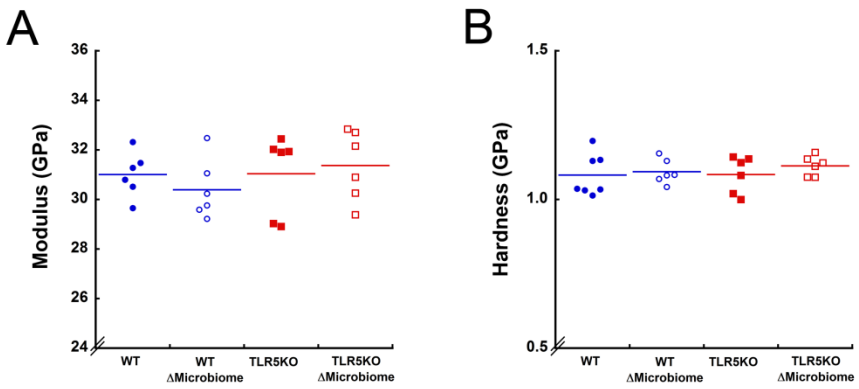

Figure 3.10. Bone tissue material properties were similar among groups.

Bone tissue material properties in the tibial diaphysis were assessed with nanoindentation. (A) Modulus and (B) hardness were similar among groups.

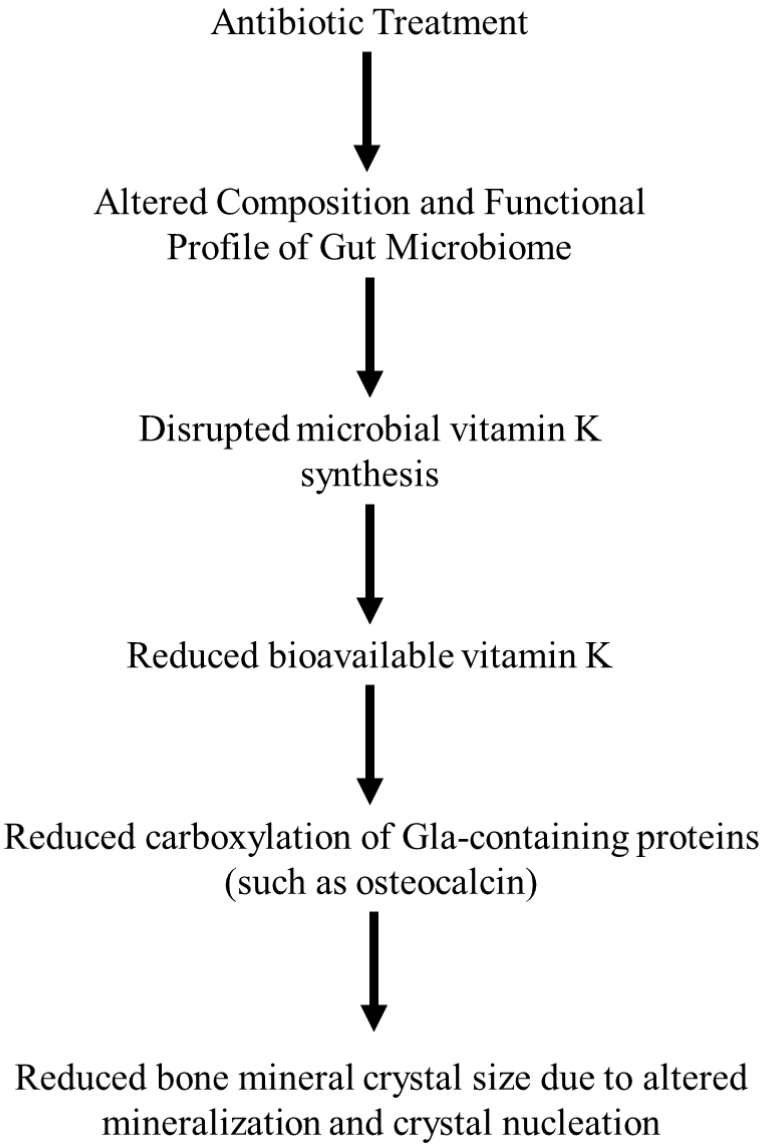

Figure 3.11. Proposed vitamin K and microbiome dependent pathway for modifying bone tissue material properties

Chapter 4- Alterations to the Gut Microbiome and Osteoarthritis

This chapter has been accepted into the journal *Osteoarthritis and Cartilage*. The article is titled "The effects of metabolic syndrome, obesity, and the gut microbiome on load-induced osteoarthritis".

Chapter 4.1 Abstract

Metabolic syndrome is characterized by obesity, hyperglycemia, hypertension, insulin resistance, and dyslipidemia. Metabolic syndrome is associated with osteoarthritis (OA), but it is unclear if the association is attributable to increased mechanical loading on joints caused by obesity or other aspects of metabolic syndrome. Here we examined the effects of metabolic syndrome, obesity, and the gut microbiome on load-induced OA. Cartilage damage was induced through cyclic compressive loading in four groups of adult male mice: Toll-like receptor-5 deficient (TLR5KO) mice that develop metabolic syndrome due to alterations in the gut microbiome, TLR5KO mice submitted to chronic antibiotics to prevent metabolic syndrome (TLR5KOΔMicrobiota), C57BL/6J mice fed a high fat diet to cause obesity (HFD), and untreated C57BL/6J mice (WT). Loading was applied for 2 weeks (n=10-11/group) or 6 weeks (n=10-11/group).After 2 weeks of loading, cartilage damage (OARSI score) was not different among groups. After 6 weeks of loading, HFD mice had increased load-induced cartilage damage, while TLR5KO mice had cartilage damage comparable to WT mice. TLR5KOΔMicrobiota mice had less cartilage damage than other groups. HFD mice had elevated serum inflammatory markers. Each group had a distinct gut microbiome composition. Conclusions: Severe obesity increased load-induced cartilage damage, while milder changes in adiposity/metabolic syndrome seen in TLR5KO mice did not. Furthermore, the effects of systemic inflammation/obesity on cartilage damage depend on the duration of mechanical

loading. Lastly, reduced cartilage damage in the TLR5KOΔMicrobiota mice suggests that the gut microbiome may influence cartilage pathology.

Chapter 4.2 Introduction

Metabolic syndrome is a cluster of conditions including abdominal obesity, hyperglycemia, hypertension, insulin resistance, and dyslipidemia that put an individual at increased risk of developing type 2 diabetes. Recent evidence suggests that abnormalities related to metabolic syndrome may exacerbate osteoarthritis (OA) pathology [242,243]. Understanding the mechanisms relating metabolic diseases and OA has the potential to improve prevention and treatment of joint disease.

Obesity is a well-recognized clinical risk factor for OA. The association between obesity and OA is commonly attributed to increases in joint loading associated with increased body mass. However, rates of OA in non-load bearing joints are greater in patients with obesity [244,245], a finding that suggests that systemic factors contribute to the risk of OA [242,246-248]. Further supporting the idea that systemic factors influences OA, patients with type 2 diabetes and metabolic syndrome have increased risk of OA [70,246,248-251], although it is unclear if the association with OA is due to increases in body mass or systemic factors.

Animal models are useful for studying the relationship between OA and metabolic syndrome. Mice fed a high fat diet (HFD) to induce an obese, diabetic state display accelerated progression of OA in both aging and surgical destabilization models of OA, and develop more severe OA after intra-articular fracture [252-254]. Leptin receptor-deficient mice (db/db) display severe obesity and develop more intense degradation of the joint following surgically-induced OA [255,256]. A limitation of these mouse models of obesity (leptin (ob/ob) or leptin-receptor deficient mice (db/db) and mice fed a HFD), is that they display severe obesity and

hyperglycemia that is more representative of a diabetic state [22,257] than that of metabolic syndrome (Table c). Furthermore, leptin is involved in mechanisms that affect chondrocyte metabolism and cartilage health [258,259], making it difficult to separate the effects of obesity from those of leptin dependent pathways in the db/db and ob/ob mice. To date the relationship between obesity, metabolic syndrome, and OA has only been studied in animals using post-traumatic, surgically-induced, or aging OA models. Little is known about the effect of in-vivo loading models that produce more modest OA pathology.

Table c Metabolic characteristics of mouse models used to study the effect of obesity, systemic inflammation and/or type 2 diabetes on OA compared to TLR5KO mouse

Metabolic Measure (Reported % Increase Compared to WT Control)	C57BL/6J Fed High Fat Diet- 60% Calories from fat	Leptin Receptor Deficient (db/db)	Leptin Deficient (ob/ob)	Toll-like receptor 5 Deficient (TLR5KO)
Blood glucose	149%[254]	159%[255]	Not reported in OA studies	16%[7]
Body mass	73%[253]; 54%[254]	47%[255]; 210%[256]	252%[256]	23%[7]
Adiposity	251%[253]	229%[256]	219%[256]	173%[7]

Obesity and the metabolic syndrome are also associated with changes in the gut microbiome [260]. The gut microbiome is the collection of trillions of micro-organisms that inhabit the gastrointestinal tract and play a key role in host metabolism, immune function, and nutrition [261]. The Toll-like receptor 5 deficient mouse (TLR5KO) spontaneously develops a metabolic syndrome phenotype due to alterations in functions of the gut microbiome. TLR5 is the receptor for bacterial flagellin, and does not have an endogenous ligand. TLR5KO mice exhibit mild hyperglycemia, mild insulin resistance, and a mild obesity [7]. TLR5KO mice do not develop metabolic syndrome when raised germ-free (never exposed to microbes) or when

submitted to chronic oral antibiotics that disrupt the gut microbiome. Therefore, the TLR5KO mouse provides a model of metabolic syndrome that can be averted by manipulating the gut microbiome.

Although prior work has indicated that metabolic abnormalities in severe obesity can influence OA development and severity, no studies have examined a mouse model of metabolic syndrome without severe obesity. Additionally, few studies have attempted to understand how manipulation of the gut microbiome may influence OA. In the present study, we tested the hypothesis that metabolic syndrome without severe obesity exacerbates the development of OA. Specifically, we used a non-surgical, load-induced model of OA and a gut-microbiome dependent model of metabolic syndrome to determine: 1) how the metabolic syndrome affects the development of load-induced OA pathology; and 2) how modification of the gut microbiota to prevent the metabolic syndrome phenotype affects the development of OA pathology.

Chapter 4.3 Materials and Methods

Chapter 4.3.1 Study Design

Animal procedures were approved by the Cornell Institutional Animal Care and Use Committee. C57BL/6J and TLR5KO (congenic strain B6.129S1-Tlr5tm1Flv/J) were acquired (Jackson Laboratory, Bar Harbor, ME) and bred via homozygous mating in a conventional animal facility. Animals were housed in plastic cages filled with ¼-inch corn cob bedding (The Andersons' Lab Bedding, Ohio), provided standard laboratory chow (Teklad LM-485 Mouse/Rat Sterilizable Diet) and water *ad libitum*, and provided a cardboard refuge environmental enrichment hut (Ketchum Manufacturing; Brockville, Ontario). Male mice were divided into four groups): 1) control C57BL/6J mice (WT); 2) TLR5KO mice that develop metabolic syndrome; 3) TLR5KO

mice receiving broad-spectrum antibiotics in their drinking water (1.0 g/L ampicillin, 0.5 g/L neomycin) to prevent the development of the metabolic syndrome phenotype (TLR5KOΔMicrobiota) [7]; and 4) C57BL/6J mice fed a HFD (60% energy from fat, Test Diet 58Y1) to induce severe obesity and a diabetic-like state (HFD) [22]. Antibiotic use and HFD began at 4 weeks of age and continued until euthanasia. The antibiotics used are poorly absorbed in the gut and therefore target the gut microbiota without influencing other regions of the body. Animals were housed 3-4 to a cage with others from the same treatment group.

Chapter 4.3.2 In-Vivo Cyclic Compression

At 20 weeks of age animals began daily, non-surgical, in vivo loading of the left tibia to induce cartilage damage. The procedure has been shown to induce cartilage damage as soon as two weeks after loading begins [262]. Compressive cyclic loading was applied to the left tibia with a 4.5N peak load for 1,200 cycles at 4 Hz for 5 days per week. The right hindlimb served as a non-loaded contralateral control. The mice were placed under general anesthesia (2% isoflurane, 1L/min) while loading was applied. Animals were exposed to loading for either 2 weeks (n=10-11/group) or 6 weeks (n=10-11/group). The sample size was determined through a priori power analysis.

Animals were euthanized after loading was completed (at 22 or 26 weeks of age). Upon euthanasia, right and left limbs and epididymal fat pads were harvested. Blood was collected through cardiac puncture at euthanasia. The knee joints from both limbs were dissected and fixed in 4% paraformaldehyde for 24 hours. Fecal pellets were collected on the day prior to euthanasia and stored at -80°C prior to analysis.

Chapter 4.3.3 Subchondral Bone and Trabecular Microarchitecture

Knee joints from animals loaded for 6 weeks were suspended in 70% ethanol and scanned by microcomputed tomography (μCT35; Scanco Medical AG, Switzerland; 55 kVp, 145 μA, 600 ms integration time, 10 μm voxel size). Images were collected at the subchondral bone plate and proximal epiphysis. An average global threshold for all samples was determined to segment mineralized and non-mineralized tissue [108] . Measures of the subchondral bone plate included thickness and tissue mineral density (TMD). Trabecular bone microarchitecture of the proximal epiphysis was examined in a region extending from the end of the subchondral bone plate to the start of the growth plate. Measurements of trabecular microarchitecture included bone volume fraction (BV/TV), trabecular thickness (Tb.Th), and trabecular separation (Tb.Sp).

Chapter 4.3.4 Assessment of Osteoarthritis in Histology Sections

Knee joints were decalcified in EDTA for 2 weeks, dehydrated in increasing ethanol gradients, and embedded in paraffin. Serial coronal sections, 6 μm thick, were taken. Sections spaced at 90 μm intervals were stained with Safranin O/Fast green for histological scoring and assessment of cartilage morphology. The OARSI scoring system was used to assess degenerative changes resulting from loading [263]. Baseline cartilage composition and cellularity in control limbs was assessed by a modified Mankin scoring system [264]. Localized thickness of cartilage was measured on sections used for histological scoring (Osteomeasure, OsteoMetrics, USA).

Chapter 4.3.5 Metabolic and Inflammatory Blood Serum Measurements

Serum was stored at -80°C and sent to the Duke Molecular Physiology Institute Biomarkers Shared Resource for analysis. Serum from 26 week old animals (n=6-10/group) was measured using a custom Proinflammatory Panel (Meso Scale Diagnostics; Rockville, Maryland) measuring IL-1β, IL-6, IL-12p70, KC, IL-10, and TNF-α, a Mouse Metabolic Kit (Meso Scale Diagnostics; Rockville, Maryland) to assess leptin and insulin, and an EndoZyme kit (Hyglos;

Bernried, Germany) to measure serum lipopolysaccharide (LPS, a bacterial molecular product). Values for IL-12p70 were below the limits of detection and were excluded (Supplementary Table f).

Chapter 4.3.6 Gut Microbiota Analysis

DNA was isolated from fecal pellets using the Mo Bio PowerSoil DNA Isolation Magnetic kit with the recommended proteinase K step to assist in cell lysis. 16S rRNA libraries were prepared using the Earth Microbiome Project protocol [162] with primers as described previously [265]. Paired-end 150x150 reads were imported into QIIME2 (https://qiime2.org) [163] and demultiplexed. The samples were analyzed using DADA2, which removes chimeric sequences, and retains unique *de novo* sequence variants [266]. Taxonomies were assigned using QIIME's machine learning classifier trained on Greengenes sequences.

Chapter 4.3.7 Statistics

The effect of load and group on OARSI score, micro-CT measures, and cartilage thickness were detected using a 2-factor repeated measures ANOVA with interactions that included individual as a random effect (JMP Pro 9.0.0). Group differences between histological scores, micro-CT measures, serum measures, body mass, and fat pad mass were determined using a one-way ANOVA with group as the factor followed by the Holm correction for multiple comparisons with α=0.05. A multivariate analysis was used to create a matrix of Pearson's product-moment correlation coefficients to identify linear relationships between OARSI and Mankin scores and indicators of systemic inflammation and metabolic syndrome (body mass, fat pad mass, serum markers) within the 6 week groups. An analysis of covariance was performed to determine if any correlations were explained by group. A Pearson's product-moment correlation

analysis was used to identify relationships between loaded limb OARSI scores and control limb subchondral bone measures.

Chapter 4.4 Results

Chapter 4.4.1 Body Mass, Fat Pad Mass, and Metabolic Profile

Body mass and serum markers of metabolism exhibited the following patterns: severe obesity in HFD mice, mild obesity in TLR5KO mice, and normal body mass in WT and TLR5KOΔMicrobiota mice. Body mass and fat pad mass were greatest in HFD mice (Fig 4.1A-1B). Body mass and fat pad mass were greater in TLR5KO mice than in WT mice or TLR5KOΔMicrobiota mice. HFD mice had the greatest serum levels of insulin (Fig 4.1C) and leptin (Fig 4.1D). TLR5KO mice had greater serum levels of insulin and leptin compared to WT mice. Mean body mass, serum insulin and serum leptin were similar between the TLR5KOΔMicrobiota and WT mice.

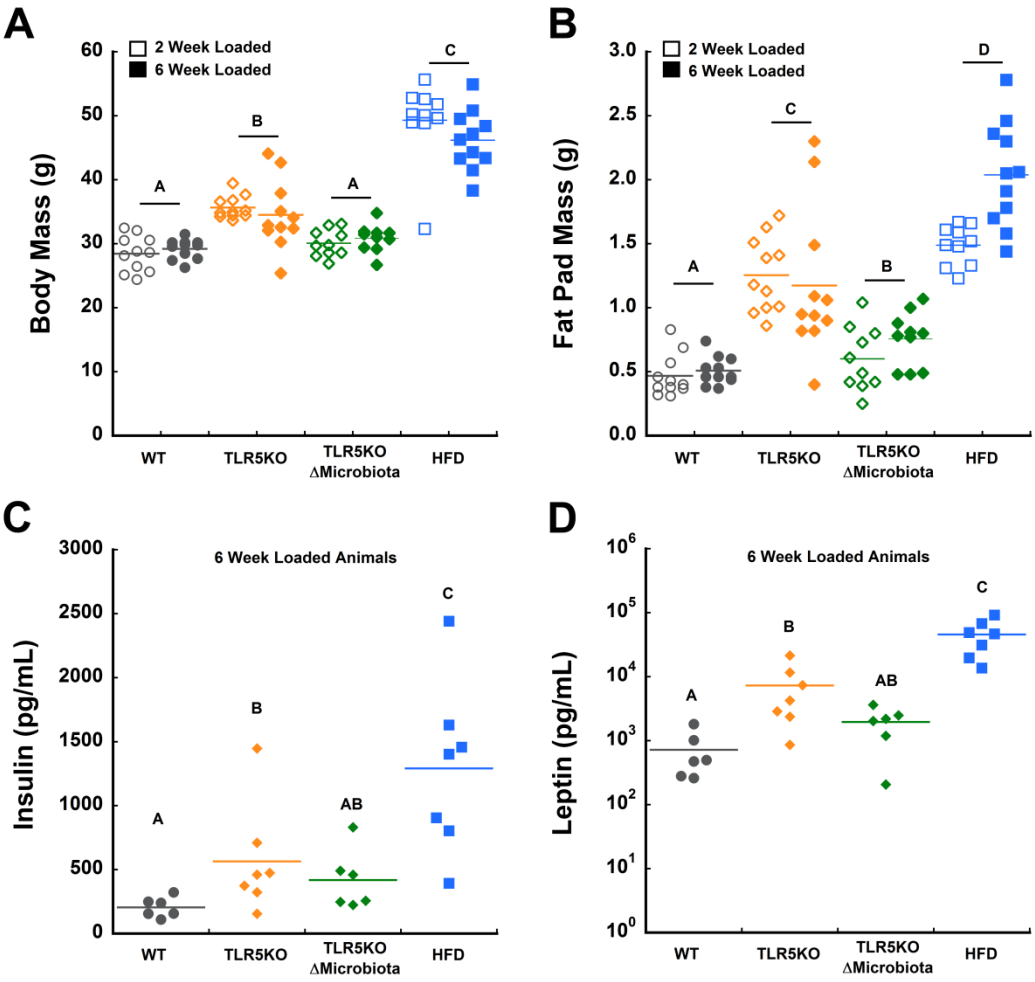

Figure 4.1. Metabolic phenotype of mice with an altered gut microbiome and fed a high fat diet.

TLR5KO mice displayed hallmarks of metabolic syndrome including increased (A) body mass, (B) epididymal fat pad mass, (C) serum insulin levels, and (D) serum leptin levels compared to WT mice. High fat diet mice had increased levels of adiposity, insulin, and leptin. Body mass and epididymal fat pad mass are pooled from 22 week and 26 week old animals. Serum is from 26-week old mice. Solid colored lines on dot plots represent the mean value. Groups sharing the same letter are not significantly different from each other ($p < 0.05$)

Chapter 4.4.2 Histology and Osteoarthritis Cartilage Pathology

Mechanical loading caused cartilage damage as measured by OARSI score following either 2 weeks (95% confidence interval of difference between groups: [0.05, 0.18]) or 6 weeks

of loading (Fig 4.2A-B, [0.10, 0.32]). At 2 weeks of loading, mean OARSI scores were similar among the loaded limbs of the four groups (Fig 4.2A). After 6 weeks of loading, HFD mice had greater OARSI scores with more surface fibrillations and vertical clefts in the loaded limbs than other groups (Fig 4.2A-B) and TLR5KOΔMicrobiota mice had lower OARSI scores in loaded limbs compared to the other groups. Control limb OARSI scores were similar among groups at 2 weeks of loading. Control limb OARSI scores at 6 weeks of loading were greater in HFD mice compared to TLR5KOΔMicrobiota mice. Control limb Mankin scores of HFD mice and TLR5KOΔMicrobiota mice were greater than those in WT mice at 6 weeks (Fig 4.2C), but were similar in animals that received loading for 2 weeks (Supplemental Fig 4.6). Cartilage thickness did not differ among groups (Supplemental Fig 4.7). No effect of mechanical loading on cartilage thickness was detected.

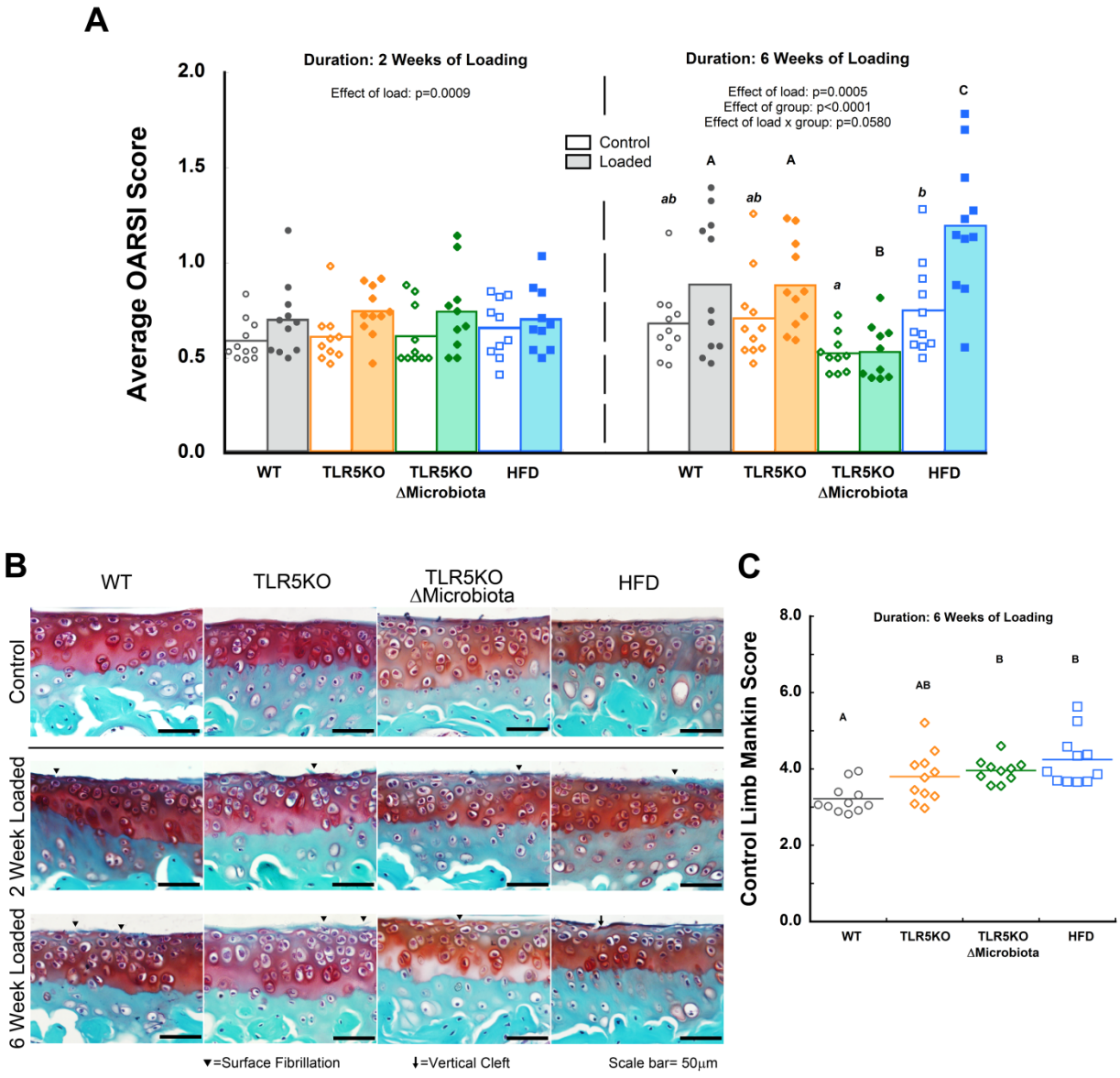

Figure 4.2. The effects of altering the gut microbiome and obesity on load-induced cartilage damage

Twenty-week old male mice were subjected to either 2 or 6 weeks of cyclic mechanical loading to induce OA pathology. (A) After both 2 weeks and 6 weeks of mechanical loading there was an effect of load on OA pathology as measured by OARSI score. No differences the effect of loading were observed among groups at 2 weeks, however, after 6 weeks of loading, HFD mice had elevated loaded limb OARSI scores compared to other groups, and TLR5KOΔMicrobiota mice had lower loaded limb OARSI scores (upper case letters used to denote group differences of loaded limb OARSI scores). Control limb OARSI scores were greater in HFD mice compared to TLR5KOΔMicrobiota mice after 6 weeks of loading (lower case letters used to denote group differences of control limb OARSI scores). (B) Example histology of control and loaded limbs is

shown with surface fibrillations and vertical clefts identified. (C) Modified Mankin scores were greater in HFD and TLR5KOΔMicrobiota mice compared to WT. Solid colored bars on plots represent mean. Groups sharing the same letter are not significantly different from each other ($p < 0.05$).

Chapter 4.4.3 Subchondral Bone Plate and Cancellous Bone Morphology

Subchondral bone TMD (Fig 4.3A) was lower in TLR5KOΔMicrobiota mice than in other groups. Subchondral bone plate thickness in TLR5KOΔMicrobiota mice (Fig 4.3C) was lower than that in WT and HFD mice. Subchondral bone plate thickness was greater in HFD mice compared to TLR5KO mice (Fig. 4.3A). Loaded limb OARSI scores were correlated with control limb subchondral bone TMD (r=0.69, [0.40, 0.86], Fig 4.3B) and control limb subchondral bone thickness (r=0.66, [0.35, 0.84], Supplemental Fig 4.8). Epiphyseal bone volume fraction was less in HFD mice than in WT mice (Fig 4.3D). Trabecular thickness and trabecular separation were less in TLR5KOΔMicrobiota mice than in other groups (Supplemental Fig. 4.9). Mechanical loading was not associated with alterations in any other measures of bone (Fig 4.3A-B, 4.3D).

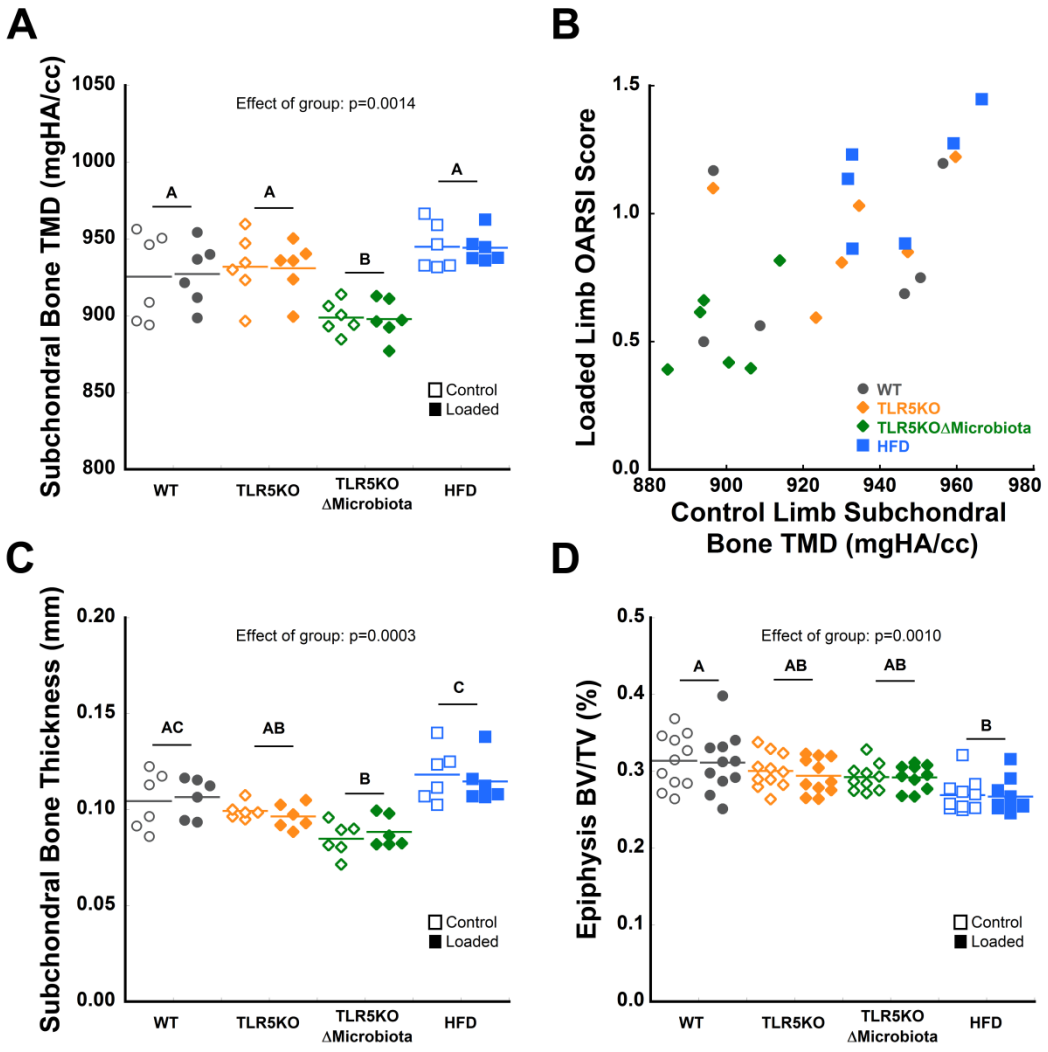

Figure 4.3. The effects of an altered gut microbiome and in-vivo cyclic compression on subchondral bone plate and cancellous bone morphology

Measures of subchondral and epiphyseal bone after 6 weeks of loading are shown. (A) TLR5KOΔMicrobiota mice showed lower levels of subchondral tissue mineral density (TMD). (B) Control limb subchondral bone TMD was correlated with loaded limb OARSI scores (r=0.69, 95% confidence interval of correlation coefficient: [0.40, 0.86]). A Pearson's product moment correlation analysis was used to identify relationships between loaded limb OARSI scores and control limb subchondral bone TMD. (C) TLR5KOΔMicrobiota mice showed lower levels of subchondral bone thickness as compared to other groups. (D) Epiphyseal bone volume fraction was less in HFD mice compared to other groups. Solid colored lines on dot plots represent mean. Groups sharing the same letter are not significantly different from each other ($p < 0.05$).

Chapter 4.4.4 Serum Inflammatory Markers From 6 Week-Loaded Animals

Serum levels of LPS, KC, and IL-10 were greatest in HFD mice (Fig 4.4A, 4.4C, 4.4D, Table d). Serum levels of TNF-α were greater in HFD mice than in TLR5KOΔMicrobiota mice. Serum levels of IL-6 were lower in TLR5KOΔMicrobiota mice compared to WT mice. Serum IL-1 levels did not differ among groups.

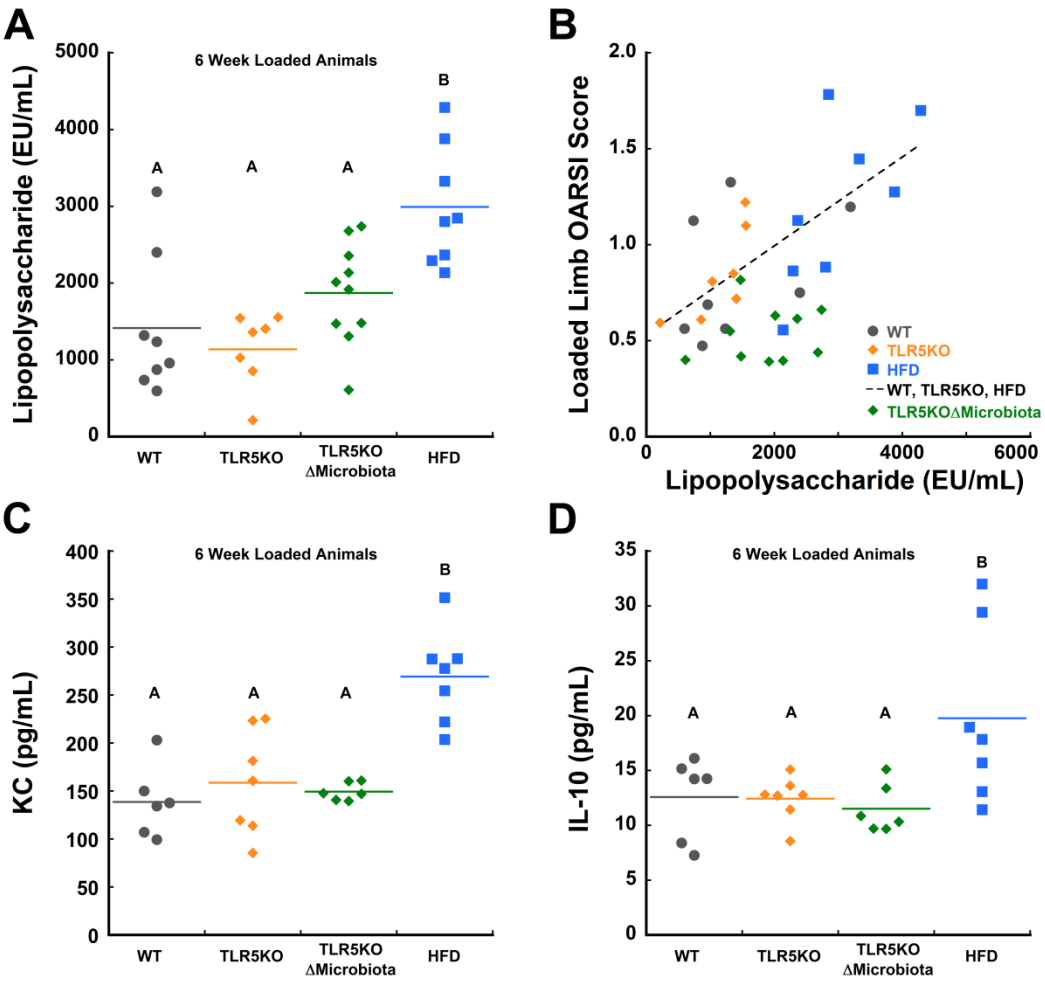

Figure 4.4. Serum inflammatory markers from 6 week-loaded animals.

Serum markers after six weeks of loading are shown. Mice fed a high fat diet had elevated (A) serum lipopolysaccharide (LPS). (B) Serum LPS was correlated with loaded limb OARSI scores in untreated animals. Among the WT, HFD, and TLR5KO groups, LPS explained 44% of the variation in OARSI score across groups (R^2 =0.44, p=0.0003). High fat diet mice also had

elevated serum levels of (C) KC and (D) IL-10. Solid colored lines on dot plots represent mean. Groups sharing the same letter are not significantly different from each other ($p < 0.05$).

Table d Serum markers of cytokines and lipopolysaccharide (LPS)

Serum Measure	WT	TLR5KO	TLR5KOΔMicrobiota	HFD
KC (pg/mL)	139±37.0	159±54.8	149±9.26	269±48.8[a,*,$]
IL-10 (pg/mL)	12.6±3.75	12.4±2.03	11.5±2.23	19.8±7.94[a,*,$]
TNF-α(pg/mL)	7.66±1.31	7.43±1.23	5.94±1.31	9.40±2.32[$]
IL-6 (pg/mL)	30.2±15.9	21.3±11.5	11.4±2.50[#]	18.7±10.6
IL-1β (pg/mL)	0.534±0.192	0.350±0.172	0.447±0.198	0.512±0.158
LPS (EU/mL)	1410±909	1140±484	1870±663	2990±779 [a,*,$]

Values are mean ± SD.
[#]TLR5KOΔMicrobiota vs.WT
[a]HFD vs. WT
[*]TLR5KO v HFD
[$]HFD v. TLR5KOΔMicrobiota

Chapter 4.4.5 Correlations Among Histological Score and Metabolic and Inflammatory Measures

Loaded limb OARSI scores were correlated with body mass (r=0.31, [0.01, 0.56], Table e, Supplemental Fig. 4.10), fat pad mass (r=0.43, [0.15, 0.65], Supplemental Fig. 4.11), KC (r=0.39, [0.00, 0.68]), IL-10 (r=0.41 [0.03, 0.69]), and LPS (r=0.54, [0.24, 0.74]). Of the parameters correlated with loaded limb OARSI scores, LPS was the only parameter that had a significant effect on loaded limb OARSI score when group was included in the regression model. Among the WT, HFD, and TLR5KO groups, LPS explained 44% of the variation in OARSI score across groups (R^2=0.44, p=0.0003, Fig 4.4B). Within the TLR5KOΔMicrobiota mice, LPS was not correlated with OARSI score. Leptin and insulin were not correlated with loaded limb OARSI score. Control limb Mankin scores were correlated with body mass (r=0.48,[0.21, 0.68]), fat pad mass (r=0.47, [0.20, 0.68]), LPS (r=0.48,[0.16, 0.71]), IL-6 (r=-0.41,[-0.69, -0.03]),

insulin (r=0.51,[0.15, 0.75]), leptin (r=0.55, [0.21, 0.77]). Control limb Mankin scores were not correlated with loaded limb OARSI scores.

Table e A correlations matrix of histological scores and metabolic and inflammatory measures after 6 weeks of loading is shown.

	Loaded OARSI	Control OARSI	Control Mankin	Body Mass	Fat Pad Mass	LPS	IL-10	IL-1β	IL-6	KC	TNF-α	Insulin	Leptin
Loaded OARSI		[-0.079,0.493]	[-0.202,0.393]	[0.012,0.560]	[0.153,0.649]	[0.236,0.743]	[0.026,0.688]	[-0.305,0.478]	[-0.107,0.611]	[0.003,0.675]	[-0.241,0.517]	[-0.166,0.572]	[-0.057,0.641]
Control OARSI	0.227		[-0.271,0.330]	[-0.130,0.453]	[-0.074,0.498]	[-0.237,0.442]	[-0.445,0.327]	[-0.371,0.419]	[-0.041,0.651]	[-0.363,0.411]	[-0.398,0.377]	[-0.366,0.408]	[-0.209,0.541]
Control Mankin	0.105	0.032		[0.209,0.682]	[0.199,0.676]	[0.161,0.705]	[-0.144,0.587]	[-0.343,0.445]	[-0.689,-0.028]	[-0.015,0.666]	[-0.184,0.559]	[0.149,0.748]	[0.209,0.774]
Body Mass	**0.312**	0.177	**0.480**		[0.766,0.926]	[0.052,0.645]	[0.214,0.776]	[-0.288,0.492]	[-0.561,0.181]	[0.601,0.907]	[0.326,0.820]	[0.712,0.936]	[0.844,0.968]
Fat Pad Mass	**0.434**	0.232	**0.472**	**0.867**		[0.027,0.631]	[0.052,0.701]	[-0.226,0.541]	[-0.515,0.243]	[0.252,0.791]	[-0.112,0.607]	[0.608,0.909]	[0.721,0.939]
LPS	**0.536**	0.116	**0.478**	**0.388**	**0.336**		[-0.081,0.627]	[-0.292,0.490]	[-0.520,0.236]	[0.250,0.791]	[-0.244,0.514]	[0.008,0.678]	[0.256,0.793]
IL-10	**0.409**	-0.069	0.258	**0.555**	**0.441**	0.316		[0.003,0.685]	[-0.320,0.451]	[0.437,0.858]	[0.390,0.842]	[0.175,0.759]	[0.102,0.726]
IL-1β	0.103	0.029	0.060	0.121	0.173	0.117	**0.397**		[-0.064,0.648]	[-0.136,0.603]	[-0.146,0.597]	[-0.240,0.531]	[-0.375,0.415]
IL-6	0.292	0.352	**-0.411**	-0.222	-0.171	-0.167	0.077	0.340		[-0.413,0.361]	[-0.250,0.509]	[-0.617,0.096]	[-0.594,0.134]
KC	**0.390**	0.029	0.375	**0.802**	**0.570**	**0.581**	**0.705**	0.274	-0.030		[0.334,0.822]	[0.442,0.860]	[0.523,0.885]
TNF-α	0.162	-0.012	0.219	**0.634**	0.332	0.158	**0.675**	0.264	0.152	**0.638**		[0.120,0.734]	[0.085,0.717]
Insulin	0.237	0.025	**0.507**	**0.862**	**0.831**	**0.394**	**0.527**	0.172	-0.302	**0.708**	**0.485**		[0.653,0.922]
Leptin	0.338	0.194	**0.552**	**0.928**	**0.878**	**0.585**	**0.470**	0.024	-0.268	**0.757**	**0.457**	**0.831**	

Bold numbers represent a significant correlation ($p<0.05$). Bottom left half of table are pairwise correlation value (*r*). Top left half of table are confidence interval of correlation.

Chapter 4.4.6 Gut Microbiota Analysis

Gut microbiota composition varied dramatically among groups at both the phyla and class level (Fig 4.5A, Supplemental Fig. 4.12). Gut microbiota composition at the phyla level was dominated by Bacteroidetes and Firmicutes (Fig 4.5B, 4.5C). The relative abundance of Bacteroidetes was greater in WT and TLR5KO mice compared to TLR5KOΔMicrobiota mice. HFD mice had the greatest abundance of Firmicutes. TLR5KOΔMicrobiota mice had the greatest abundance of Proteobacteria (Fig 4.5D). Principal coordinate analysis based on Bray-Curtis dissimilarity indicated that each group uniquely clustered together and had a distinct microbial community structure (Fig 4.5E, Supplemental Fig. 4.13). The diversity of the gut microbiota, as measured by the Shannon Diversity index, was reduced in the TLR5KOΔMicrobiota mice compared to other groups (Fig 4.5F).

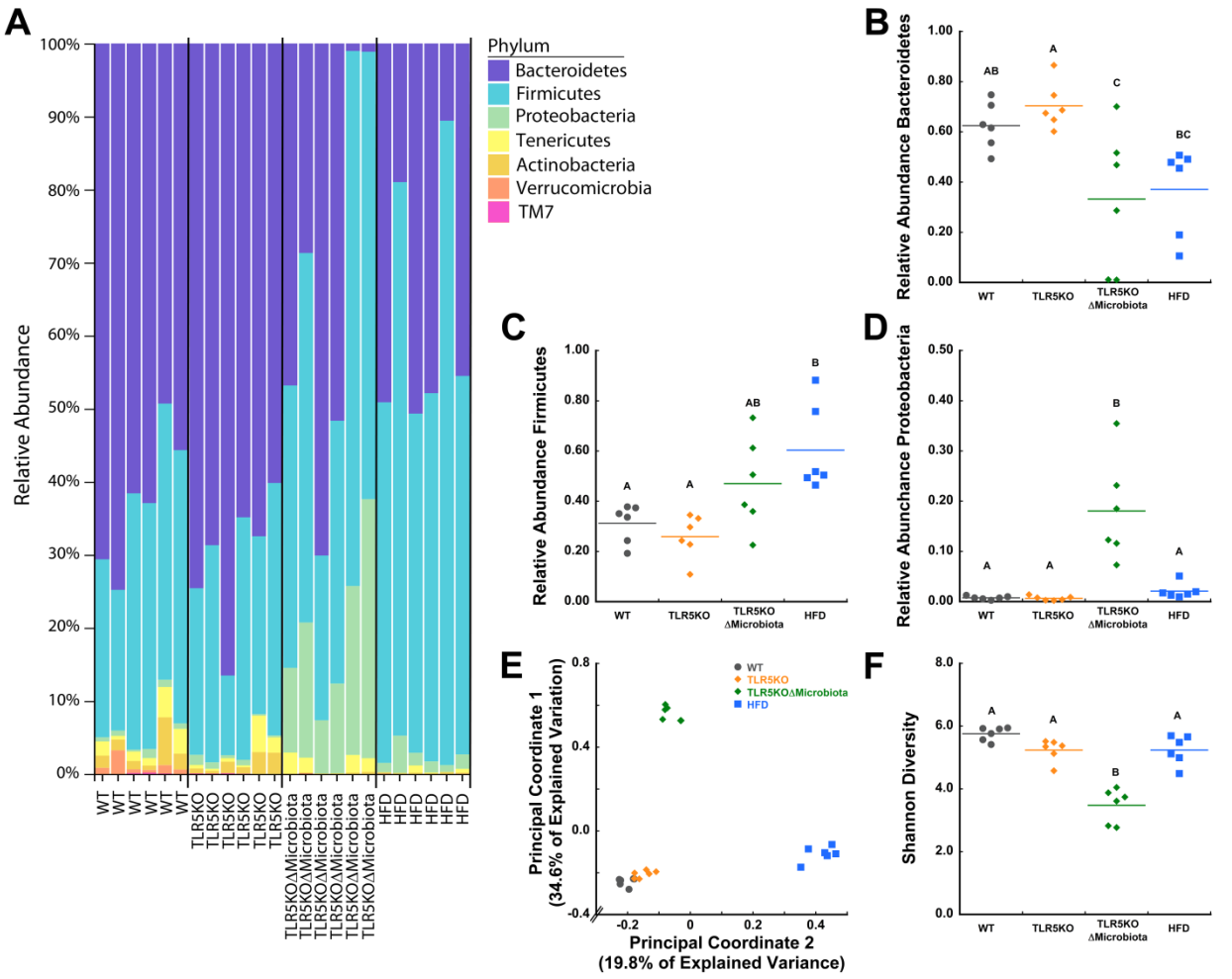

Figure 4.5. Gut microbiome analysis of 6 week-loaded animals

The taxonomic profile of the gut microbiota from animals after six weeks of loading is shown. (A) There are large differences in the relative abundance of organisms at the phyla level. (B) The relative abundance of Bacteroidetes was greatest in TLR5KO and WT mice. (C) The relative abundance of Firmicutes was greatest in HFD mice and (D) the relative abundance of Proteobacteria was greatest in TLR5KOΔMicrobiota mice. (E) Principal coordinate analysis based on the Bray-Curtis dissimilarity shows that each group forms its own distinct clusters from each other. Bacterial diversity was dramatically reduced in TLR5KOΔMicrobiota mice (F). Solid colored lines on dot plots represent mean. * $p < 0.05$

Chapter 4.5 Discussion

In the current study, we examined the role of obesity, a metabolic syndrome-like phenotype, and the composition of the gut microbiome in the development of OA using an in-

vivo tibial loading model. We demonstrate that alterations in obesity, the gut microbiome, and elevated levels of systemic inflammatory mediators can influence the development of load-induced cartilage damage, although the effects require time to manifest. Additionally, we demonstrate that the metabolic syndrome-like phenotype characteristic of the TLR5KO mouse is not sufficient to increase load-induced cartilage damage.

We attribute a portion of the increased load-induced cartilage damage in HFD mice to increased systemic inflammation. We see elevated levels of serum KC in the HFD mice, consistent with previous reports in HFD mice submitted to post-traumatic OA [(253)], and in patients with OA that have increased serum IL-8 (the human analog of KC) [(267)]. The elevated serum levels of IL-10 in HFD mice in the current study may reflect an active anti-inflammatory response to the OA pathology, consistent with findings of elevated levels of IL-10 in the synovial fluid of patients with OA [(268)]. Serum LPS was elevated in HFD mice, and was the only systemic factor examined in this study that explained differences in OARSI score across groups. Serum LPS has been associated with low-grade inflammation and is thought to play a role in the development of OA in individuals with obesity and metabolic syndrome [(269)]. Others have shown that mice fed a high fat diet develop an altered gut microbiome and a more permeable intestinal barrier, leading to elevated LPS levels and systemic inflammation [(270)]. LPS can also initiate local inflammatory responses within the joint that may enhance the effects of mechanical loads [(269)]. Consistent with our results, serum and synovial fluid LPS levels are associated with signs of OA in patients [(271)], supporting a possible role of LPS in the pathogenesis of OA cartilage pathology.

Adiposity is thought to influence OA pathology [(242,272)]. In our study HFD mice had the greatest levels of adiposity and the greatest loaded limb OARSI scores. However, several TLR5KO mice displayed fat pad mass within the range seen in HFD mice, yet did not have

increased OARSI scores in loaded limbs like that seen in HFD mice (Supplemental Fig. 4.11). Additionally, serum factors associated with increased adiposity, such as leptin and insulin, were not associated with loaded limb OARSI score. Hence, our findings suggest that adiposity does not fully explain the increased cartilage damage in the current study.

Our findings suggest that the effects of systemic inflammation, adiposity, and the gut microbiome on load-induced cartilage damage are time dependent. After 2 weeks of loading, loaded limb OARSI scores were similar among groups, but after 6 weeks of loading HFD mice had greater loaded limb OARSI scores. Hence, the additional four weeks of loading may be required for systemic inflammation and adiposity to have an effect on OA cartilage pathology. Similarly, TLR5KOΔMicrobiota mice display less cartilage damage after 6 weeks of loading but not after 2 weeks, suggesting that the effect of the gut microbiome is time dependent as well. The effect of time is not surprising as joint degeneration in humans occurs over decades [(273)]. Our findings may have implications for clinical treatment for patients with obesity or metabolic syndrome. For example, if a patient has a recent load-induced injury subsequent treatments that correct metabolic abnormalities may slow subsequent development and progression of OA.

High fat diet and TLR5KO mice both exhibited clear signs of metabolic abnormalities and excess adiposity, but only HFD mice exhibited signs of more severe OA with prolonged loading. Compared to WT, The HFD mice showed severely elevated insulin levels (530% increase) and severe obesity (261% increase in fat pad mass). The TLR5KO mice had mild increases in insulin levels (175% increase) and mild obesity (149% increase in fat pad mass) compared to WT. We attribute the different degrees of cartilage pathology in the HFD and TLR5KO mice to one of three possibilities: First, the severity of metabolic abnormalities in TLR5KO mice may have been insufficient to worsen cartilage pathology. Larger changes in

systemic inflammation and/or adiposity may be required to increase load-induced cartilage damage. Second, metabolic syndrome and the related systemic environment in the TLR5KO mice may require more time to become evident in cartilage pathology (just as HFD mice required more than 2 weeks). Last, we must consider the possibility that TLR5 signaling within the joint may contribute to OA; TLR5 is expressed at higher levels in synovial tissue of OA patients compared to healthy individuals [(274)].

The TLR5KOΔMicrobiota mice display less cartilage damage after 6 weeks of loading compared to other groups and little difference between the loaded and control limbs. The reduced cartilage damage is likely not explained by adiposity or systemic inflammation, two factors that were comparable in TLR5KOΔMicrobiota and WT mice. The antibiotics used here to disrupt the gut microbiota are poorly absorbed at the gut lining, thus making it unlikely that antibiotics have a direct effect on joint tissues. Others have shown that oral antibiotic treatment can lead to reduced OA joint pathology in humans [(275)] and animals [(276)]. We consider the most likely explanation for the reduced cartilage damage in the TLR5KOΔMicrobiota mice is alterations in the gut microbiome. We see large differences in the composition of the gut microbiota between TLR5KOΔMicrobiota and WT mice. The gut microbiome may influence distant organs through three different mechanisms: regulation of nutrient/vitamin absorption, interactions with the immune system at the gut lining, and translocation of microbe-associated molecular patterns (MAMPs) from the gut to the circulation [(98)]. The TLR5KOΔMicrobiota did not display overt signs of impaired nutrient absorption; TLR5KOΔMicrobiota mice had comparable body mass to WT mice. However, we cannot ignore the possibility that vitamins derived from the gut microbiota may influence cartilage damage mechanisms. Immune regulation at the gut lining may contribute to the reduced OARSI scores, as modification of the

constituents of the gut microbiota are known to influence inflammation and/or immune activation at the gut lining and circulating immune cells and cytokines. Additionally, modification of the gut microbiota could have altered the translocation of MAMPs across the gut endothelium and into the systemic circulation. LPS is one example of a MAMP commonly observed in the blood [277]. A larger study with more stringent controls of the microbiome constituents, and that included WT mice treated with antibiotics is required to better understand the specific mechanisms behind the reduced OARSI scores in the TLR5KOΔMicrobiota group. The distinct gut microbial communities may also help to explain the opposite trends in OA cartilage pathology between the TLR5KOΔMicrobiota and HFD mice.

Additionally, it remains possible that the reduced OARSI scores and increased Mankin scores in the TLR5KOΔMicrobiota mice may be secondary to changes in bone tissue and cartilage. Alterations in bone tissue have recently been shown to influence OA cartilage pathology [278,279]. The TLR5KOΔMicrobiota mice had reduced subchondral bone plate TMD and thickness, which may help explain the reduced effect of mechanical loading, since subchondral bone TMD and bone thickness were both correlated with loaded limb OARSI score [280]. We also recently showed that the same modifications to the gut microbiome in the current study were associated with reductions in whole bone strength caused by changes in bone tissue material properties [133]. The relationship between subchondral bone properties and load-induced cartilage damage is complex and warrants further investigation [281]. With regard to cartilage properties, TLR5KOΔMicrobiota mice had increased control limb Mankin scores. It is possible that the alterations to the gut microbiome had a direct effect on cartilage health, although it does not appear that the increased Mankin scores influenced load-induced cartilage damage.

A number of strengths of the current study are worth noting. First, the study is unique in the examination of metabolic syndrome without severe obesity on the development of OA. Previous studies looking at metabolic disease and OA have focused solely on HFD models and leptin/leptin receptor deficient models. Second, the current study is the first to demonstrate an effect of HFD on OA in an in-vivo loading animal model without surgery or trauma. Third, the study examines modifications to the gut microbiota that influence load-induced OA. The reduced response to 6 weeks of loading in the TLR5KOΔMicrobiota is interesting and warrants further investigation to understand if the gut microbiome influences OA development [282].

A number of limitations are worth noting. First, the severity of OA cartilage pathology was small compared to more severe OA animal models [253,283]. The use of a greater load magnitude would lead to higher OARSI scores and increased sensitivity to small group differences. However, the milder form of OA cartilage pathology here provides insight into the earlier stages of OA development and/or OA generated by more common, lower magnitude loads. Second, it is not clear in this study if HFD mice had elevated severity or accelerated progression of OA cartilage pathology at 6 weeks. HFD models have been shown to develop both increased severity [253] and accelerated progression of OA [254]. It is possible that if the current study extended beyond 6 weeks, OA cartilage pathology in other groups might become as severe as in HFD mice. Lastly, the metabolic syndrome phenotype of the TLR5KO mice was not completely confirmed as only one direct measure of metabolic syndrome (abdominal adiposity) was assessed. However, the other parameters related to metabolic syndrome (body mass and serum insulin) are consistent with the previous characterization of the TLR5KO mouse [7].

We conclude the following: 1) severe adiposity and systemic inflammation increased load-induced cartilage damage after 6 weeks of loading, while milder adiposity and metabolic abnormalities in TLR5KO mice did not worsen OA pathology; 2) the effect of systemic factors on OA development appeared to be related to the duration of increased mechanical loading; 3) changes in the gut microbiota may contribute to the severity of load-induced OA cartilage pathology and subchondral bone morphology.

Chapter 4.6 Acknowledgements

The authors thank Lyudmila Lukashova of the HSS microCT core facility, Laura Vasquez-Bolanos, Adrian Alepuz, and the Cornell CARE staff for their experimental assistance.

Chapter 4.7 Author Contributions

Authors' roles: Conceived and designed the experiments: JDG, MCHM, SRG, CJH. Acquisition, analysis, and interpretation of the data: JDG, CJH, SNZ, ML, DTH, TNS, GGG. Wrote and Revised Manuscript: JDG, CJH, MCHM, SRG. Critical revision and final approval of the manuscript: All authors.

Chapter 4.8 Role of the Funding Source

This research was supported in part by the National Institute of Arthritis and Musculoskeletal and Skin Diseases of the National Institutes of Health (U.S) under Award Number AR068061. The content of the work is solely the responsibility of the authors and does not necessarily represent the official views of the National Institutes of Health.

Chapter 4.9 Supplementary Material

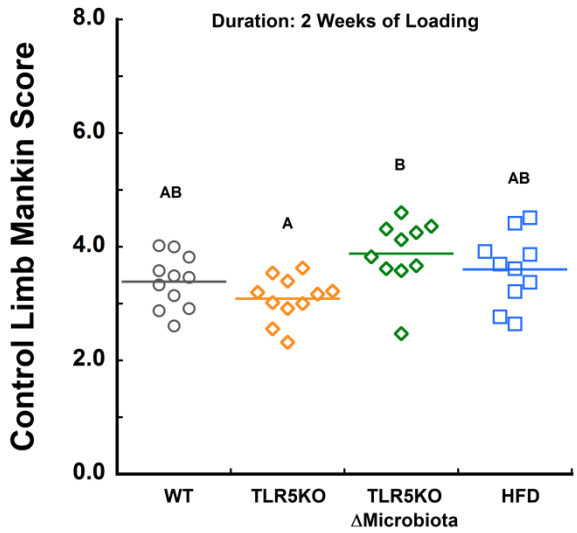

Figure 4.6. Control limb Mankin scores from 2 week loaded animals

After 2 weeks of loading, TLR5KOΔMicrobiota mice had increased Mankin scores compared to TLR5KO mice . Solid colored lines on dot plots represent mean. Means sharing the same letter are not significantly different from each other ($p < 0.05$).

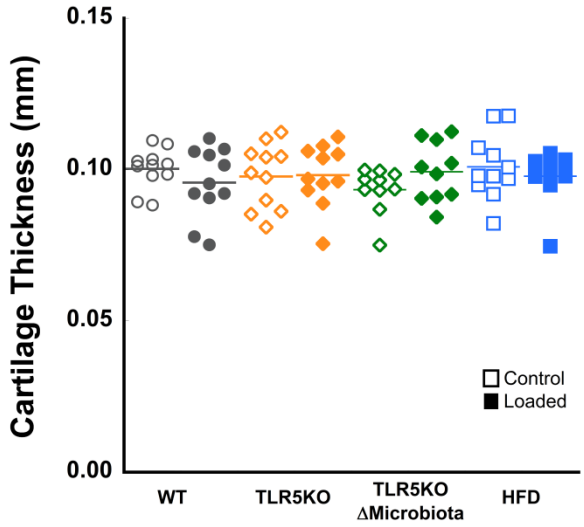

Figure 4.7. Cartilage thickness from 6 week loaded animals

Cartilage thickness measured in loaded and control limbs after six weeks of loading is shown. There was no effect of load or group detected on cartilage thickness. Solid colored lines on dot plots represent mean.

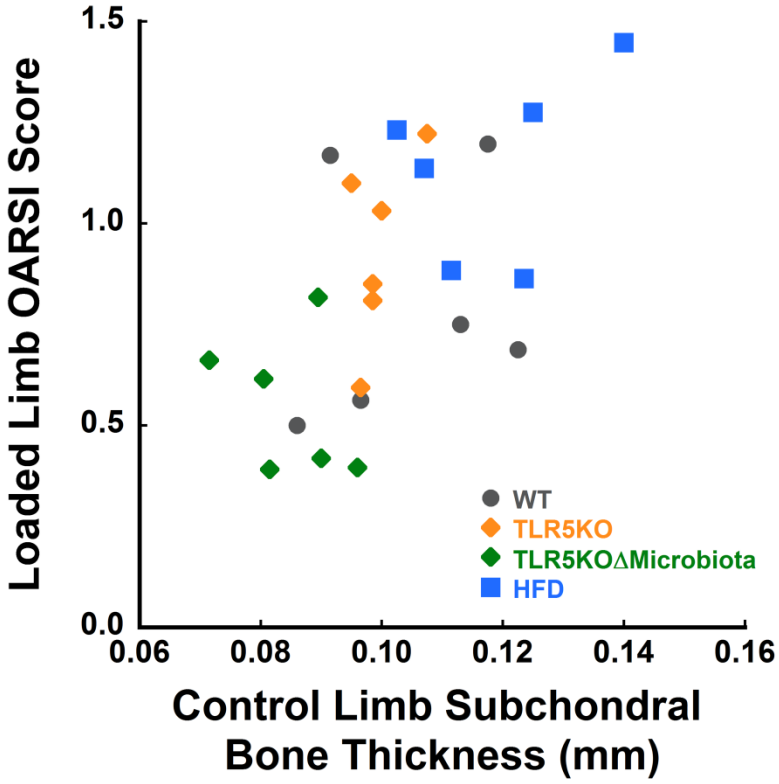

Figure 4.8. Correlation between subchondral bone thickness and loaded limb OARSI score

Control limb subchondral bone thickness measured by micro-computed tomography was correlated with loaded limb OARSI score at six weeks (r=0.66, [0.35, 0.84]). A Pearson's product-moment correlation analysis was used to identify relationships between loaded limb OARSI scores and control limb subchondral bone thickness.

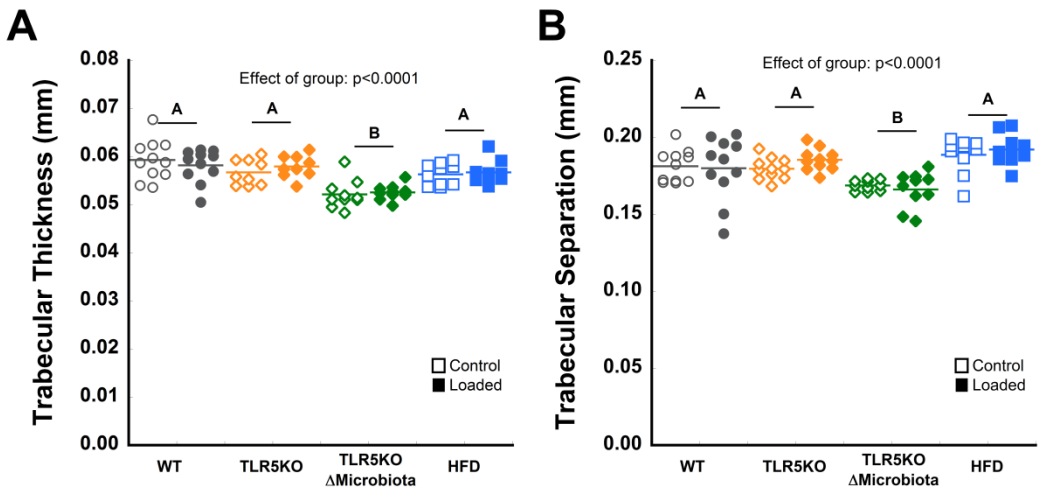

Figure 4.9. Trabecular bone microarchitecture in the proximal tibia epiphysis in 6 week-loaded animals

Microcomputed tomography was used to assess the trabecular bone microarchitecture of the proximal tibia epiphysis in loaded and control limbs of animals loaded for a duration of 6 weeks. There was no effect of load detected on trabecular thickness or separation. TLR5KOΔMicrobiota mice had lower trabecular thickness and separation compared to other groups. Solid colored lines on dot plots represent mean.

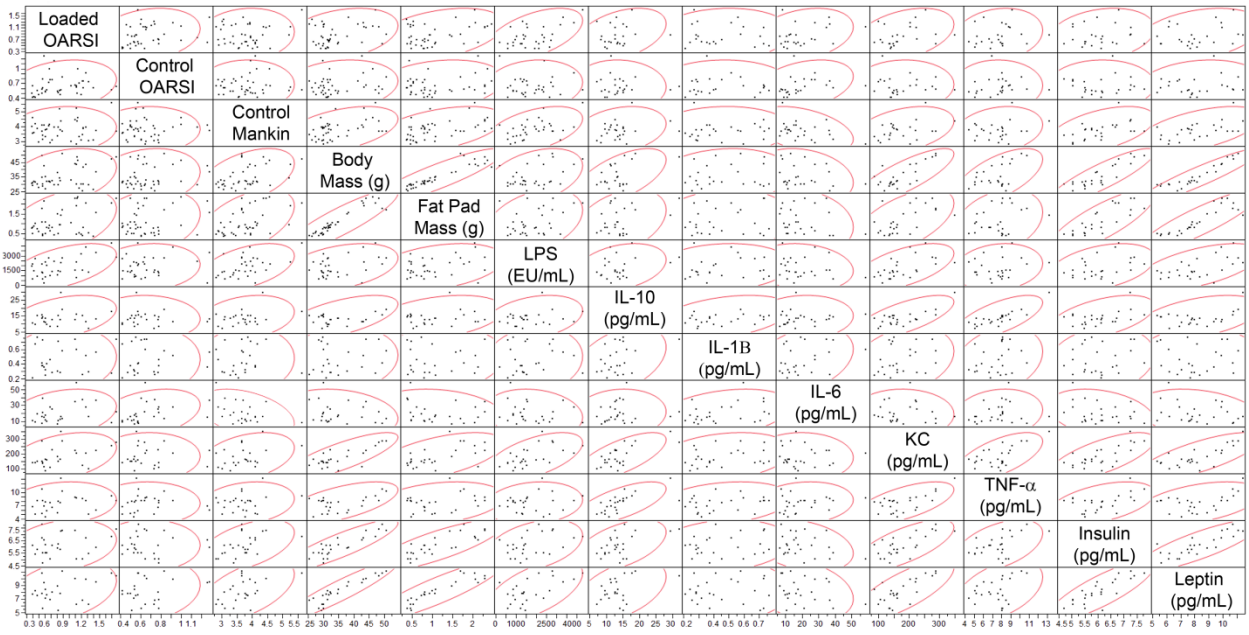

Figure 4.10. Scatterplot of Correlation Matrix from Table e

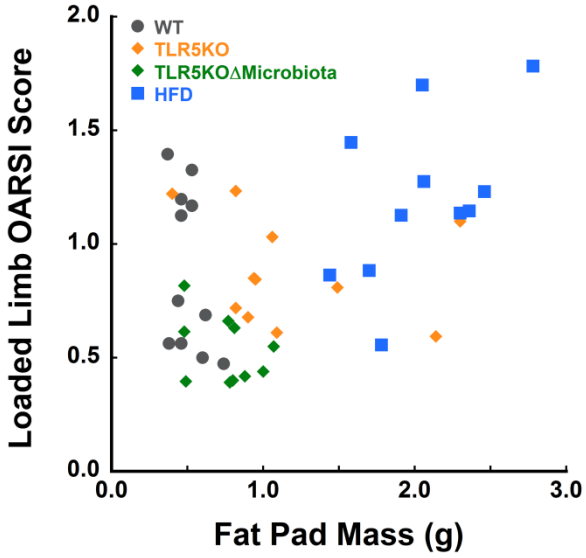

Figure 4.11. Correlation between fat pad mass and loaded limb OARSI score

Epididymal fat pad mass was correlated with loaded limb OARSI score in animals loaded for six weeks (r=0.43, [0.15, 0.65]). A Pearson's product-moment correlation analysis was used to identify relationships between loaded limb OARSI scores and control limb subchondral bone thickness.

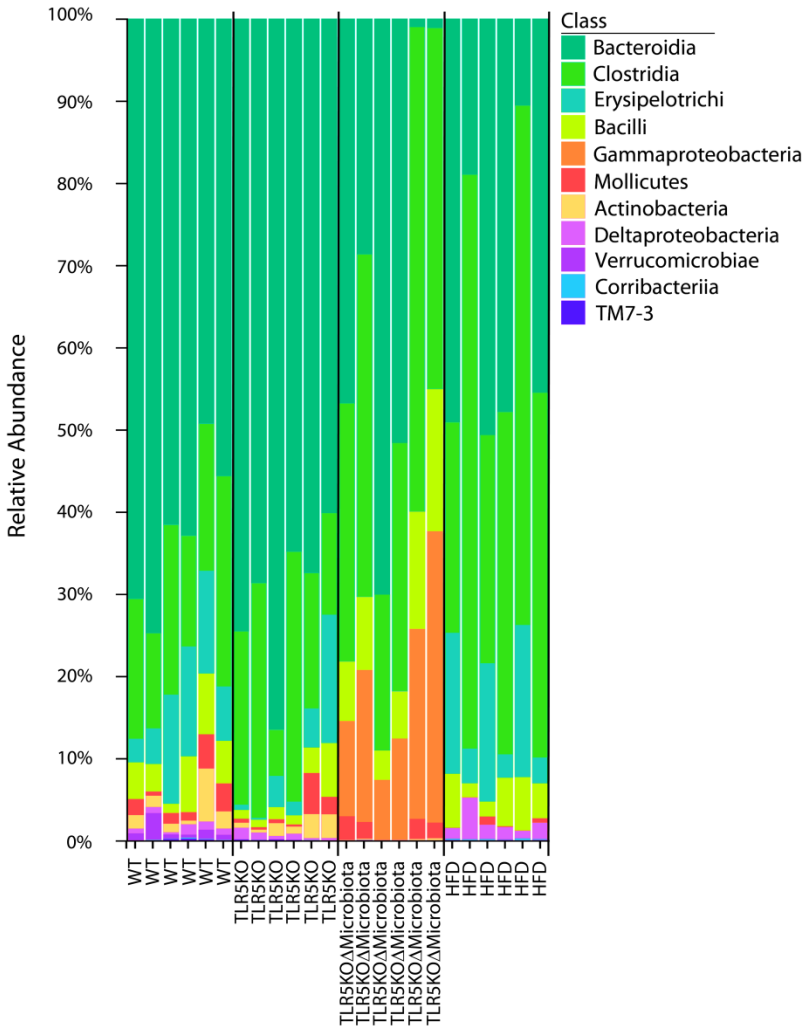

Figure 4.12. Relative abundance of fecal microbiota by phylogenetic class is shown.

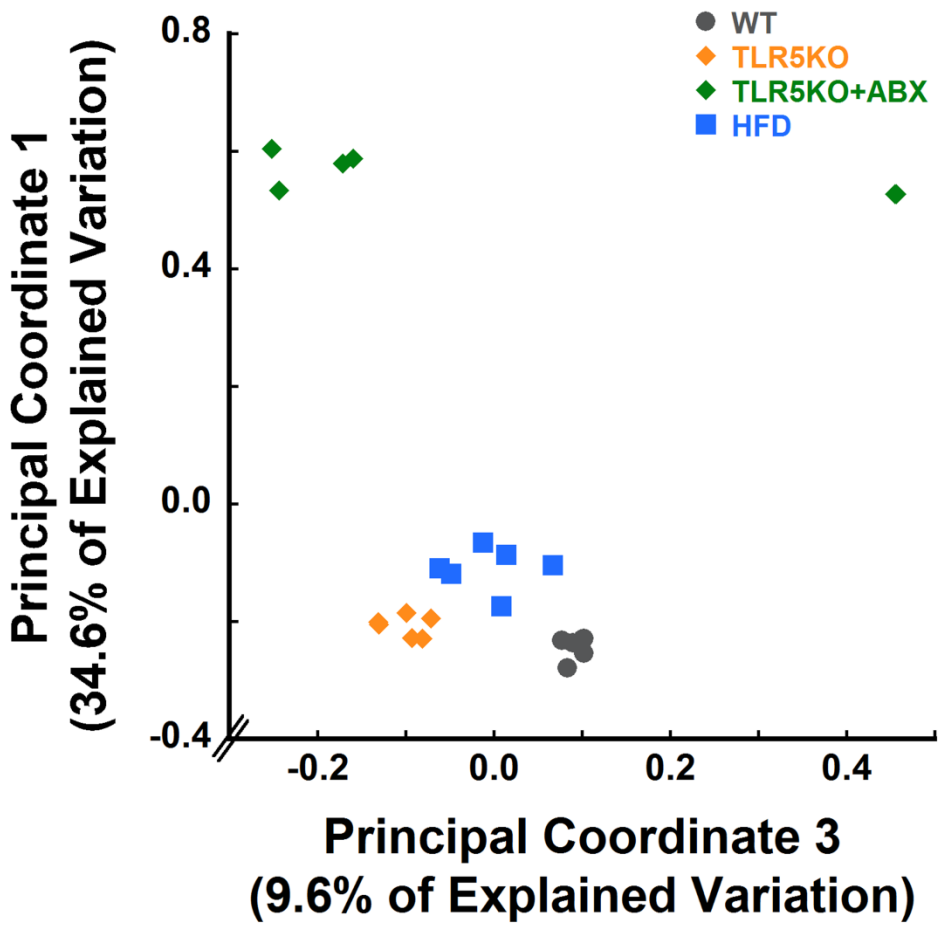

Figure 4.13. Principle coordinate analysis of fecal samples

Gut microbiota was characterized from fecal samples of animals loaded for a duration of 6 weeks. Principal coordinate analysis based on the Bray-Curtis dissimilarity was performed. Each point represents a single sample and the Bray-Curtis dissimilarity between each point represents how compositionally different each sample is from each other. Each group forms its own distinct clusters.

Table f The lower limit of detection for the serum markers evaluated are shown.

Serum Marker	Mean Lower Limit of Detection (pg/ml)
Leptin	11.7
Insulin	43.1
IL-1β	0.149
IL-6	1.08
KC	0.447
IL-10	0.609
IL-12p70	16.3
TNF-α	0.126

Chapter 5- Summary and Future Directions

Chapter 5.1 Summary

The gut microbiome influences host functions that are associated with bone and joint. Alterations in the gut microbiome lead to diseases and conditions that put an individual at increased risk of developing bone and joint diseases such as osteoporosis and osteoarthritis. Therefore, the objective of this research was to establish an initial understanding of how the gut microbiome can influence both bone and joint. Specifically, we use genetic manipulation, chronic antibiotic treatment, and diet to disrupt the composition and functions of the gut microbiome. We then used mechanical testing methods, Raman spectroscopy, and in-vivo cyclic compressive loading to understand how the alterations in the gut microbiome influence bone mechanical performance, bone tissue composition, and osteoarthritis pathology.

Few studies have examined the role of the gut microbiome in bone and joint. Prior work in the bone field has demonstrated that the disruption or absence of the gut microbiome can influence bone mass and structure. However, the studies are limited by experimental

methodology (age of animals, imaging techniques) and have conflicting findings. None of the previous studies examined the effect of alterations in the gut microbiome on bone mechanical performance or bone tissue composition and material properties. Prior work connecting the gut microbiome to joint disease is limited as well. Initial studies have investigated how systemic inflammation and obesity may contribute to increased risk and increased severity of osteoarthritis. However, the majority of the existing studies are limited by not evaluating the composition or functions of the gut microbiome and related pathways, or by the use of extreme animal models (high fat diet fed mice, leptin deficient mice) and injury models (intra-articular fracture, destabilization of the medial meniscus). Further investigation of each suspected pathway connecting the composition and function of the gut microbiome to bone and joint is required to begin translating the knowledge to therapeutics. Additionally, by exploring milder forms of obesity, non-traumatic injury models, and novel gut microbiome manipulation techniques, we can help fill current gaps of knowledge in the field. The work presented in this thesis seeks to address these current limitations and gaps in knowledge.

Chapter 5.1.1 Aim 1

In this aim, we characterized how alterations in the gut microbiome influence bone phenotype and mechanical performance at skeletal maturity. We examined alterations in the gut microbiome due to both genotypic alterations and chronic treatment with antibiotics. TLR5KO mice had larger cross-sectional area and moment of inertia compared to WT mice, but similar peak bending moment. Accounting for differences in cross-sectional femoral geometry demonstrated that TLR5KO mice had lower whole bone bending strength. Disruption of the gut microbiota with chronic antibiotics in WT mice did not result in changes in total area or moment

of inertia, but led to decreased cortical area and thickness. Disruption of the gut microbiota with chronic antibiotics in TLR5KO mice resulted in decreased cortical area, marrow area, cortical thickness, and moment of inertia. Long-term disruption of the gut microbiota in both genotypes led to reductions in whole bone bending strength beyond what could be explained by changes in cross-sectional femoral geometry. Trabecular bone microarchitecture was not influenced by the disruption of the gut microbiota or by genotype. Dramatic changes in the composition of the gut microbiota were detected with antibiotic treatment. The composition of the gut microbiome was dominated by the phylum Bacteroidetes in untreated animals, but the composition of the gut microbiome was dominated by the phylum Proteobacteria in animals treated with antibiotics. The changes in B and T cells detected in TLR5KO and antibiotic treated mice are one potential route the gut microbiome could influence bone. The results from this Aim together suggest that disruption of the gut microbiota can influence bone tissue material properties and composition.

Chapter 5.1.2 Aim 2

In this aim, we characterized the effects of disrupting the gut microbiome on bone tissue composition and the functional profile of the gut microbiome. We examined alterations in the gut microbiome due to genotypic alterations and chronic treatment with antibiotics. High-density spatial mapping of the posterior region of the tibial diaphysis revealed increased crystallinity in TLR5KO mice with a disrupted gut microbiome compared to untreated TLR5KO mice. Cross-sectional analysis confirmed the changes in TLR5KO ΔMicrobiome mice in crystallinity and measured decreased carbonate substitution as well. Cross-sectional analysis also revealed decreased crystallinity and increased carbonate substitution in WT ΔMicrobiome mice compared to untreated WT mice. Bone mineral crystallinity was less in TLR5KO mice compared to WT mice. Similar tissue modulus and hardness were measured among groups using nano-indentation,

suggesting other tissue-scale mechanical properties may be responsible for the impaired mechanical performance measured in whole bone testing. The functional capacity of the gut microbiome was uniquely different as a result of both antibiotic treatment and genotype. Disruption of the gut microbiota with oral antibiotics led to differential changes in microbial gene pathways involved in vitamin synthesis, short chain fatty acid fermentation, and bacterial cell wall components. Vitamin K is suspected to play a role in the observed changes in bone tissue composition. Microbial gene pathways relating to vitamin K synthesis were disrupted in mice receiving oral antibiotics. Furthermore, the resulting vitamin K levels measured in the cecum, liver, and kidney were altered in ΔMicrobiome mice. The results from this Aim suggest that the gut microbiome has the potential to influence bone tissue composition through changes in a variety of microbial gene pathways. As multiple pathways were effected by the antibiotic treatment, further study is required to test how each pathway can lead to changes in bone matrix.

Chapter 5.1.3 Aim 3

In this aim, we investigated the influence of the composition of the gut microbiome, gut microbiome-derived inflammation and metabolic syndrome on the development of osteoarthritis. We used a model of metabolic syndrome dependent on the gut microbiome, diet induced obesity, and an in-vivo tibial cyclic compressive loading model to induce modest osteoarthritis pathology in mice. We found that varying levels of obesity, the composition of the gut microbiome, and systemic inflammation can influence load-induced cartilage damage, though the effect of each condition takes sufficient time to manifest. We see greater levels of load-induced cartilage damage in severely obese mice after 6 weeks of loading, but not after 2 weeks of loading. The increased cartilage damage in high fat diet mice are likely a result of the systemic inflammation and severe adiposity levels in this group. The systemic levels of bacterial lipopolysaccharide are

elevated in high fat diet mice and are correlated with loaded-limb OARSI score, suggesting that lipopolysaccharide may have a direct effect on cartilage health or initiate an inflammatory cascade. We determined that the effect of a metabolic syndrome phenotype without severe obesity did not increase load-induced cartilage damage after 2 or 6 weeks of loading. We demonstrated that disruption of the gut microbiome and the subsequent prevention of the metabolic syndrome in TLR5KO mice did not influence cartilage damage after two weeks of loading but led to less load-induced cartilage damage after 6 weeks of loading. The TLR5KOΔMicrobiota mice had reduced subchondral bone plate tissue mineral density and thickness, as well as increased control limb Mankin scores, suggesting that the measured osteoarthritis pathology may be a combination of effects on bone and cartilage. The results from Aim 3 suggest that the gut microbiome has the potential to influence the severity of load-induced osteoarthritis, either through a direct influence on bone or cartilage health, or through indirect pathways that involve the systemic state of the animal.

Chapter 5.1.4 Synthesis

The studies contained within this thesis are some of the first findings to demonstrate an effect of the gut microbiome on bone and joint. The results of Aim 1 demonstrate that not only can the gut microbiome modify bone mass and architecture at skeletal maturity, but that alterations to the composition of the gut microbiome also can impair whole bone mechanical performance. The findings from the first study suggest that bone tissue material properties and bone tissue composition can be regulated by the gut microbiome. Aim 2 then evaluates how alterations in the gut microbiome influence bone tissue composition by using Raman spectroscopy. This aim examines the functional capacity of the gut microbiome to understand potential pathways for the changes in bone tissue composition. The results of the second study

demonstrate that disruption of the gut microbiome in mice leads to altered bone mineral crystallinity and carbonate substitution. Microbial gene pathways relating to vitamin synthesis, bacterial cell wall components, and short-chain fatty acid fermentation are disrupted and may each play a role in the changes in bone tissue composition. The role of gut microbiome-derived vitamin K in bone mineral crystallinity is a promising area that requires further investigation. Osteoarthritis is the degenerative disease that involves both changes to subchondral bone and cartilage. In the third study, we evaluate how alterations in the gut microbiome may influence the development of load-induced osteoarthritis pathology. The results of the third study demonstrate that severe obesity and systemic inflammation are able to increase cartilage damage, while mild obesity and moderate metabolic disturbances are not sufficient to increase osteoarthritis pathology. Our findings suggest that the gut microbiome may modulate the development of OA in both beneficial and detrimental ways. The mechanism behind the changes in OA pathology may involve the effects of the microbiome on bone. Together, the results suggest that the composition and functional capacity of the gut microbiome play a key role in both bone and joint.

We see that disruption of the gut microbiome in the TLR5KO mice has a distinct effect in both bone and joint throughout the thesis. In Aims 1 and 2, we see that disruption of the gut microbiome in TLR5KO leads to an altered gut microbiome and impaired bone strength, as well as increased crystallinity. In Aim 3, we see that disruption of the gut microbiome in TLR5KO mice, led to less load-induced cartilage damage. It is intriguing how disruption of the gut microbiome can have a detrimental effect on bone strength, however, when evaluating the joint we find a protective effect. A few explanations may explain the discrepant results: 1) A different gut microbiome dependent mechanism is involved in the changes in bone compared to the

changes in the joint. For example, an LPS dependent mechanism may be more relevant for a connecting the gut microbiome to joint health, whereas a vitamin-K dependent mechanism may have larger detectable effects on bone; 2) The changes observed in bone in Aims 1 and 2, may influence the effect of joint loading and cartilage damage. Previous studies have demonstrated that differences in bone properties, can lead to different levels of load-induced cartilage damage [281]. As the TLR5KO mice with a disrupted gut microbiome have impaired tissue material properties and increased mineral crystal size, it is possible the bone would behave differently under the applied loading in Aim 3. We clearly do see an effect in the bone of TLR5KO mice with a disrupted gut microbiome in Aim 3 consistent with Aim 1. In Aim 1 we see that TLR5KO mice treated with antibiotics have decreased tissue mineral density in cortical bone of the tibial metaphyseal shell, consistent with findings in Aim 3 that show reduced tissue mineral density in the subchondral bone plate.; 3) Vitamin K has been connected to both bone and joint disease [220,223,284], and also can impact the immune system. We see increased levels of vitamin K in TLR5KO mice with a disrupted gut microbiome in Aim 2. It is possible that altering the levels of vitamin K has one effect on bone phenotype and then a completely different effect on joint health.

Throughout the thesis it is clear that the TLR5KO genotype plays a role in the results in each Aim. In Aim 1 we see that TLR5KO mice have impaired bone tissue material properties. Then in Aim 3, we see that the TLR5KO mice do not have increased load-induced cartilage, despite the excess adiposity and metabolic status. It is possible that the TLR5KO do not show increased load-induced cartilage damage as was expected, as these mice have impaired bone tissue material properties, suggesting they would behave differently when subjected to cyclic compressive loading. We also see a different effect of disrupting the gut microbiome depending

on genotype in both Aim 1 and 2. It is clear disrupting the gut microbiome in the TLR5KO genotype leads to different changes in the composition and function of the gut microbiome than compared to the WT mice. This suggests that if WT mice with a disrupted gut microbiome were subjected to cyclic-compressive loading as were mice in Aim 3, that a different effect on cartilage damage may be observed. Further study can be devoted towards understanding the genotypic differences, and how those stemming in the gut microbiome lead to other downstream effects. It is possible that the impaired immune status in TLR5KO mice, or the increased adiposity are primary contributors to the genotypic differences. Even the divergent effects of antibiotic treatment on the metagenomic profiles of the gut microbiome may in turn be a downstream effect of an impaired immune system. It may be beneficial to further investigate which microbe populations are responsible for which functions both before and after antibiotic treatment, and then to see how it differs between the genotypes. Further investigation to connect the differing shifts in abundance of microbe populations to the shifts in the functional profile, will allow for a deeper understanding of which microbiota are responsible for which pathways.

We demonstrate that the metagenomic profile is greatly disrupted in animals treated with antibiotics, and that tissue vitamin K levels are impacted as well in Aim 2. It is worth considering how the metagenomic profile may connect to the findings in Aim 3. Vitamin K has been linked to osteoarthritis incidence previously. However, as the overall functional pathways are severely disrupted in mice treated with antibiotics, there are many downstream pathways and products of the microbiome that can influence the results. Pathways for bacterial cell wall and capsule components are disrupted in mice treated with antibiotics. These products have the potential to cause an inflammatory response in the body or joint, and in fact have been connected to inflammatory arthritis models in mice [(285)]. Additionally, high fat diet fed mice may also see

large changes in functional profile as a results of the long-term diet changes. Applying the metagenomic analysis performed in Aim 2 on high fat diet fed mice, can allow us to further investigate microbiome related mechanisms for the increased load induced cartilage.

Chapter 5.1.5 Strengths

The primary strength of the first two Aims in the thesis are the novelty of characterizing bone mechanical performance and tissue composition for the first time in relation to the the gut microbiome. The investigation of bone mechanical performance in relation to the gut microbiome is the first of its kind and demonstrated that bone tissue composition and mechanical performance can be influenced by changes in the gut microbiome. Previous studies have focused solely on bone microarchitecture and bone mass, neglecting to investigate if whole bone mechanical performance is influenced by the gut microbiome. The second study further evaluates the impaired bone mechanical performance, and is the first study to investigate how alterations in the gut microbiome can influence bone tissue composition. Another key strength and novelty of the second study, is the investigation of gut microbiome functional pathways and the potential effect of the pathways on bone composition. Previous studies have solely evaluated the composition of the gut microbiota in relation to bone phenotype. The primary strength of the third study is the use of a novel gut-microbiome derived animal model of metabolic syndrome. Prior studies focused on high fat diet induced models that are extreme in the presentation of obesity and metabolic syndrome. Furthermore, the study uses a novel in-vivo loading model that allows for: 1) the generation of a more modest, non-traumatic form of osteoarthritis, compared to the post-traumatic injury models; 2) the evaluation of how duration of loading and time exposed to systemic factors can influence osteoarthritis pathology.

Chapter 5.1.6 Limitations

Despite the novelty of the studies, several limitations must be considered when interpreting the results. First, the use of chronic, long-term antibiotics to generate consistent changes in the gut microbiome does not simulate treatment in humans. More commonly used antibiotic treatment regimens of 1-2 weeks were not used in the studies, as shorter term treatments with antibiotics generate only a transient change in the gut microbiome, rather than a sustained alteration in the gut microbiome. Though the use of antibiotics in this study does not mimic common clinical treatment, the resulting, sustained change in the gut microbiome can be compared to sustained changes in the gut microbiome that are a result of diet, disease, or other lifestyle factors. Another major limitation of the two studies focused on bone is that bone turnover was not assessed. Assessment of bone turnover using dynamic histomorphometry can help to understand the mechanism behind the changes in bone mechanical performance and tissue composition in mice with an altered gut microbiome. Prior work has found that colonization of germ-free mice with microbiota increased bone formation rate and mineral apposition rate [198]. As we did not observe changes in cancellous bone volume fraction and preliminary studies in the cortex suggest no differences in bone formation at skeletal maturity, measures of bone remodeling are unlikely to provide further insight into the observed bone phenotypes. However, performing dynamic histomorphometry can determine if bone turnover played a role in the current thesis and provide further insight into a gut microbiome dependent mechanism. Another limitation of the work is that only two methods of manipulating the gut microbiome were used. The gut microbiome is an incredibly complex ecosystem with trillions of bacteria. Modifications to the gut microbiome that involve different genotypic alterations,

different antibiotic regimens and types, different diets, or gut microbiota transplantation will each have a unique impact on the gut microbiome, and thus potentially on bone and joint as well. Future work will have to work towards more clearly understanding the gut microbiome as a network, as well as the mechanisms driving differences to be able to apply the findings in this thesis towards clinical applications.

Chapter 5.2 Future Work

The results of the current thesis lay the ground work for several interesting future areas of study regarding the influence of the gut microbiome on bone and joint. Understanding the key mechanisms connecting alterations in the gut microbiome to the impairment of bone mechanical performance and the severity of load-induced cartilage remain to be explored. The most attractive future lines of investigation involve isolating the mechanisms responsible for the relationships between the microbiome and bone and joint. Future work will be directed towards testing each pathway suspected (immune system, nutrient absorption and vitamin synthesis, and bacterial translocation), and testing how these pathways may interact. Many of the pathways can have effects on one another, and so unraveling the complex system will take multiple approaches.

Chapter 5.2.1 Continued Research Avenues

Chapter 5.2.1.1 Determining the Role of Vitamin K and Non-Collagenous Proteins in Gut Microbiome Related Bone Tissue Changes

Based on the results from Chapter 3, vitamin-K dependent pathways are suspected to play a role in the changes in bone tissue composition and mechanical performance observed in Aim 1 and Aim 2. Vitamin-K synthesized by the gut microbiome is responsible for the carboxylation of

several non-collagenous proteins present in bone [286]. Non-collagenous proteins account for about 5% of the organic content of bone and can influence bone mineral crystal nucleation and growth. Non-collagenous proteins such as osteocalcin and matrix Gla protein require vitamin-K to carboxylate the protein into its active form. Osteocalcin and other non-collagenous proteins have been implicated as factors influencing bone quality. Mice deficient in osteocalcin and matrix Gla protein have altered bone mineral crystallinity [287]. Therefore, a line of investigation that evaluates the role of vitamin K and non-collagenous proteins in gut microbiome related changes in bone tissue is required. Experiments that utilize warfarin to block vitamin K can be useful to isolate the effects of vitamin K. Determining if the effects of using warfarin are present in mice both with a normal and disrupted gut microbiome will be an important study to conduct. Disruption of the synthesis of vitamin-K can also be achieved through modification of the gut microbiome. Different antibiotic cocktails and diets can be used to help target which microbes are primarily responsible for the vitamin-K synthesis. Through the use of osteocalcin-deficient mice, matrix Gla protein deficient mice, and administration of antibiotics to disrupt the ability of the gut microbiome to synthesize vitamin-K, we can determine if the gut microbiome related bone tissue changes are dependent on vitamin-K carboxylation of osteocalcin or matrix Gla protein. The influence of genotype on vitamin-K dependent changes in bone composition is another area for investigation, as we found in Aim 2 that disruption of the gut microbiome had differential effects on the gut metagenome and vitamin K levels in the TLR5KO mice. Additional areas for investigation of vitamin-K dependent changes in bone tissue composition are when the changes to bone tissue occur (at initial disruption of the gut microbiome or during the entire growth period), if the changes in bone tissue composition are permanent, and if the

changes to bone tissue properties can be recovered (perhaps through modifications to the gut microbiome).

Lastly, gut microbiome mediated changes in vitamin-k content may influence bone tissue through modification of the immune system or by regulation of osteoblastogenesis/osteoclastogenesis. Vitamin-K has been associated with inflammatory cytokine concentrations [286,288], as well as in the regulation of B-cell development and antibody production [289]. Vitamin K has recently been shown to regulate osteoblastogenesis and osteoclastogenesis, suggesting another route vitamin K may influence bone [290].

Chapter 5.2.1.2 Understanding How the Gut Microbiome Can Be Used to Improve the Systemic Obesity State and Osteoarthritis Pathology

As obesity is a widespread epidemic in the United States, and clinical/experimental data suggest increased incidence of OA in obese populations. As we may not be able to stop the obesity epidemic, it is important to understand how we can combat the negative effects of obesity on OA development. Based on the results from Aim 3, we have demonstrated that severe obesity in the high fat diet mouse is sufficient to increase load-induced cartilage damage. The results suggest that systemic inflammation and severe obesity contributed to the OA severity. The severity of load-induced cartilage damage was also correlated with serum levels of bacterial lipopolysaccharide (LPS). Additionally we found there are large changes in the composition of the microbiome associated with high fat diet feeding. Therefore, an interesting and impactful line of investigation would be to further investigate the mechanism behind the increase load-induced cartilage damage in mice fed a high fat diet, with a focus on understanding how the gut microbiome may be implicated and can be used to improve or prevent OA pathology. Evidence has shown that high fat diet feeding leads to increased levels of LPS in the intestine, leading to gut inflammation via TLR-4, leading to increased intestinal permeability, and then increased

serum LPS levels that cause systemic inflammation and can accelerate obesity [270]. Experiments should evaluate different methods of modifying the gut microbiome (antibiotics, diets, prebiotics, genotype) to prevent OA pathology in high fat diet fed mice. For example, prebiotics can be used to promote commensal bacteria that reduce inflammatory levels and was recently demonstrated to improve OA pathology in a post-traumatic OA mouse model [282]. Alternative diets, such as a Mediterranean diet, as well as varying degrees of fat % in the high fat diet can be investigated. Modifying the gut microbiome through chronic antibiotic treatment is another promising potential route to combat increased cartilage damage associated with obesity. In Aim 3 we demonstrated that alterations to the gut microbiome induced by chronic antibiotic treatment led to reduced load-induced cartilage damage. Previous literature shows that modulation of the gut microbiota of high fat diet fed mice with oral antibiotics is able to improve insulin signaling and glucose tolerance by reducing circulating LPS levels and inflammatory cytokines such as IL-6 and TNF-α [291,292]. Mice treated with a cocktail of ampicillin, neomycin, and metrodinozole have a commensal flora dominated by phylum Proteobacteria [291], similar to the results presented in this thesis. The results from Aim 3 and prior work suggest that altering the gut microbiome with antibiotics in mice fed a high fat diet may be sufficient to mitigate systemic inflammation and metabolic disturbances, and prevent the increased severity of load-induced cartilage damage. Alternative antibiotic cocktails can be used to explore the effects of different microbiota populations on load-induced cartilage damage, with a hope to understand which microbiota populations are responsible. LPS, may be one of several MAMP's that are elevated and involved in the increased systemic inflammation and cartilage damage in high fat diet mice. Mice on a high fat diet have increased intestinal permeability leading to increased leakage of bacteria and/or bacterial products such as lipopolysaccharide [293]. Systemic profiling of other potential

MAMPs such as peptidoglycan, flagellin, and cell free DNA should be conducted [98], as it is not clear if LPS is the only elevated MAMP in high fat diet mice. The use of bacterial LPS binding molecules can be used to block any potential effects of LPS and determine if systemic LPS plays a role in the inflammation and cartilage pathology [294]. Gut microbiome compositional and metagenomic profiling can be used to evaluate if the gene pathways related to the production of any of these MAMPs is functionally altered. Additionally, the use of various toll-like receptor deficient mice can be used to further test the effects of certain MAMPs, as each TLR has specific bacterial products/components they detect. The TLR4-deficient mouse may be an interesting study group to include for example, as TLR4 is the toll-like receptor responsible for detecting lipopolysaccharide. High fat diet feeding does not increase pro-inflammatory cytokine levels in TLR4-deficient mice [270]. TLR-4 deficient mice have also previously been shown to be protected from collagen-induced arthritis, supporting a potential role for TLR4 signaling in arthritis disease progression [285].

Chapter 5.2.1.3 Understanding The Role of TGF-β and the Immune System in Changes in Bone Tissue Composition

The gut microbiome has a large impact on both the development and function of the immune system. Therefore, it is important to further understand the role of the immune system in gut microbiome related changes in bone tissue. One route the gut microbiome may influence the immune system and subsequent bone matrix properties, is through regulation or modification of protein- and mineral-rich extracellular material produced by osteoblasts and osteocytes. One key example, is the highly conserved anti-inflammatory cytokine, TGF-β. TGF-β has been shown to be a key modulator of the gut microbiome and immune cells. TGF-β has also been shown to influence the mechanical properties and composition of bone matrix [295]. TGF-β can regulate the

expression of osteocalcin, osteopontin, osteonectin, type I collagen, and matrix metalloproteinases, and thus has the ability to influence bone matrix properties and composition [296-298]. Knockout-mice used to target signaling pathways related to TGF-β demonstrated that growth factor signaling can regulate the mechanical properties of bone matrix independently of changes in bone mass and architecture [295], similar to what was found in mice with an altered gut microbiome in the current thesis. TGF-β is mainly activated and produced by intestinal epithelial cells after stimulation by short chain fatty acids, or by dendritic cells after direct contact with gut microbiota [299]. TGF-β is also a major factor driving the development and functioning of lymphocytes that help maintain the gut barrier [299]. A recent study also demonstrated that short chain fatty acids (butyrate) produced by commensal gut bacteria activates TGF-β expression in intestinal epithelial cells [300]. Additionally, Toll-like receptor deficiency can decrease TGF-β induced extracellular matrix protein deposition [301], further supporting a link between the gut microbiome and TGF-β induced changes in bone matrix. Therefore, it is possible that altered interactions between the immune system and the gut microbiome lead to changes in TGF-β activation/expression, resulting in altered expression of proteins in bone. A line of investigation evaluating the potential role of TGF-β in the changes in bone found in mice with an altered gut microbiome is an interesting and exciting future area of work. To test the role of TGF-β, 1D11 antibody treatment can be used to inhibit TGF-β signaling [302], as well as other novel TGF-Beta inhibitors [303]. There are transgenic mouse models that manipulate the TGF-β that can be used as well. For example, Smad 3 deficient mice can be used as Smad 3 is an important molecule in the TGF-β signaling pathway that leads to changes in bone. Investigating which gut microbiota populations are most closely associated with TGF-β levels will be important, as certain microbiota members such as Clostridiales provide a transforming growth factor rich environment

that promotes Treg cell populations in the gut [300]. Additional assays to understand the changes in the immune system would be necessary and would potentially include: flow cytometry to investigate the specific immune cell populations (Treg cell), as well as analysis of growth factors and cytokines in the serum and small intestine. Furthermore, there are many links between TGF-β and osteoarthritis [304,305] that may also be worth investigating, given the evidence connecting TGF-β and the gut microbiome.

Chapter 5.2.2 New Research Avenues

Chapter 5.2.2.1 Influence of the Maternal Mouse Gut Microbiome and the Gut Microbiome Early in Life on Bone Phenotype

In the studies presented in this thesis, alterations to the gut microbiome through antibiotic treatment have begun at 4 weeks of age. However, a critical development window for bone [306] and the immune system [307] occurs in-utero and during the initial 4 weeks of life . The femoral cortical area of C57BL/6J mice nearly quadruples between embryonic day 18.5 and 28 days post-birth, achieving 48% of the cortical area the mouse will reach by 1 year of age [191]. Poor bone development early in life can lead to reductions in peak bone mass, and thus a higher risk of osteoporotic fracture in adulthood. The maternal microbiome is transferred to offspring during birth and is then shaped by subsequent nutrient intake from mother's breast milk [3]. The maternal microbiome can have serious consequences on the health of offspring. Maternal antibiotic treatment used to target gram-negative bacteria was able to prevent the development of diabetes in offspring of mice genetically pre-disposed to diabetes [308]. Additionally, changes in the maternal microbiome after antibiotic treatment has been shown to influence susceptibility to inflammatory bowel disease, as well as the resulting composition of the gut microbiome in offspring until 21 weeks of age or longer [309]. The clear effect of the maternal gut microbiome on

offspring health and disease susceptibility suggests that disruption of the maternal gut microbiome may influence bone phenotype in offspring. Additionally, as the gut microbiome during the first 4 weeks of life is crucial for the development and education of the immune system [310], it important to understand how changes in this time window may impact adult bone phenotype. A line of investigation that evaluates how changes in the maternal gut microbiome and the gut microbiome in early life (birth-4 weeks of age) can influence the bone phenotype of offspring can be very informative for clinical management of mother's during pregnancy. If treatment of the maternal gut microbiome during pregnancy can improve bone mass and quality in the offspring, then fracture risk in adult age can be reduced. Determining the effect of the disruption of the maternal gut microbiome on the bone phenotype of offspring can have clinical relevance, as the use or disuse of antibiotics during pregnancy may have implications on bone health and disease for the mother and child. Studies should evaluate when changes in bone composition initially occur in offspring, if the changes are reversible post-birth, and what modifications to the maternal gut microbiome are beneficial or detrimental. It will be interesting to evaluate the effects of disrupting the gut microbiome at different ages in the offspring (starting at birth) to better understand how and when the changes in bone occur.

Chapter 5.2.2.2 Influence of Natural Mouse Gut Microbiome on Bone Phenotype

The results from this thesis and prior work clearly demonstrate that the gut microbiome has important consequences on health and disease. However, the majority of our current understanding of the gut microbiome are based on research performed on mice raised in tightly controlled laboratory conditions. Recently it has been demonstrated that the gut microbiome of mice raised in a tightly controlled laboratory environment is dramatically different than the gut microbiome of their genetic counterparts living in the wild [311]. Furthermore, the differences in

the gut microbiome between lab mice and mice with a "natural gut microbiome" led to detectable effects in overall animal health and immune system function. The natural gut microbiome beneficially modulated host responses to inflammatory stimuli, improved overall host fitness, and improved resistance to infection and tumorogenesis. The findings are not surprising as the natural gut microbiome have evolved and adapted over time to increase animal survival, while the gut microbiome of laboratory mice has been heavily modified based on controlled environment and genetics. Therefore, the natural mouse gut microbiome provides a useful model to further our understanding of how the gut microbiome can influence bone phenotype. Additionally, by understanding how the natural gut microbiome may have positive or negative effects on bone health, we can evaluate the composition, function, and products of the natural gut microbiome to further evaluate potential mechanisms. Investigating the effects of the natural mouse gut microbiome on bone phenotype can provide key insights into how immune changes stemming from the gut microbiome can influence bone. Monitoring immune cell changes and the systemic inflammatory environment resulting from the natural gut microbiome can be informative as beneficial changes in the immune system occur in mice with a natural gut microbiome. Studies that use gut microbiome transplantation can be conducted where germ-free mice are gavaged with either natural mouse gut microbiome or WT mouse gut microbiome and the subsequent changes in bone phenotype are monitored over time.

References Cited

1. Yatsunenko T, Rey FE, Manary MJ, Trehan I, Dominguez-Bello MG, Contreras M, et al. Human gut microbiome viewed across age and geography. Nature. 2012;486(7402):222-7.
2. Nagpal R, Yadav H, Marotta F. Gut Microbiota: The Next-Gen Frontier in Preventive and Therapeutic Medicine? Front Med. Perspective 2014;1(15).
3. Lozupone CA, Stombaugh JI, Gordon JI, Jansson JK, Knight R. Diversity, stability and resilience of the human gut microbiota. Nature. 2012;489(7415):220-30.
4. David LA, Materna AC, Friedman J, Campos-Baptista MI, Blackburn MC, Perrotta A, et al. Host lifestyle affects human microbiota on daily timescales. Genome Biol. 2014;15(7):R89.
5. Jernberg C, Löfmark S, Edlund C, Jansson JK. Long-term impacts of antibiotic exposure on the human intestinal microbiota. Microbiology. 2010;156(11):3216-23.
6. Reyniers JA. The pure-culture concept and gnotobiotics. Ann N Y Acad Sci. 1959;78(1):3-16.

7. Vijay-Kumar M, Aitken JD, Carvalho FA, Cullender TC, Mwangi S, Srinivasan S, et al. Metabolic syndrome and altered gut microbiota in mice lacking Toll-like receptor 5. Science. 2010;328(5975):228-31.
8. Luczynski P, McVey Neufeld K-A, Oriach CS, Clarke G, Dinan TG, Cryan JF. Growing up in a Bubble: Using Germ-Free Animals to Assess the Influence of the Gut Microbiota on Brain and Behavior. Int J Neuropsychopharmacol. 2016;19(8):pyw020.
9. Ericsson AC, Franklin CL. Manipulating the Gut Microbiota: Methods and Challenges. ILAR Journal. 2015;56(2):205-17.
10. Ericsson AC, Franklin CL. Manipulating the Gut Microbiota: Methods and Challenges. ILAR J. 2015;56(2):205-17.
11. Laukens D, Brinkman BM, Raes J, De Vos M, Vandenabeele P. Heterogeneity of the gut microbiome in mice: guidelines for optimizing experimental design. FEMS Microbiol Rev. 2016;40(1):117-32.
12. Lundberg R, Toft MF, August B, Hansen AK, Hansen CHF. Antibiotic-treated versus germ-free rodents for microbiota transplantation studies. Gut Microbes. 2016;7(1):68-74.
13. Aron-Wisnewsky J, Clement K. The gut microbiome, diet, and links to cardiometabolic and chronic disorders. Nat Rev Nephrol. 2016;12(3):169-81.
14. Jovel J, Patterson J, Wang W, Hotte N, O'Keefe S, Mitchel T, et al. Characterization of the Gut Microbiome Using 16S or Shotgun Metagenomics. Front Microbiol. 2016;7:459.
15. Sharpton TJ. An introduction to the analysis of shotgun metagenomic data. Front Plant Sci. 2014;5:209.
16. Turnbaugh PJ, Ridaura VK, Faith JJ, Rey FE, Knight R, Gordon JI. The Effect of Diet on the Human Gut Microbiome: A Metagenomic Analysis in Humanized Gnotobiotic Mice. Sci Transl Med. 2009;1(6):6ra14.
17. David LA, Maurice CF, Carmody RN, Gootenberg DB, Button JE, Wolfe BE, et al. Diet rapidly and reproducibly alters the human gut microbiome. Nature. 2014;505(7484):559-63.
18. Wu GD, Chen J, Hoffmann C, Bittinger K, Chen Y-Y, Keilbaugh SA, et al. Linking Long-Term Dietary Patterns with Gut Microbial Enterotypes. Science 2011;334(6052):105-8.
19. Read MN, Holmes AJ. Towards an Integrative Understanding of Diet–Host–Gut Microbiome Interactions. Front Immunol. 2017;8:538.
20. Singh RK, Chang H-W, Yan D, Lee KM, Ucmak D, Wong K, et al. Influence of diet on the gut microbiome and implications for human health. J Transl Med. 2017;15(1):73.
21. Cordain L, Eaton SB, Sebastian A, Mann N, Lindeberg S, Watkins BA, et al. Origins and evolution of the Western diet: health implications for the 21st century. Am J Clin Nutr 2005;81(2):341-54.
22. Wang C-Y, Liao JK. A Mouse Model of Diet-Induced Obesity and Insulin Resistance. Methods Mol Biol. 2012;821:421-33.
23. Turnbaugh PJ, Ley RE, Mahowald MA, Magrini V, Mardis ER, Gordon JI. An obesity-associated gut microbiome with increased capacity for energy harvest. Nature. 2006;444(7122):1027-131.
24. Murphy EA, Velazquez KT, Herbert KM. Influence of High-Fat-Diet on Gut Microbiota: A Driving Force for Chronic Disease Risk. Curr Opin Clin Nutr Metab Care. 2015;18(5):515-20.

25. Turnbaugh PJ, Backhed F, Fulton L, Gordon JI. Marked alterations in the distal gut microbiome linked to diet-induced obesity. Cell Host Microbe. 2008;3(4):213-23.
26. Turnbaugh PJ. Microbes and Diet-Induced Obesity: Fast, Cheap, and Out of Control. Cell host & microbe.21(3):278-81.
27. Zhang M, Yang X-J. Effects of a high fat diet on intestinal microbiota and gastrointestinal diseases. World J Gastroenterol. 2016;22(40):8905-9.
28. Singh RK, Chang H-W, Yan D, Lee KM, Ucmak D, Wong K, et al. Influence of diet on the gut microbiome and implications for human health. J Transl Med. 2017;15:73.
29. Wu GD, Chen J, Hoffmann C, Bittinger K, Chen Y-Y, Keilbaugh SA, et al. Linking Long-Term Dietary Patterns with Gut Microbial Enterotypes. Science. 2011;334(6052):105.
30. Quigley EMM. Prebiotics and probiotics; modifying and mining the microbiota. Pharmacol Res. 2010;61(3):213-8.
31. Holscher HD. Dietary fiber and prebiotics and the gastrointestinal microbiota. Gut Microbes. 2017;8(2):172-84.
32. Langdon A, Crook N, Dantas G. The effects of antibiotics on the microbiome throughout development and alternative approaches for therapeutic modulation. Genome Med. 2016;8:39.
33. Zaman SB, Hussain MA, Nye R, Mehta V, Mamun KT, Hossain N. A Review on Antibiotic Resistance: Alarm Bells are Ringing. Cureus. 2017;9(6):e1403.
34. Tasnim N, Abulizi N, Pither J, Hart MM, Gibson DL. Linking the Gut Microbial Ecosystem with the Environment: Does Gut Health Depend on Where We Live? Front Microbiol. 2017;8(1935).
35. Jin Y, Wu S, Zeng Z, Fu Z. Effects of environmental pollutants on gut microbiota. Environ Pollut. 2017;222:1-9.
36. Goodrich JK, Waters JL, Poole AC, Sutter JL, Koren O, Blekhman R, et al. Human genetics shape the gut microbiome. Cell. 2014;159(4):789-99.
37. Saraswati S, Sitaraman R. Aging and the human gut microbiota—from correlation to causality. Front Microbiol. 2014;5:764.
38. O'Toole PW, Claesson MJ. Gut microbiota: Changes throughout the lifespan from infancy to elderly. Int Dairy J. 2010;20(4):281-91.
39. Ciorba MA. A Gastroenterologist's Guide to Probiotics. Clin Gastroenterol Hepatol. 2012;10(9):960-8.
40. Shanahan F. Probiotics in Perspective. Gastroenterology. 2010;139(6):1808-12.
41. Schwarzer M, Makki K, Storelli G, Machuca-Gayet I, Srutkova D, Hermanova P, et al. Lactobacillus plantarum strain maintains growth of infant mice during chronic undernutrition. Science. 2016;351(6275):854-7.
42. Belkaid Y, Hand T. Role of the Microbiota in Immunity and inflammation. Cell. 2014;157(1):121-41.
43. Cerf-Bensussan N, Gaboriau-Routhiau V. The immune system and the gut microbiota: friends or foes? Nat Rev Immunol. 2010;10(10):735-44.
44. Rooks MG, Garrett WS. Gut microbiota, metabolites and host immunity. Nat Rev Immunol. 2016;16(6):341-52.
45. Wu H-J, Wu E. The role of gut microbiota in immune homeostasis and autoimmunity. Gut Microbes. 2012;3(1):4-14.

46. McGuckin MA, Lindén SK, Sutton P, Florin TH. Mucin dynamics and enteric pathogens. Review Article 2011;9:265.
47. Cullender TC, Chassaing B, Janzon A, Kumar K, Muller CE, Werner JJ, et al. Innate and adaptive immunity interact to quench microbiome flagellar motility in the gut. Cell Host Microbe. 2013;14(5):571-81.
48. Frantz AL, Rogier EW, Weber CR, Shen L, Cohen DA, Fenton LA, et al. Targeted deletion of MyD88 in intestinal epithelial cells results in compromised antibacterial immunity associated with downregulation of polymeric immunoglobulin receptor, mucin-2, and antibacterial peptides. Mucosal Immunol. 2012;5(5):501-12.
49. Ubeda C, Lipuma L, Gobourne A, Viale A, Leiner I, Equinda M, et al. Familial transmission rather than defective innate immunity shapes the distinct intestinal microbiota of TLR-deficient mice. The Journal of Experimental Medicine. 2012;209(8):1445-56.
50. Hooper LV, Littman DR, Macpherson AJ. Interactions Between the Microbiota and the Immune System. Science. 2012;336(6086):1268.
51. Levy M, Kolodziejczyk AA, Thaiss CA, Elinav E. Dysbiosis and the immune system. Nat Rev Immunol. Review 2017;17(4):219-32.
52. Qin J, Li R, Raes J, Arumugam M, Burgdorf KS, Manichanh C, et al. A human gut microbial gene catalogue established by metagenomic sequencing. Nature. 10.1038/nature08821 2010;464(7285):59-65.
53. Sharon G, Garg N, Debelius J, Knight R, Dorrestein Pieter C, Mazmanian Sarkis K. Specialized Metabolites from the Microbiome in Health and Disease. Cell Metabolism.20(5):719-30.
54. Bäckhed F, Ding H, Wang T, Hooper LV, Koh GY, Nagy A, et al. The gut microbiota as an environmental factor that regulates fat storage. Proc Natl Acad Sci U S A. 2004;101(44):15718-23.
55. Rabot S, Membrez M, Bruneau A, Gérard P, Harach T, Moser M, et al. Germ-free C57BL/6J mice are resistant to high-fat-diet-induced insulin resistance and have altered cholesterol metabolism. The FASEB Journal. December 1, 2010 2010;24(12):4948-59.
56. Kübeck R, Bonet-Ripoll C, Hoffmann C, Walker A, Müller VM, Schüppel VL, et al. Dietary fat and gut microbiota interactions determine diet-induced obesity in mice. Molecular Metabolism. 2016/12/01/ 2016;5(12):1162-74.
57. Devaraj S, Hemarajata P, Versalovic J. The Human Gut Microbiome and Body Metabolism: Implications for Obesity and Diabetes. Clin Chem. 2013;59(4):617-28.
58. Holmes E, Li Jia V, Marchesi Julian R, Nicholson Jeremy K. Gut Microbiota Composition and Activity in Relation to Host Metabolic Phenotype and Disease Risk. Cell Metab. 2012;16(5):559-64.
59. Rowland I, Gibson G, Heinken A, Scott K, Swann J, Thiele I, et al. Gut microbiota functions: metabolism of nutrients and other food components. European Journal of Nutrition. 2017/04/09 2017.
60. Tan J, McKenzie C, Potamitis M, Thorburn AN, Mackay CR, Macia L. Chapter Three - The Role of Short-Chain Fatty Acids in Health and Disease. In: Alt FW, editor. Advances in Immunology. 121: Academic Press; 2014. p. 91-119.
61. Hao G, Zhang B, Gu M, Chen C, Zhang Q, Zhang G, et al. Vitamin K intake and the risk of fractures: A meta-analysis. Medicine. 2017;96(17):e6725.

62. Higgs J, Derbyshire E, Styles K. Nutrition and osteoporosis prevention for the orthopaedic surgeon: A wholefoods approach. EFORT Open Reviews. 2017;2(6):300-8.
63. Rayman MP. Diet, nutrition and osteoarthritis. BMC Musculoskeletal Disorders. 2015;16(Suppl 1):S7-S.
64. Berenbaum F, Eymard F, Houard X. Osteoarthritis, inflammation and obesity. Curr Opin Rheumatol. 2013;25(1):114-8.
65. Hardy R, Cooper MS. Bone loss in inflammatory disorders. J Endocrinol. Jun 2009;201(3):309-20.
66. Clemente JC, Manasson J, Scher JU. The role of the gut microbiome in systemic inflammatory disease. BMJ. 2018;360.
67. Boulangé CL, Neves AL, Chilloux J, Nicholson JK, Dumas M-E. Impact of the gut microbiota on inflammation, obesity, and metabolic disease. Genomic Med. 2016;8(1):42.
68. Poiana C, Capatina C. Fracture Risk Assessment in Patients With Diabetes Mellitus. J Clin Densitom. 2017;20(3):432-43.
69. King LK, March L, Anandacoomarasamy A. Obesity & osteoarthritis. Indian J Med Res. 2013;138(2):185-93.
70. Williams MF, London DA, Husni EM, Navaneethan S, Kashyap SR. Type 2 diabetes and osteoarthritis: a systematic review and meta-analysis. J Diabetes Complications. 2016;30(5):944-50.
71. Gonnelli S, Caffarelli C, Nuti R. Obesity and fracture risk. Clin Cases Miner Bone Metab. 2014;11(1):9-14.
72. Courties A, Sellam J, Berenbaum F. Metabolic syndrome-associated osteoarthritis. Curr Opin Rheumatol. 2017;29(2):214-22.
73. Zhuo Q, Yang W, Chen J, Wang Y. Metabolic syndrome meets osteoarthritis. Nat Rev Rheumatol. 2012;8:729.
74. Yoshiya T, Shingo N, Yosuke O. Osteoblasts and Osteoclasts in Bone Remodeling and Inflammation. Curr Drug Targets Inflamm Allergy 2005;4(3):325-8.
75. Shaw AT, Gravallese EM. Mediators of inflammation and bone remodeling in rheumatic disease. Semin Cell Dev Biol 2016;49:2-10.
76. Tilg H, Moschen AR, Kaser A, Pines A, Dotan I. Gut, inflammation and osteoporosis: basic and clinical concepts. Gut. 2008;57(5):684-94.
77. Mundy GR. Osteoporosis and inflammation. Nutr Rev. 2007;65(12 Pt 2):S147-51.
78. Guilak F, Fermor B, Keefe FJ, Kraus VB, Olson SA, Pisetsky DS, et al. The Role of Biomechanics and Inflammation in Cartilage Injury and Repair. Clin Orthop Relat Res. 2004;423:17-26.
79. Goldring MB, Otero M. Inflammation in osteoarthritis. Curr Opin Rheumatol. 2011;23(5):471-8.
80. Sokolove J, Lepus CM. Role of inflammation in the pathogenesis of osteoarthritis: latest findings and interpretations. Ther Adv Musculoskelet Dis. 2013;5(2):77-94.
81. Abbas Ali Imani F, Seyed Fazlollah M, Sepideh S, Samaneh Y, Mohammad Reza N. Toll-Like Receptors: Role in Inflammation and Commensal Bacteria. Inflamm Allergy Drug Targets 2011;10(3):198-207.
82. Pendyala S, Walker JM, Holt PR. A High-Fat Diet Is Associated With Endotoxemia That Originates From the Gut. Gastroenterology. 2012;142(5):1100-1.e2.

83. Hajam IA, Dar PA, Shahnawaz I, Jaume JC, Lee JH. Bacterial flagellin—a potent immunomodulatory agent. Exp Mol Med. 2017;49:e373.
84. Giannelli V, Di Gregorio V, Iebba V, Giusto M, Schippa S, Merli M, et al. Microbiota and the gut-liver axis: Bacterial translocation, inflammation and infection in cirrhosis. World J Gastroenterol. 2014;20(45):16795-810.
85. Andersen K, Kesper MS, Marschner JA, Konrad L, Ryu M, Kumar Vr S, et al. Intestinal Dysbiosis, Barrier Dysfunction, and Bacterial Translocation Account for CKD–Related Systemic Inflammation. J Am Soc Nephrol 2016.
86. Sun J, Kato I. Gut microbiota, inflammation and colorectal cancer. Genes & Diseases. 2016;3(2):130-43.
87. Hussain Mian A, Saito H, Alles N, Shimokawa H, Aoki K, Ohya K. Lipopolysaccharide-induced bone resorption is increased in TNF type 2 receptor-deficient mice in vivo. J Bone Miner Metab. 2008;26(5):469-77.
88. Fujita S, Kikuchi T, Sobue T, Suzuki M, Koide M, Noguchi T. Lipopolysaccharide Mediated Enhancement of Bone Metabolism in Estrogen Deficient Mice. J Periodontol 2008;79(11):2173-81.
89. Kassem A, Lindholm C, Lerner UH. Toll-Like Receptor 2 Stimulation of Osteoblasts Mediates Staphylococcus Aureus Induced Bone Resorption and Osteoclastogenesis through Enhanced RANKL. PLoS One. 2016;11(6):e0156708.
90. Muthukuru M, Darveau RP. TLR signaling that induces weak inflammatory response and SHIP1 enhances osteogenic functions. Bone Res. Article 2014;2:14031.
91. Takami M, Kim N, Rho J, Choi Y. Stimulation by Toll-Like Receptors Inhibits Osteoclast Differentiation. J Immunol. 2002;169(3):1516.
92. Bobacz K, Sunk IG, Hofstaetter JG, Amoyo L, Toma CD, Akira S, et al. Toll-like receptors and chondrocytes: The lipopolysaccharide-induced decrease in cartilage matrix synthesis is dependent on the presence of toll-like receptor 4 and antagonized by bone morphogenetic protein 7. Arthritis Rheum. 2007;56(6):1880-93.
93. Sillat T, Barreto G, Clarijs P, Soininen A, Ainola M, Pajarinen J, et al. Toll-like receptors in human chondrocytes and osteoarthritic cartilage. Acta Orthop. 2013;84(6):585-92.
94. Barreto G, Sandelin J, Salem A, Nordström DC, Waris E. Toll-like receptors and their soluble forms differ in the knee and thumb basal osteoarthritic joints. Acta Orthop. 2017;88(3):326-33.
95. Gómez R, Villalvilla A, Largo R, Gualillo O, Herrero-Beaumont G. TLR4 signalling in osteoarthritis—finding targets for candidate DMOADs. Nat Rev Rheumatol. 2014;11:159.
96. Ohira H, Tsutsui W, Fujioka Y. Are Short Chain Fatty Acids in Gut Microbiota Defensive Players for Inflammation and Atherosclerosis? J Atheroscler Thromb. 2017;24(7):660-72.
97. Ríos-Covián D, Ruas-Madiedo P, Margolles A, Gueimonde M, de los Reyes-Gavilán CG, Salazar N. Intestinal Short Chain Fatty Acids and their Link with Diet and Human Health. Front Microbiol. 2016;7(185).
98. Hernandez CJ, Guss JD, Luna M, Goldring SR. Links Between the Microbiome and Bone. J Bone Miner Res. 2016;31(9):1638-46.
99. Mosekilde L. The effect of modelling and remodelling on human vertebral body architecture. Technol Health Care. 1998;6(5-6):287-97.

100. Pisani P, Renna MD, Conversano F, Casciaro E, Di Paola M, Quarta E, et al. Major osteoporotic fragility fractures: Risk factor updates and societal impact. World J Orthop. 2016;7(3):171-81.
101. Carpintero P, Caeiro JR, Carpintero R, Morales A, Silva S, Mesa M. Complications of hip fractures: A review. World J Orthop. 2014;5(4):402-11.
102. Fratzl P, Gupta HS, Paschalis EP, Roschger P. Structure and mechanical quality of the collagen-mineral nano-composite in bone. J Mater Chem. 2004;14(14):2115-23.
103. Rho J-Y, Kuhn-Spearing L, Zioupos P. Mechanical properties and the hierarchical structure of bone. Med Eng Phys. 1998;20(2):92-102.
104. Boskey AL. Bone composition: relationship to bone fragility and antiosteoporotic drug effects. BoneKEy Rep. 2013;2.
105. Wang X. Cortical Bone Mechanics and Composition: Effects of Age and Gender. In: Silva MJ, editor. Skeletal Aging and Osteoporosis: Biomechanics and Mechanobiology. Berlin, Heidelberg: Springer Berlin Heidelberg; 2013. p. 53-85.
106. Parkinson IH, Fazzalari NL. Characterisation of Trabecular Bone Structure. In: Silva MJ, editor. Skeletal Aging and Osteoporosis: Biomechanics and Mechanobiology. Berlin, Heidelberg: Springer Berlin Heidelberg; 2013. p. 31-51.
107. Li H, Zhang H, Tang Z, Hu G. Micro-computed tomography for small animal imaging: Technological details. PROG NAT SCI. 2008;18(5):513-21.
108. Bouxsein ML, Boyd SK, Christiansen BA, Guldberg RE, Jepsen KJ, Müller R. Guidelines for assessment of bone microstructure in rodents using micro–computed tomography. J Bone Miner Res. 2010;25(7):1468-86.
109. Vasilić B, Rajapakse CS, Wehrli FW. Classification of trabeculae into three-dimensional rodlike and platelike structures via local inertial anisotropy. Medical Physics. 2009;36(7):3280-91.
110. Cowin S. Bone mechanics handbook. New York: Informa Healthcare; 2008.
111. Lewis G, Nyman JS. The use of nanoindentation for characterizing the properties of mineralized hard tissues: State-of-the art review. Journal of Biomedical Materials Research Part B: Applied Biomaterials. 2008/10/01 2008;87B(1):286-301.
112. Zysset PK. Indentation of bone tissue: a short review. Osteoporosis International. 2009/06/01 2009;20(6):1049-55.
113. Morris MD, Mandair GS. Raman Assessment of Bone Quality. Clin Orthop Relat Res. 2011;469(8):2160-9.
114. Mandair GS, Morris MD. Contributions of Raman spectroscopy to the understanding of bone strength. BoneKEy Rep. Review 2015;4.
115. Yerramshetty JS, Akkus O. The associations between mineral crystallinity and the mechanical properties of human cortical bone. Bone. 2008;42(3):476-82.
116. Akkus O, Adar F, Schaffler MB. Age-related changes in physicochemical properties of mineral crystals are related to impaired mechanical function of cortical bone. Bone. 2004;34(3):443-53.
117. Raghavan M, Sahar ND, Kohn DH, Morris MD. Age-specific profiles of tissue-level composition and mechanical properties in murine cortical bone. Bone. 2012;50(4):942-53.
118. Gamsjaeger S, Robins SP, Tatakis DN, Klaushofer K, Paschalis EP. Identification of Pyridinoline Trivalent Collagen Cross-Links by Raman Microspectroscopy. Calcif Tissue Int. 2017;100(6):565-74.

119. Nyman JS, Granke M, Singleton RC, Pharr GM. Tissue-level Mechanical Properties of Bone Contributing to Fracture Risk. Curr Osteoporos Rep. 2016;14(4):138-50.
120. Seeman E. Bone Modeling and Remodeling. 2009-06-26 2009;19(3):219-33.
121. Langdahl B, Ferrari S, Dempster DW. Bone modeling and remodeling: potential as therapeutic targets for the treatment of osteoporosis. Ther Adv Musculoskelet Dis. 2016;8(6):225-35.
122. Fox AJ, Bedi A, Rodeo SA. The Basic Science of Articular Cartilage: Structure, Composition, and Function. Sports Health. 2009;1(6):461-8.
123. Goldring MB. Articular Cartilage Degradation in Osteoarthritis. HSS J. 2012;8(1):7-9.
124. Li G, Yin J, Gao J, Cheng TS, Pavlos NJ, Zhang C, et al. Subchondral bone in osteoarthritis: insight into risk factors and microstructural changes. Arthritis Res Ther. 2013;15(6):223.
125. Burr DB, Gallant MA. Bone remodelling in osteoarthritis. Nat Rev Rheumatol. 2012;8:665.
126. van der Kraan PM, van den Berg WB. Osteophytes: relevance and biology. Osteoarthr Cartil. 2007;15(3):237-44.
127. Holyoak DT, Tian YF, van der Meulen MCH, Singh A. Osteoarthritis: Pathology, mouse models, and nanoparticle injectable systems for targeted treatment. Ann Biomed Eng. 2016;44(6):2062-75.
128. Christiansen BA, Guilak F, Lockwood KA, Olson SA, Pitsillides AA, Sandell LJ, et al. Non-invasive mouse models of post-traumatic osteoarthritis. Osteoarthr Cartil. 2015;23(10):1627-38.
129. Furman Bridgette D, Strand J, Hembree WC, Ward Benjamin D, Guilak F, Olson Steven A. Joint degeneration following closed intraarticular fracture in the mouse knee: A model of posttraumatic arthritis. J Orthop Res. 2007;25(5):578-92.
130. Christiansen BA, Anderson MJ, Lee CA, Williams JC, Yik JHN, Haudenschild DR. Musculoskeletal changes following non-invasive knee injury using a novel mouse model of post-traumatic osteoarthritis. Osteoarthr Cartil. 2012;20(7):773-82.
131. Ko FC, Dragomir C, Plumb DA, Goldring SR, Wright TM, Goldring MB, et al. In vivo cyclic compression causes cartilage degeneration and subchondral bone changes in mouse tibiae. Arthritis & Rheum. 2013;65(6):1569-78.
132. Johnell O, Kanis JA. An estimate of the worldwide prevalence and disability associated with osteoporotic fractures. Osteoporos Int. 2006;17(12):1726-33.
133. Guss JD, Horsfield MW, Fontenele FF, Sandoval TN, Luna M, Apoorva F, et al. Alterations to the Gut Microbiome Impair Bone Strength and Tissue Material Properties. J Bone Miner Res. 2017;32(6):1343-53.
134. Lucas AR, Melton Iii LJ, Crowson CS, O'Fallon WM. Long-term Fracture Risk Among Women With Anorexia Nervosa: A Population-Based Cohort Study. Mayo Clin Proc. 1999;74(10):972-7.
135. Kane AV, Dinh DM, Ward HD. Childhood Malnutrition and the Intestinal Microbiome Malnutrition and the microbiome. Pediatr Res. 2015;77(0):256-62.
136. Kostic AD, Xavier RJ, Gevers D. The Microbiome in Inflammatory Bowel Disease: Current Status and the Future Ahead. Gastroenterology. 2014;146(6):1489-99.
137. Van staa T-P, Cooper C, Samuels Brusse L, Leufkens H, Javaid MK, Arden NK. Inflammatory bowel disease and the risk of fracture. Gastroenterology. 2003;125(6):1591-7.

138. Vestergaard P, Krogh K, Rejnmark L, Laurberg S, Mosekilde L. Fracture risk is increased in Crohn's disease, but not in ulcerative colitis. Gut. 2000;46(2):176-81.
139. Cao JJ. Effects of obesity on bone metabolism. J Orthop Surg Res. 2011;6:30-.
140. Ivers RQ, Cumming RG, Mitchell P, Peduto AJ. Diabetes and Risk of Fracture: the Blue Mountains Eye Study. Diabetes Care. 2001;24(7):1198-203.
141. Oei L, Rivadeneira F, Zillikens MC, Oei EHG. Diabetes, Diabetic Complications, and Fracture Risk. Curr Osteoporos Rep. 2015;13(2):106-15.
142. Oei L, Zillikens MC, Dehghan A, Buitendijk GHS, Castaño-Betancourt MC, Estrada K, et al. High Bone Mineral Density and Fracture Risk in Type 2 Diabetes as Skeletal Complications of Inadequate Glucose Control: the Rotterdam Study. Diabetes Care. 2013;36(6):1619-28.
143. Yatsunenko T, Rey FE, Manary MJ, Trehan I, Dominguez-Bello MG, Contreras M, et al. Human gut microbiome viewed across age and geography. Nature. 2012;486(7402):222-7.
144. Phillips ML. Gut Reaction: Environmental Effects on the Human Microbiota. Environ Health Perspect. 2009;117(5):A198-A205.
145. Rescigno M. Intestinal microbiota and its effects on the immune system. Cell Microbiol. Jul 2014;16(7):1004-13.
146. Carvalho FA, Koren O, Goodrich JK, Johansson ME, Nalbantoglu I, Aitken JD, et al. Transient inability to manage proteobacteria promotes chronic gut inflammation in TLR5-deficient mice. Cell Host Microbe. 2012;12(2):139-52.
147. Round JL, Mazmanian SK. The gut microbiota shapes intestinal immune responses during health and disease. Nat Rev Immunol. 2009;9(5):313-23.
148. Sjögren K, Engdahl C, Henning P, Lerner UH, Tremaroli V, Lagerquist MK, et al. The gut microbiota regulates bone mass in mice. J Bone Miner Res. 2012;27(6):1357-67.
149. Yan J, Herzog JW, Tsang K, Brennan CA, Bower MA, Garrett WS, et al. Gut microbiota induce IGF-1 and promote bone formation and growth. PNAS. 2016;113(47):E7554-E63.
150. Cho I, Yamanishi S, Cox L, Methe BA, Zavadil J, Li K, et al. Antibiotics in early life alter the murine colonic microbiome and adiposity. Nature. 2012;488(7413):621-6.
151. Cox LM, Yamanishi S, Sohn J, Alekseyenko AV, Leung JM, Cho I, et al. Altering the intestinal microbiota during a critical developmental window has lasting metabolic consequences. Cell. 2014;158(4):705-21.
152. Nobel YR, Cox LM, Kirigin FF, Bokulich NA, Yamanishi S, Teitler I, et al. Metabolic and metagenomic outcomes from early-life pulsed antibiotic treatment. Nat Commun. 2015;6:7486.
153. Hayashi F, Smith KD, Ozinsky A, Hawn TR, Yi EC, Goodlett DR, et al. The innate immune response to bacterial flagellin is mediated by Toll-like receptor 5. Nature. 2001;410(6832):1099-103.
154. Jepsen KJ, Silva MJ, Vashishth D, Guo XE, van der Meulen MC. Establishing biomechanical mechanisms in mouse models: practical guidelines for systematically evaluating phenotypic changes in the diaphyses of long bones. J Bone Miner Res. Jun 2015;30(6):951-66.
155. Vijay-Kumar M, Sanders CJ, Taylor RT, Kumar A, Aitken JD, Sitaraman SV, et al. Deletion of TLR5 results in spontaneous colitis in mice. J Clin Invest. 2007;117(12):3909-21.

156. MacGregor RR, Graziani AL. Oral Administration of Antibiotics: A Rational Alternative to the Parenteral Route. Clin Infect Dis. 1997;24(3):457-67.
157. Doube M, Klosowski MM, Arganda-Carreras I, Cordelieres FP, Dougherty RP, Jackson JS, et al. BoneJ: Free and extensible bone image analysis in ImageJ. Bone. 2010;47(6):1076-9.
158. Turner CH, Burr DB. Basic biomechanical measurements of bone: A tutorial. Bone. 1993;14(4):595-608.
159. Lima SF, Teixeira AGV, Higgins CH, Lima FS, Bicalho RC. The upper respiratory tract microbiome and its potential role in bovine respiratory disease and otitis media. Sci Rep. 2016;6:29050.
160. Nonnenmacher C, Dalpke A, Mutters R, Heeg K. Quantitative detection of periodontopathogens by real-time PCR. J Microbiol Methods. 2004;59(1):117-25.
161. Boutin S, Graeber SY, Weitnauer M, Panitz J, Stahl M, Clausznitzer D, et al. Comparison of microbiomes from different niches of upper and lower airways in children and adolescents with cystic fibrosis. PLoS One. 2015;10(1):e0116029.
162. Caporaso JG, Lauber CL, Walters WA, Berg-Lyons D, Huntley J, Fierer N, et al. Ultra-high-throughput microbial community analysis on the Illumina HiSeq and MiSeq platforms. ISME J. 2012;6(8):1621-4.
163. Caporaso JG, Kuczynski J, Stombaugh J, Bittinger K, Bushman FD, Costello EK, et al. QIIME allows analysis of high-throughput community sequencing data. Nat Methods. 2010;7(5):335-6.
164. Bokulich NA, Subramanian S, Faith JJ, Gevers D, Gordon JI, Knight R, et al. Quality-filtering vastly improves diversity estimates from Illumina amplicon sequencing. Nat Methods. 2013;10(1):57-9.
165. McDonald D, Price MN, Goodrich J, Nawrocki EP, DeSantis TZ, Probst A, et al. An improved Greengenes taxonomy with explicit ranks for ecological and evolutionary analyses of bacteria and archaea. ISME J. 2012;6(3):610-8.
166. Edgar RC. Search and clustering orders of magnitude faster than BLAST. Bioinformatics. 2010;26(19):2460-1.
167. Purwada A, Jaiswal MK, Ahn H, Nojima T, Kitamura D, Gaharwar AK, et al. Ex vivo engineered immune organoids for controlled germinal center reactions. Biomaterials. 2015;63:24-34.
168. Purwada A, Tian YF, Huang W, Rohrbach KM, Deol S, August A, et al. Self-Assembly Protein Nanogels for Safer Cancer Immunotherapy. Adv Healthc Mater. 2016;5(12):1413-9.
169. Mirpuri J, Raetz M, Sturge CR, Wilhelm CL, Benson A, Savani RC, et al. Proteobacteria-specific IgA regulates maturation of the intestinal microbiota. Gut Microbes. 2014;5(1):28-39.
170. Hernandez C, Beaupre G, Keller T, al. e. The influence of bone volume fraction and ash fraction on bone strength and modulus. Bone. 2001;29(1):74-8.
171. Jepsen KJ, Andarawis-Puri N. The amount of periosteal apposition required to maintain bone strength during aging depends on adult bone morphology and tissue-modulus degradation rate. J Bone Miner Res. 2012;27(9):1916-26.
172. Ionova-Martin SS, Wade JM, Tang S, Shahnazari M, Ager JW, 3rd, Lane NE, et al. Changes in cortical bone response to high-fat diet from adolescence to adulthood in mice. Osteoporos Int. 2011;22(8):2283-93.

173. Lozupone CA, Stombaugh JI, Gordon JI, Jansson JK, Knight R. Diversity, stability and resilience of the human gut microbiota. Nature. 2012;489(7415):220-30.
174. Schulfer A, Blaser MJ. Risks of Antibiotic Exposures Early in Life on the Developing Microbiome. PLoS Pathog. 2015;11(7):e1004903.
175. Chung H, Pamp Sünje J, Hill Jonathan A, Surana Neeraj K, Edelman Sanna M, Troy Erin B, et al. Gut Immune Maturation Depends on Colonization with a Host-Specific Microbiota. Cell.149(7):1578-93.
176. Shin NR, Whon TW, Bae JW. Proteobacteria: microbial signature of dysbiosis in gut microbiota. Trends Biotechnol. 2015;33(9):496-503.
177. D'Amico L, Roato I. Cross-talk between T cells and osteoclasts in bone resorption. Bonekey Rep. 2012;1:82.
178. Kawai T, Matsuyama T, Hosokawa Y, Makihira S, Seki M, Karimbux NY, et al. B and T lymphocytes are the primary sources of RANKL in the bone resorptive lesion of periodontal disease. Am J Pathol. 2006;169(3):987-98.
179. Manilay JO, Zouali M. Tight relationships between B lymphocytes and the skeletal system. Trends Mol Med. 2014;20(7):405-12.
180. Weitzmann MN, Pacifici R. The role of T lymphocytes in bone metabolism. Immunol Rev. 2005;208:154-68.
181. Zhao B, Ivashkiv LB. Negative regulation of osteoclastogenesis and bone resorption by cytokines and transcriptional repressors. Arthritis Res Ther. 2011;13(4):234.
182. de Onis M, Garza C, Victora CG. The WHO Multicentre Growth Reference Study: strategy for developing a new international growth reference. Forum Nutr. 2003;56:238-40.
183. Viguet-Carrin S, Hoppler M, Membrez Scalfo F, Vuichoud J, Vigo M, Offord EA, et al. Peak bone strength is influenced by calcium intake in growing rats. Bone. 2014;68:85-91.
184. Donnelly E, Chen DX, Boskey AL, Baker SP, van der Meulen MC. Contribution of mineral to bone structural behavior and tissue mechanical properties. Calcif Tissue Int. 2010;87(5):450-60.
185. O'Sullivan M, O'Morain C. Nutrition in inflammatory bowel disease. Best Pract Res Clin Gastroenterol. 2006;20(3):561-73.
186. Bianchi ML. Inflammatory bowel diseases, celiac disease, and bone. Arch Biochem Biophys. 2010;503(1):54-65.
187. Hamdani G, Gabet Y, Rachmilewitz D, Karmeli F, Bab I, Dresner-Pollak R. Dextran sodium sulfate-induced colitis causes rapid bone loss in mice. Bone. 2008;43(5):945-50.
188. Irwin R, Lee T, Young VB, Parameswaran N, McCabe LR. Colitis-induced bone loss is gender dependent and associated with increased inflammation. Inflamm Bowel Dis. 2013;19(8):1586-97.
189. Potgieter M, Bester J, Kell DB, Pretorius E. The dormant blood microbiome in chronic, inflammatory diseases. FEMS Microbiol Rev. 2015;39(4):567-91.
190. Sanger TJ, Norgard EA, Pletscher LS, Bevilacqua M, Brooks VR, Sandell LJ, et al. Developmental and genetic origins of murine long bone length variation. J Exp Zool B Mol Dev Evol. 2011;316B(2):146-61.
191. Price C, Herman BC, Lufkin T, Goldman HM, Jepsen KJ. Genetic variation in bone growth patterns defines adult mouse bone fragility. J Bone Miner Res. Nov 2005;20(11):1983-91.

192. Blanton LV, Charbonneau MR, Salih T, Barratt MJ, Venkatesh S, Ilkaveya O, et al. Gut bacteria that prevent growth impairments transmitted by microbiota from malnourished children. Science. 2016;351(6275).
193. Wallach S, Feinblatt JD, Carstens JH, Jr., Avioli LV. The bone "quality" problem. Calcif Tissue Int. 1992;51(3):169-72.
194. Hernandez CJ, Keaveny TM. A biomechanical perspective on bone quality. Bone. 2006;39(6):1173-81.
195. Hillier TA, Stone KL, Bauer DC, et al. Evaluating the value of repeat bone mineral density measurement and prediction of fractures in older women: The study of osteoporotic fractures. Arch Intern Med. 2007;167(2):155-60.
196. Schuit SCE, van der Klift M, Weel AEAM, de Laet CEDH, Burger H, Seeman E, et al. Fracture incidence and association with bone mineral density in elderly men and women: the Rotterdam Study. Bone.34(1):195-202.
197. Hernandez CJ, Keaveny TM. A biomechanical perspective on bone quality. Bone. Dec 2006;39(6):1173-81. Epub 2006/08/01.
198. Yan J, Herzog JW, Tsang K, Brennan CA, Bower MA, Garrett WS, et al. Gut microbiota induce IGF-1 and promote bone formation and growth. PNAS. 2016;113(47):E7554.
199. Thomas T, Gilbert J, Meyer F. Metagenomics - a guide from sampling to data analysis. Microb Inform Exp. 2012;2:3-.
200. Pacifici R. Bone Remodeling and the Microbiome. Cold Spring Harb Perspect Med. 2018;8(4).
201. Heaney RP. Chapter 27 - Nutrition and Risk for Osteoporosis. In: Marcus R, Feldman D, Kelsey J, editors. Osteoporosis (Second Edition). San Diego: Academic Press; 2001. p. 669-700.
202. Shea MK, Booth SL. Role of vitamin K in the regulation of calcification. Int Congr Ser. 2007;1297:165-78.
203. Gourion-Arsiquaud S, Faibish D, Myers E, Spevak L, Compston J, Hodsman A, et al. Use of FTIR Spectroscopic Imaging to Identify Parameters Associated With Fragility Fracture. J Bone Miner Res. 2009;24(9):1565-71.
204. Kim G, Boskey AL, Baker SP, van der Meulen MCH. Improved prediction of rat cortical bone mechanical behavior using composite beam theory to integrate tissue level properties. J Biomech. 2012;45(16):2784-90.
205. Hunt HB, Donnelly E. Bone Quality Assessment Techniques: Geometric, Compositional, and Mechanical Characterization from Macroscale to Nanoscale. Clin Rev Bone Miner Metab. 2016;14(3):133-49.
206. Paschalis EP, Mendelsohn R, Boskey AL. Infrared Assessment of Bone Quality: A Review. Clin Orthop Relat Res. 2011;469(8):2170-8.
207. Zimmermann EA, Busse B, Ritchie RO. The fracture mechanics of human bone: influence of disease and treatment. BoneKEy Rep. Review 2015;4.
208. Overbeek R, Begley T, Butler RM, Choudhuri JV, Chuang H-Y, Cohoon M, et al. The Subsystems Approach to Genome Annotation and its Use in the Project to Annotate 1000 Genomes. Nucleic Acids Res. 2005;33(17):5691-702.
209. Goodrich JK, Di Rienzi SC, Poole AC, Koren O, Walters WA, Caporaso JG, et al. Conducting a Microbiome Study. Cell. 2014;158(2):250-62.

210. Donnelly E, Baker SP, Boskey AL, van der Meulen MCH. Effects of surface roughness and maximum load on the mechanical properties of cancellous bone measured by nanoindentation. J Biomed Mater Res A. 2006;77(2):426-35.
211. Gamsjaeger S, Masic A, Roschger P, Kazanci M, Dunlop JWC, Klaushofer K, et al. Cortical bone composition and orientation as a function of animal and tissue age in mice by Raman spectroscopy. Bone. 2010;47(2):392-9.
212. Kazanci M, Fratzl P, Klaushofer K, Paschalis EP. Complementary Information on In Vitro Conversion of Amorphous (Precursor) Calcium Phosphate to Hydroxyapatite from Raman Microspectroscopy and Wide-Angle X-Ray Scattering. Calcif Tissue Int. 2006;79(5):354-9.
213. Donnelly E, Boskey AL, Baker SP, van der Meulen MCH. Effects of tissue age on bone tissue material composition and nanomechanical properties in the rat cortex. J Biomed Mater Res A. 2010;92(3):1048-56.
214. Oliver WC, Pharr GM. An improved technique for determining hardness and elastic modulus using load and displacement sensing indentation experiments. J Mater Res. 1992;7(6):1564-83.
215. Walther B, Karl JP, Booth SL, Boyaval P. Menaquinones, Bacteria, and the Food Supply: The Relevance of Dairy and Fermented Food Products to Vitamin K Requirements. Adv Nutr. 2013;4(4):463-73.
216. Nguyen TLA, Vieira-Silva S, Liston A, Raes J. How informative is the mouse for human gut microbiota research? Dis Model Mech. 10.1242/dmm.017400 2015;8(1):1.
217. Thijssen HHW, Drittij-Reijnders MJ. Vitamin K distribution in rat tissues: dietary phylloquinone is a source of tissue menaquinone-4. Br J Nutr. 1994;72(3):415-25.
218. Karl JP, Fu X, Dolnikowski GG, Saltzman E, Booth SL. Quantification of phylloquinone and menaquinones in feces, serum, and food by high-performance liquid chromatography–mass spectrometry. J Chromatogr B. 2014;963:128-33.
219. Bi X, Patil CA, Lynch CC, Pharr GM, Mahadevan-Jansen A, Nyman JS. Raman and Mechanical Properties Correlate at Whole Bone- and tissue-levels in a genetic mouse model. J Biomech. 2011;44(2):297-303.
220. Gundberg CM, Lian JB, Booth SL. Vitamin K-Dependent Carboxylation of Osteocalcin: Friend or Foe? Adv Nutr. 2012;3(2):149-57.
221. Morgan S, Poundarik AA, Vashishth D. Do Non-Collagenous Proteins Affect Skeletal Mechanical Properties? Calcif Tissue Int. 2015;97(3):281-91.
222. Poundarik AA, Diab T, Sroga GE, Ural A, Boskey AL, Gundberg CM, et al. Dilatational band formation in bone. PNAS. 10.1073/pnas.1201513109 2012;109(47):19178.
223. Cheung AM, Tile L, Lee Y, Tomlinson G, Hawker G, Scher J, et al. Vitamin K Supplementation in Postmenopausal Women with Osteopenia (ECKO Trial): A Randomized Controlled Trial. PLoS Med. 2008;5(10):1-12.
224. Burr DB, Akkus O. Chapter 1 - Bone Morphology and Organization. Basic and Applied Bone Biology. San Diego: Academic Press; 2014. p. 3-25.
225. Hunter GK, Hauschka PV, Poole AR, Rosenberg LC, Goldberg HA. Nucleation and inhibition of hydroxyapatite formation by mineralized tissue proteins. Biochem J. 1996;317(Pt 1):59-64.
226. Murshed M, Schinke T, McKee MD, Karsenty G. Extracellular matrix mineralization is regulated locally; different roles of two gla-containing proteins. J Cell Bio. 2004;165(5):625-30.

227. Poundarik A, Gundberg C, Vashishth D. Non-collageneous proteins influence bone crystal size and morphology: A SAXS study. 2011 IEEE 37th Annual Northeast Bioengineering Conference (NEBEC)2011. p. 1-2.
228. Poundarik AA, Boskey A, Gundberg C, Vashishth D. Biomolecular regulation, composition and nanoarchitecture of bone mineral. Sci Rep. 2018;8:1191.
229. Stock SR. The Mineral–Collagen Interface in Bone. Calcif Tissue Int. 2015;97(3):262-80.
230. Boskey AL, Gadaleta S, Gundberg C, Doty SB, Ducy P, Karsenty G. Fourier transform infrared microspectroscopic analysis of bones of osteocalcin-deficient mice provides insight into the function of osteocalcin. Bone. 1998;23(3):187-96.
231. Shen C-L, Cao JJ, Dagda RY, Chanjaplammootil S, Lu C, Chyu M-C, et al. Green tea polyphenols benefits body composition and improves bone quality in long-term high-fat diet–induced obese rats. Nutr Res. 2012;32(6):448-57.
232. Shapses SA, Pop LC, Wang Y. Obesity is a concern for bone health with aging. Nutr Res. 2017;39:1-13.
233. Lecka-Czernik B, Stechschulte LA, Czernik PJ, Dowling AR. High bone mass in adult mice with diet-induced obesity results from a combination of initial increase in bone mass followed by attenuation in bone formation; implications for high bone mass and decreased bone quality in obesity. Mol Cell Endocrinol. 2015;410:35-41.
234. Ionova-Martin SS, Wade JM, Tang S, Shahnazari M, Ager JW, Lane NE, et al. Changes in cortical bone response to high-fat diet from adolescence to adulthood in mice. Osteoporos Int. 2011;22(8):2283-93.
235. Yamaguchi M, Taguchi H, Hua Gao Y, Igarashi A, Tsukamoto Y. Effect of vitamin K2 (menaquinone-7) in fermented soybean (natto) on bone loss in ovariectomized rats1999. 23-9 p.
236. Kim M, Na W, Sohn C. Vitamin K1 (phylloquinone) and K2 (menaquinone-4) supplementation improves bone formation in a high-fat diet-induced obese mice. J Clin Biochem Nutr. 2013;53(2):108-13.
237. Okano T, Shimomura Y, Yamane M, Suhara Y, Kamao M, Sugiura M, et al. Conversion of Phylloquinone (Vitamin K1) into Menaquinone-4 (Vitamin K2) in Mice: Two possible routes fro menaquinone-4 accumulation in cerebra of mice. J Biol Chem. 2008;283(17):11270-9.
238. Tabb MM, Sun A, Zhou C, Grün F, Errandi J, Romero K, et al. Vitamin K2 Regulation of Bone Homeostasis Is Mediated by the Steroid and Xenobiotic Receptor SXR. J Biol Chem. 2003;278(45):43919-27.
239. Bi X, Grafe I, Ding H, Flores R, Munivez E, Jiang Ming M, et al. Correlations Between Bone Mechanical Properties and Bone Composition Parameters in Mouse Models of Dominant and Recessive Osteogenesis Imperfecta and the Response to Anti-TGF-β Treatment. J Bone Miner Res. 2016;32(2):347-59.
240. Silva M, Brodt M, Wopenka B, Thomopoulos S, Williams D, Wassen M, et al. Decreased Collagen Organization and Content Are Associated With Reduced Strength of Demineralized and Intact Bone in the SAMP6 Mouse. J Bone Miner Res. 2009;21(1):78-88.
241. Kavukcuoglu NB, Patterson-Buckendahl P, Mann AB. Effect of osteocalcin deficiency on the nanomechanics and chemistry of mouse bones. J Mech Behav Biomed Mater. 2009;2(4):348-54.

242. Aspden RM. Obesity punches above its weight in osteoarthritis. Nat Rev Rheumatol. 2011;7(1):65-8.
243. Courties A, Gualillo O, Berenbaum F, Sellam J. Metabolic stress-induced joint inflammation and osteoarthritis. Osteoarthr Cartil. 2015;23(11):1955-65.
244. Dahaghin S, Bierma-Zeinstra SM, Koes BW, Hazes JM, Pols HA. Do metabolic factors add to the effect of overweight on hand osteoarthritis? The Rotterdam Study. Ann Rheum Dis. 2007;66.
245. Yusuf E, Nelissen RG, Ioan-Facsinay A, Stojanovic-Susulic V, DeGroot J, van Osch G, et al. Association between weight or body mass index and hand osteoarthritis: a systematic review. Ann Rheum Dis. 2010;69(4):761.
246. Puenpatom RA, Victor TW. Increased Prevalence of Metabolic Syndrome in Individuals with Osteoarthritis: An Analysis of NHANES III Data. Postgrad Med J. 2009;121(6):9-20.
247. Sellam J, Berenbaum F. Is osteoarthritis a metabolic disease? Joint Bone Spine. 2013;80(6):568-73.
248. Yoshimura N, Muraki S, Oka H, Tanaka S, Kawaguchi H, Nakamura K, et al. Accumulation of metabolic risk factors such as overweight, hypertension, dyslipidaemia, and impaired glucose tolerance raises the risk of occurrence and progression of knee osteoarthritis: a 3-year follow-up of the ROAD study. Osteoarthr Cartil. 2012;20(11):1217-26.
249. Schett G, Kleyer A, Perricone C, Sahinbegovic E, Iagnocco A, Zwerina J, et al. Diabetes Is an Independent Predictor for Severe Osteoarthritis: Results from a longitudinal cohort study. Diabetes Care. 2013;36(2):403-9.
250. Louati K, Vidal C, Berenbaum F, Sellam J. Association between diabetes mellitus and osteoarthritis: systematic literature review and meta-analysis. RMD Open. 2015;1(1).
251. Monira Hussain S, Wang Y, Cicuttini FM, Simpson JA, Giles GG, Graves S, et al. Incidence of total knee and hip replacement for osteoarthritis in relation to the metabolic syndrome and its components: A prospective cohort study. Semin Arthritis Rheum. 2014;43(4):429-36.
252. Griffin TM, Fermor B, Huebner JL, Kraus VB, Rodriguiz RM, Wetsel WC, et al. Diet-induced obesity differentially regulates behavioral, biomechanical, and molecular risk factors for osteoarthritis in mice. Arthritis Res Ther. 2010;12(4):R130.
253. Louer CR, Furman BD, Huebner JL, Kraus VB, Olson SA, Guilak F. Diet-Induced Obesity Significantly Increases the Severity of Post-Traumatic Arthritis in Mice. Arthritis & Rheum. 2012;64(10):3220-30.
254. Mooney RA, Sampson ER, Lerea J, Rosier RN, Zuscik MJ. High-fat diet accelerates progression of osteoarthritis after meniscal/ligamentous injury. Arthritis Res Ther. 2011;13(6):R198.
255. Ribeiro M, López de Figueroa P, Nogueira-Recalde U, Centeno A, Mendes AF, Blanco FJ, et al. Diabetes-accelerated experimental osteoarthritis is prevented by autophagy activation. Osteoarthr Cartil. 2016;24(12):2116-25.
256. Griffin TM, Huebner JL, Kraus VB, Guilak F. Extreme obesity due to impaired leptin signaling in mice does not cause knee osteoarthritis. Arthritis Rheum. 2009;60(10):2935-44.
257. King AJF. The use of animal models in diabetes research. Br J Pharmacol. 2012;166(3):877-94.

258. Scotece M, Mobasheri A. Leptin in osteoarthritis: Focus on articular cartilage and chondrocytes. Life Sciences. 2015;140(Supplement C):75-8.
259. Dumond H, Presle N, Terlain B, Mainard D, Loeuille D, Netter P, et al. Evidence for a key role of leptin in osteoarthritis. Arthritis & Rheum. 2003;48(11):3118-29.
260. Tilg H, Kaser A. Gut microbiome, obesity, and metabolic dysfunction. J Clin Invest. 2011;121(6):2126-32.
261. Shreiner AB, Kao JY, Young VB. The gut microbiome in health and in disease. Curr Opin Gastroenterol. 2015;31(1):69-75.
262. Ko FC, Dragomir C, Plumb DA, Goldring SR, Wright TM, Goldring MB, et al. In vivo cyclic compression causes cartilage degeneration and subchondral bone changes in mouse tibiae. Arthritis Rheum. 2013;65(6):1569-78.
263. Glasson SS, Chambers MG, Van Den Berg WB, Little CB. The OARSI histopathology initiative – recommendations for histological assessments of osteoarthritis in the mouse. Osteoarthr Cartil. 2010;18, Supplement 3:S17-S23.
264. Xu L, Flahiff CM, Waldman BA, Wu D, Olsen BR, Setton LA, et al. Osteoarthritis-like changes and decreased mechanical function of articular cartilage in the joints of mice with the chondrodysplasia gene (cho). Arthritis Rheum. 2003;48(9):2509-18.
265. Walters W, Hyde ER, Berg-Lyons D, Ackermann G, Humphrey G, Parada A, et al. Improved Bacterial 16S rRNA Gene (V4 and V4-5) and Fungal Internal Transcribed Spacer Marker Gene Primers for Microbial Community Surveys. mSystems. 2016;1(1).
266. Callahan BJ, McMurdie PJ, Rosen MJ, Han AW, Johnson AJA, Holmes SP. DADA2: High-resolution sample inference from Illumina amplicon data. Nat Methods. 2016;13:581.
267. Kaneko S, Satoh T, Chiba J, Ju C, Inoue K, Kagawa J. Interleukin–6 and interleukin–8 levels in serum and synovial fluid of patients with osteoarthritis. Cytokines Cell Mol Ther. 2000;6(2):71-9.
268. Martel-Pelletier J, Alaaeddine N, Pelletier JP. Cytokines and their role in the pathophysiology of osteoarthritis. Front Biosci. 1999;4:D694-703.
269. Huang Z, Kraus VB. Does lipopolysaccharide-mediated inflammation have a role in OA? Nat Rev Rheumatol. 2015;12:123.
270. Kim K-A, Gu W, Lee I-A, Joh E-H, Kim D-H. High Fat Diet-Induced Gut Microbiota Exacerbates Inflammation and Obesity in Mice via the TLR4 Signaling Pathway. PLoS One. 2012;7(10):e47713.
271. Huang ZY, Stabler T, Pei FX, Kraus VB. Both systemic and local lipopolysaccharide (LPS) burden are associated with knee OA severity and inflammation. Osteoarthr Cartil. 2016;24(10):1769-75.
272. Poonpet T, Honsawek S. Adipokines: Biomarkers for osteoarthritis? World J Orthop. 2014;5(3):319-27.
273. Lohmander LS, Englund PM, Dahl LL, Roos EM. The Long-term Consequence of Anterior Cruciate Ligament and Meniscus Injuries. Am J Sports Med. 2007;35(10):1756-69.
274. Chamberlain ND, Vila OM, Volin MV, Volkov S, Pope RM, Swedler W, et al. TLR5, a Novel and Unidentified Inflammatory Mediator in Rheumatoid Arthritis that Correlates with Disease Activity Score and Joint TNF-α Levels. J Immunol. 2012;189(1):475-83.

275. Brandt KD, Mazzuca SA, Katz BP, Lane KA, Buckwalter KA, Yocum DE, et al. Effects of doxycycline on progression of osteoarthritis: Results of a randomized, placebo-controlled, double-blind trial. Arthritis Rheum. 2005;52(7):2015-25.
276. Yu LP, Smith GN, Brandt KD, Myers SL, O'Connor BL, Brandt DA. Reduction of the severity of canine osteoarthritis by prophylactic treatment with oral doxycycline. Arthritis Rheum. 1992;35(10):1150-9.
277. Gnauck A, Lentle RG, Kruger MC. Chasing a ghost? – Issues with the determination of circulating levels of endotoxin in human blood. Crit Rev Clin Lab Sci. 2016;53(3):197-215.
278. Holyoak DT, Otero M, Armar NS, Ziemian SN, Otto A, Cullinane D, et al. Collagen XI mutation lowers susceptibility to load-induced cartilage damage in mice. J Orthop Res. 2018;36(2):711-20.
279. Hardcastle SA, Dieppe P, Gregson CL, Davey Smith G, Tobias JH. Osteoarthritis and bone mineral density: are strong bones bad for joints. BoneKEy Rep. 2015;4.
280. Peters AE, Akhtar R, Comerford EJ, Bates KT. The effect of ageing and osteoarthritis on the mechanical properties of cartilage and bone in the human knee joint. Sci Rep. 2018;8(1):5931.
281. Adebayo OO, Ko FC, Wan PT, Goldring SR, Goldring MB, Wright TM, et al. Role of subchondral bone properties and changes in development of load-induced osteoarthritis in mice. Osteoarthr Cartil. 2017;25(12):2108-2118.
282. Schott EM, Farnsworth CW, Grier A, Lillis JA, Soniwala S, Dadourian GH, et al. Targeting the gut microbiome to treat the osteoarthritis of obesity. JCI Insight. 2018;3(8).
283. Glasson SS, Blanchet TJ, Morris EA. The surgical destabilization of the medial meniscus (DMM) model of osteoarthritis in the 129/SvEv mouse. Osteoarthr Cartil. 2007;15(9):1061-9.
284. Misra D, Booth SL, Tolstykh I, Felson DT, Nevitt MC, Lewis CE, et al. Vitamin K deficiency is associated with incident knee osteoarthritis. The American journal of medicine. 2013;126(3):243-8.
285. Pierer M, Wagner U, Rossol M, Ibrahim S. Toll-Like Receptor 4 Is Involved in Inflammatory and Joint Destructive Pathways in Collagen-Induced Arthritis in DBA1J Mice. PLoS One. 2011;6(8):e23539.
286. Shiraki M, Tsugawa N, Okano T. Recent advances in vitamin K-dependent Gla-containing proteins and vitamin K nutrition. Osteoporos Sarcopenia. 2015;1(1):22-38.
287. Boskey AL, Mendelsohn R. Infrared spectroscopic characterization of mineralized tissues. Vib Spectrosc. 2005;38(1-2):107-14.
288. Shea MK, Dallal GE, Dawson-Hughes B, Ordovas JM, O'Donnell CJ, Gundberg CM, et al. Vitamin K, circulating cytokines, and bone mineral density in older men and women. Am J Clin Nutr. 2008;88(2):356-63.
289. Ross AC, Chen Q, Ma Y. Vitamin A and Retinoic Acid in the Regulation of B-Cell Development and Antibody Production. Vitam Horm. 2011;86:103-26.
290. Palermo A, Tuccinardi D, D'Onofrio L, Watanabe M, Maggi D, Maurizi AR, et al. Vitamin K and osteoporosis: Myth or reality? Metabolism. 2017;70:57-71.
291. Carvalho BM, Guadagnini D, Tsukumo DML, Schenka AA, Latuf-Filho P, Vassallo J, et al. Modulation of gut microbiota by antibiotics improves insulin signalling in high-fat fed mice. Diabetologia. 2012;55(10):2823-34.

292. Cani PD, Bibiloni R, Knauf C, Waget A, Neyrinck AM, Delzenne NM, et al. Changes in Gut Microbiota Control Metabolic Endotoxemia-Induced Inflammation in High-Fat Diet–Induced Obesity and Diabetes in Mice. Diabetes. 2008;57(6):1470.
293. Winer Daniel A, Luck H, Tsai S, Winer S. The Intestinal Immune System in Obesity and Insulin Resistance. Cell Metab. 2016;23(3):413-26.
294. Chaby R. Lipopolysaccharide-binding molecules: transporters, blockers and sensors. Cell Mol Life Sci 2004;61(14):1697-713.
295. Balooch G, Balooch M, Nalla RK, Schilling S, Filvaroff EH, Marshall GW, et al. TGF-β regulates the mechanical properties and composition of bone matrix. Proc Natl Acad Sci U S A. 2005;102(52):18813-8.
296. Harris SE, Bonewald LF, Harris MA, Sabatini M, Dallas S, Feng JQ, et al. Effects of transforming growth factor β on bone nodule formation and expression of bone morphogenetic protein 2, osteocalcin, osteopontin, alkaline phosphatase, and type I collagen mRNA in long-term cultures of fetal rat calvarial osteoblasts. J Bone Miner Res. 1994;9(6):855-63.
297. Rydziel S, Varghese S, Canalis E. Transforming growth factor β1 inhibits collagenase 3 expression by transcriptional and post-transcriptional mechanisms in osteoblast cultures. J Cell Physiol. 1998;170(2):145-52.
298. Kang JS, Alliston T, Delston R, Derynck R. Repression of Runx2 function by TGF-β through recruitment of class II histone deacetylases by Smad3. The EMBO J. 2005;24(14):2543-55.
299. Bauché D, Marie JC. Transforming growth factor β: a master regulator of the gut microbiota and immune cell interactions. Clin Transl Immunology. 2017;6(4):e136.
300. Martin-Gallausiaux C, Béguet-Crespel F, Marinelli L, Jamet A, Ledue F, Blottière HM, et al. Butyrate produced by gut commensal bacteria activates TGF-beta1 expression through the transcription factor SP1 in human intestinal epithelial cells. Sci Rep. 2018;8(1):9742.
301. Pushpakumar S, Ren L, Kundu S, Gamon A, Tyagi SC, Sen U. Toll-like Receptor 4 Deficiency Reduces Oxidative Stress and Macrophage Mediated Inflammation in Hypertensive Kidney. Sci Rep. 2017;7(1):6349.
302. Edwards James R, Nyman Jeffry S, Lwin Seint T, Moore Megan M, Esparza J, O'Quinn Elizabeth C, et al. Inhibition of TGF-β signaling by 1D11 antibody treatment increases bone mass and quality in vivo. J Bone Miner Res. 2010;25(11):2419-26.
303. de Gramont A, Faivre S, Raymond E. Novel TGF-β inhibitors ready for prime time in onco-immunology. Oncoimmunology. 2017;6(1):e1257453.
304. Shen J, Li S, Chen D. TGF-β signaling and the development of osteoarthritis. Bone Res. 2014;2:14002.
305. Xie L, Tintani F, Wang X, Li F, Zhen G, Qiu T, et al. Systemic neutralization of TGF-β attenuates osteoarthritis. Ann N Y Acad Sci. 2016;1376(1):53-64.
306. Price C, Herman Brad C, Lufkin T, Goldman Haviva M, Jepsen Karl J. Genetic Variation in Bone Growth Patterns Defines Adult Mouse Bone Fragility. J Bone Miner Res. 2009;20(11):1983-91.
307. Landreth KS. Critical windows in development of the rodent immune system. Hum Exp Toxicol. 2002;21(9-10):493-8.

308. Hu Y, Peng J, Tai N, Hu C, Zhang X, Wong FS, et al. Maternal antibiotic treatment protects offspring from diabetes development in NOD mice by generation of tolerogenic antigen-presenting cells. J Immunol. 2015;195(9):4176-84.
309. Schulfer AF, Battaglia T, Alvarez Y, Bijnens L, Ruiz VE, Ho M, et al. Intergenerational transfer of antibiotic-perturbed microbiota enhances colitis in susceptible mice. Nat Microbiol. 2018;3(2):234-42.
310. Chu DM, Meyer KM, Prince AL, Aagaard KM. Impact of maternal nutrition in pregnancy and lactation on offspring gut microbial composition and function. Gut Microbes. 2016;7(6):459-70.
311. Rosshart SP, Vassallo BG, Angeletti D, Hutchinson DS, Morgan AP, Takeda K, et al. Wild Mouse Gut Microbiota Promotes Host Fitness and Improves Disease Resistance. Cell. 2017;171(5):1015-28.e13.